VOLUME 8 NUMBER 2 2017 ISSN 2218-7987

International Journal of Mathematics and Physics

Al-Farabi Kazakh National University

The International Journal of Mathematics and Physics is a peer-reviewed international journal covering all branches of mathematics and physics. The Journal welcomes papers on modern problems of mathematics and physics, in particular, Applied Mathematics, Algebra, Mathematical Analysis, Differential Equations, Mechanics, Informatics, Mathematical Modeling, Applied Physics, Radio Physics, Thermophysics, Nuclear Physics, Nanotechnology, and etc.

International Journal of Mathematics and Physics is published twice a year by al-Farabi Kazakh National University, 71 al-Farabi ave., 050040, Almaty, Kazakhstan
website: http://ijmph.kaznu.kz/

Any inquiry for subscriptions should be send to:
Prof. Tlekkabul Ramazanov, al-Farabi Kazakh National University
71 al-Farabi ave., 050040, Almaty, Kazakhstan
e-mail: Tlekkabul.Ramazanov@kaznu.kz

 Printed in Kazakhstan

EDITORIAL

The most significant scientific achievements are attained through joint efforts of different sciences, mathematics and physics are among them. Therefore publication of the Journal, which shows results of current investigations in the field of mathematics and physics, will allow wider exhibition of scientific problems, tasks and discoveries.

One of the basic goals of the Journal is to promote extensive exchange of information between scientists from all over the world. We propose publishing service for original papers and materials of Mathematical and Physical Conferences (by selection) held in different countries and in the Republic of Kazakhstan.

Creation of the special International Journal of Mathematics and Physics is of great importance because a vast amount of scientists are willing to publish their articles and it will help to widen the geography of future dissemination. We will also be glad to publish papers of scientists from all the continents.

The Journal will publish experimental and theoretical investigations on Mathematics, Physical Technology and Physics. Among the subject emphasized are modern problems of Applied Mathematics, Algebra, Mathematical Analysis, Differential Equations, Mechanics, Informatics, Mathematical Modeling, Astronomy, Space Research, Theoretical Physics, Plasma Physics, Chemical Physics, Radio Physics, Thermophysics, Nuclear Physics, Nanotechnology, and etc.

The Journal is issued on the base of al-Farabi Kazakh National University. Leading scientists from different countries of the world agreed to join the Editorial Board of the Journal.

The Journal is published twice a year by al-Farabi Kazakh National University. We hope to receive papers from many laboratories which are interested in applications of the scientific principles of mathematics and physics and are carrying out researches on such subjects as production of new materials or technological problems.

IRSTI 27.35.39

[1]Sh.R. Myrzakul, [2]E. Gudekli, [3]A.M. Syzdyk, [4*] K.R. Yesmakhanova

[1]Faculty of Physics and Technology, al-Farabi Kazakh National University, Almaty, Kazakhstan
[2]Department of Physics, Istanbul University, Istanbul, Turkey
[3]Faculty of physics and technical sciences, L.N. Gumilyov Eurasian National University, Astana, Kazakhstan
[4]Faculty of Mechanics and Mathematics, L.N. Gumilyov Eurasian National University, Astana, Kazakhstan
[*]e-mail: kryesmakhanova@gmail.com

The nonlocal nonlinear Schrödinger and Maxwell – Bloch equation

Abstract. In this paper, the nonlocal nonlinear Schrödinger and Maxwell – Bloch equations are is introduced. A particular case of this system, namely the Schrödinger equation, is integrable by the inverse scattering method as shown in the work of M. Ablowitz and Z. Musslimani. Following their idea, we prove the integrability of the nonlocal nonlinear Schrödinger and Maxwell – Bloch equation using its Lax pairs. Also the Darboux transformations are constructed, and soliton solutions are obtained from different "seed" solutions using them. One–fold, two–fold and N–fold determinant representations are obtained by this transformation. Moreover, soliton and solitons–like solutions, such as dynamic and topological soliton, periodic, domain walls, kink, lamp, bright and dark solitons, bright and dark rogue waves, bright and dark positons, etc., of this equation are built. In future papers, we will investigate the conservation laws of the nonlocal nonlinear Schrödinger and Maxwell – Bloch equation using the Lax pair.
Key words: nonlocal nonlinear Schrödinger and Maxwell – Bloch equation, Lax representation, Darboux transformation.

Introduction

It is known that the nature of nonlinear real systems is one of the basic notions in modern science. Nonlinearity is the property which is applied in almost all fields of science. A nonlinear phenomenon is usually modeled in terms of nonlinear ordinary and/or differential equations in particular cases. Most of such nonlinear differential equations (NDE) are completely integrable. That is they accept some classes of interesting exact solutions, such as solitons, dromions, destructive waves, semilaritons, king, etc. They draw both mathematical and physical interest. Investigations of solitons, positons, brakes, dromions, "destructive waves" have become one of the interesting and highly active areas for research in modern science and technology during the last several decades. In particular, many of the completely integrable NDEs have already been established and investigated [1-8].

Among such integrable nonlinear systems, the Schrödinger and Maxwell – Bloch equations have a crucial role. The Schrödinger and Maxwell – Bloch equations describe solitons in fibers with resonance and erbium systems and have a (1+1) – dimension [9]. Using the Darboux transformation, the (1+1)-dimensional Schrödinger and Maxwell – Bloch equations were analyzed in [9], where soliton and periodic solutions were constructed from various "seeds".

Recently, a (2+1) –dimensional Schrödinger and Maxwell – Bloch equation was introduced in [10]. In this section, our aim is to built a Darboux transformation for (2+1) – dimensional Schrödinger and Maxwell – Bloch equation and to obtain soliton solutions. It is well known that the Darboux transformation is an effective way to get different solutions of integrable equations [11]. For instence destructive waves and positon solutions were constructed using the Darboux transformation for one and two Hirota-Maxwell-Bloch equations in [11], [12]. The authors found soliton and positon solutions via the Darboux transformation as a representation of the determinant for the inhomogeneous Hirota-Maxwell-Bloch equation [12], [13].

In this work we consider one of the generalizations of the nonlinear Schrödinger equation, namely the (1+1)-dimensional nonlocal nonlinear Schrödinger and Maxwell – Bloch equation. This equation is a generalization of the (1+1) – dimensional nonlocal nonlinear Schrödinger equation, which was investigated in the papers of M.J. Ablowitz and Ziad H. Musslimani, Li-Yuan Ma, Zuo-Nong Zhu, T. A. Gadzhimuradov A. M. Agalarov et all. [13-16].

A Lax pair of the (1+1)-dimensional nonlocal focusing nonlinear Schrödinger – Maxwell – Bloch equation

In this section we study the nonlocal nonlinear Schrödinger and Maxwell – Bloch equation, which reads as

$$\begin{gathered} iq_t(x,t)+q_{xx}(x,t)+ \\ +2q(x,t)q^*(-x,t)q(x,t)-2p(x,t)=0, \end{gathered} \quad (1)$$

$$\begin{gathered} iq_t^*(-x,t)+q_{xx}^*(-x,t)- \\ -2q^*(-x,t)q(x,t)q^*(-x,t)+2p^*(-x,t)=0, \end{gathered} \quad (2)$$

$$p_x(x,t)=2[q(x,t)\eta(x,t)-i\omega p(-x,t)], \quad (3)$$

$$p_x^*(-x,t)=2[q^*(-x,t)\eta(x,t)-i\omega p^*(-x,t)], \quad (4)$$

$$\eta_x(x,t)=q(x,t)p^*(-x,t)-q^*(-x,t)p(x,t), \quad (5)$$

where $*$ denotes complex conjugation and q, p are complex functions of the real variables x and t. The equations (1)-(2) are called the nonlocal nonlinear Schrödinger equations and they were introduced by M. Ablowitz and Z. Musslimani in [10]. The nonlocal nonlinear Schrödinger equation is obtained from a new and simple reduction of the well-known AKNS system. It admits a Lax pair and an infinite number of conservation laws. The IST for decaying data is developed and a one breathing soliton solution is construced. The IST requires different scattering data symmetries than the classical NLS equation. A nonlocal NLS hierarchy and novel nonlocal Painleve´ type equations are also obtained.

Now consider equations (1) – (5) so called Schrödinger and Maxwell – Bloch equation. The system of equations (1) - (5) admits a Lax pair representation and possesses an infinite number of conservation laws; hence, it is integrable. Using the inverse scattering method, corresponding to rapidly decaying initial data, one can linearize the equation and аштв solutions to the system of equations (1)-(5) including pure soliton solutions. Some of the essential properties of the nonlocal NLS equation are derived from the classical NLS equation where the nonlocal nonlinear term $q^*(-x,t)$, $p^*(-x,t)$ are replaced by $q^*(x,t)$, $p^*(x,t)$. Infact, we note that the system of equations (1) – (2) and the classical NLS share the symmetry that when $x\to -x$, $t\to -t$ and a complex conjugate is taken, then the equation stays invariant [16].

Corresponding Lax representation for the nonlocal nonlinear Schrödinger –Maxwell – Bloch equation (1) – (5) can be written as follows

$$\psi_x = A\psi, \quad (6)$$

$$\psi_t = B\psi, \quad (7)$$

where $\psi=\begin{pmatrix}\psi_1(x,t,\lambda)\\ \psi_2(x,t,\lambda)\end{pmatrix}$ is the eigenfunction corresponding to λ and A, B are 2×2 matrices given by

$$A=-i\lambda\sigma_3+A_0,$$

$$B=\lambda^2 B_2+\lambda B_1+B_0+\frac{1}{\lambda-\omega}B_{-1}.$$

Here λ is the complex eigenvalue constant, σ_3 is the Pauli matrix and $A_0, B_2, B_1, B_0, B_{-1}$ are 2×2 matrices as follows

$$\sigma_3=\begin{pmatrix}1 & 0\\ 0 & -1\end{pmatrix},$$

$$A_0=\begin{pmatrix}0 & q(x,t)\\ -q^*(-x,t) & 0\end{pmatrix},$$

$$B_2 = -2i\sigma_3 = \begin{pmatrix} -2i & 0 \\ 0 & 2i \end{pmatrix},$$

$$B_1 = \begin{pmatrix} 0 & 2q(x,t) \\ -2q^*(-x,t) & 0 \end{pmatrix},$$

$$B_0 = i\begin{pmatrix} q(x,t)q^*(-x,t) & q_x(x,t) \\ -q_x^*(-x,t) & -q(x,t)q^*(-x,t) \end{pmatrix},$$

$$B_{-1} = \begin{pmatrix} \eta(x,t) & -p(x,t) \\ p^*(-x,t) & -\eta(x,t) \end{pmatrix}.$$

So the Lax representation of the integrable nonlocal nonlinear Schrödinger – Maxwel l– Bloch equation is given by *A* and *B*. It can be seen that from the compatibility condition from $\psi_{xt} = \psi_{tx}$ we can obtain the zero curvature equation of the system of equations (6) and (7).

$$A_t - B_x + AB - BA = 0.$$

In the next section, one-fold Darboux transformation of the nonlocal nonlinear Schrödinger – Maxwell–Bloch equation will be obtained.

The one-fold Darboux transformation for the nonlocal nonlinear Schrödinger and Maxwell – Bloch equation

Using the Darboux transformation for the AKNS system [11], consider the transformation of the linear system of equations (6)-(7)

$$\psi^{[1]} = T\psi = (\lambda I - M)\psi. \tag{8}$$

The function $\psi^{[1]}$ is assumed to satisfy

$$\begin{aligned} \psi_x^{[1]} &= A^{[1]}\psi^{[1]}, \\ \psi_t^{[1]} &= B^{[1]}\psi^{[1]} \end{aligned} \tag{9}$$

where $A^{[1]}$ and $B^{[1]}$ are matrices depending on $q^{[1]}(x,t), q^{*[1]}(-x,t)$ and λ. Here M and I are matrices of the forms

$$M = \begin{pmatrix} m_{11} & m_{12} \\ m_{21} & m_{22} \end{pmatrix}, \quad I = \begin{pmatrix} 1 & 0 \\ 0 & 1 \end{pmatrix}. \tag{10}$$

The relation between $q^{[1]}(x,t), q^{*[1]}(-x,t)$ and $A^{[1]} - B^{[1]}$ is the same as the relation between functions $q(x,t)$, $q^*(-x,t)$ and $A - B$. In order to make the system (9) invariant under the transformation (8), T must satisfy the following equations

$$T_x + TA = A^{[1]}T, \tag{11}$$

$$T_t + TB = B^{[1]}T. \tag{12}$$

The relation between $q(x,t), q^*(-x,t)$ and $q^{[1]}(x,t), q^{*[1]}(x,t)$ can be derived from these equations, which is actually the Darboux transformation of the nonlocal nonlinear Schrödinger and Maxwell – Bloch equation (1)-(5).

From the above identities, after simplifications and comparisons of the coefficients from equation (11), it follows that

$$\lambda^0: \quad M_x = A_0^{[1]}M - MA_0, \tag{13}$$

$$\lambda^1: \quad A_0^{[1]} = A_0 + i[M, \sigma_3], \tag{14}$$

$$\lambda^2: \quad iI\sigma_3 = iI\sigma_3. \tag{15}$$

Finally, from (13)-(15) we obtain solutions

$$\begin{aligned} q^{[1]} &= q - 2im_{12}, \\ q^{*[1]} &= q^* - 2im_{21}, \end{aligned} \tag{16}$$

Similarly, comparing the coefficients of λ^i of the two sides of the equation (12) gives us

$$\lambda^0: M_t = B_0^{[1]}M - MB_0, \tag{17}$$

$$\lambda^1: B_0 - MB_1 = B_0^{[1]} - B_1^{[1]}M, \tag{18}$$

$$\lambda^2: B_1 - MB_2 = B_1^{[1]} - B_2^{[1]}M. \tag{19}$$

$$\lambda^3 : IB_2 = B_2^{[1]} I, \tag{20}$$

$$\frac{1}{\lambda-\omega} : \omega B_{-1} - MB_{-1} = \omega B_{-1}^{[1]} - B_{-1}^{[1]} M. \tag{21}$$

Then the system of equations (17)-(21) yields

$$\eta^{[1]} = \frac{1}{\Delta}\left\{(\omega - m_{11})^2 + m_{12}^*(\omega - m_{11})p - |m_{12}|^2 \eta - m_{12}(\omega - m_{11}^*)p^*\right\}, \tag{22}$$

$$p^{[1]} = -\frac{1}{\Delta}\left\{\eta(\omega - m_{11})m_{12} - p^* m_{12}^2 + p(w - m_{11})^2\right\}, \tag{23}$$

$$p^{*[1]} = -\frac{1}{\Delta}\left\{2(\omega - m_{22})m_{12}^* \mu + p m_{12}^{*2} - p^*(\omega - m_{22})^2\right\}. \tag{24}$$

These solutions (16) and (22)-(24) imply the one-fold Darboux transformation of the nonlocal nonlinear Schrödinger and Maxwell – Bloch equation.

Now assume that

$$M = H\Lambda H^{-1}, \tag{25}$$

where

$$H = \begin{pmatrix} \psi_1(\lambda_1, x, t) & \psi_1(\lambda_2, x, t) \\ \psi_2(\lambda_1, x, t) & \psi_2(\lambda_2, x, t) \end{pmatrix} = \begin{pmatrix} \psi_{1,1} & \psi_{1,2} \\ \psi_{2,1} & \psi_{2,2} \end{pmatrix}, \quad \Lambda = \begin{pmatrix} \lambda_1 & 0 \\ 0 & \lambda_2 \end{pmatrix}, \tag{26}$$

and $\det H \neq 0$, where λ_1 and λ_2 are complex constants. In order to satisfy the constraints of A_0 as mentioned above, we first note that if $\delta = +1$, then

$$\psi^+ = \psi^{-1}, \quad A_0^+ = -A_0,$$

$$\lambda_2 = -\lambda_1^*, \quad H = \begin{pmatrix} \psi_1(\lambda_1, x, t) & -\psi_2^*(\lambda_1, x, t) \\ \psi_2(\lambda_1, x, t) & \psi_1^*(\lambda_1, x, t) \end{pmatrix} = \begin{pmatrix} \psi_1 & -\psi_2^* \\ \psi_2 & \psi_1^* \end{pmatrix}, \tag{27}$$

$$H^{-1} = \frac{1}{\Delta}\begin{pmatrix} \psi_1^*(\lambda_1 x, t) & \psi_2^*(\lambda_1, x, t) \\ -\psi_2(\lambda_1, x, t) & \psi_1(\lambda_1, x, t) \end{pmatrix} = \begin{pmatrix} \psi_1^* & \psi_2^* \\ -\psi_2 & \psi_1 \end{pmatrix},$$

where $\Delta = |\psi_1|^2 + |\psi_2|^2$.

From (24) use formula (27) we obtain

$$M = \frac{1}{\Delta}\begin{pmatrix} \lambda_1 |\psi_1|^2 - \lambda_1^* |\psi_2|^2 & (\lambda_1 + \lambda_1^*)\psi_1 \psi_2^* \\ (\lambda_1 + \lambda_1^*)\psi_2 \psi_1^* & \lambda_1 |\psi_2|^2 - \lambda_1^* |\psi_1|^2 \end{pmatrix}. \tag{28}$$

In the following section we give the determinant representation of the Darboux transformation for the nonlocal nonlinear Schrödinger and Maxwell – Bloch equation.

The determinant representation of Darboux transformation for the nonlocal nonlinear Schrödinger – Maxwell–Bloch equation

Here the determinant representation is obtained for the one-fold, two-fold and n-fold Darboux transformation of the (1+1)-dimensional nonlocal nonlinear Schrödinger and Maxwell – Bloch equation. The reduction condition on the eigenfunctions are $\psi_{2,2i} = \psi^*_{1,2i-1}$, $\psi_{2,2i-1} = -\psi^*_{1,2i}$ and for the eigenvalues are $\lambda_{2i} = -\lambda^*_{2i-1}$.

The determinant representation of the one-fold Darboux transformation of the nonlocal nonlinear Schrödinger – Maxwell–Bloch equation implies the following theorem (as [12]- [14]).

Theorem 1. The one-fold Darboux transformation of the nonlocal nonlinear Schrödinger – Maxwell–Bloch equation is

$$T_1(\lambda, \lambda_1, \lambda_2) = \lambda I - M = \lambda I + t_0^{[1]} = \frac{1}{\Delta_1}\begin{pmatrix} (T_1)_{11} & (T_1)_{12} \\ (T_1)_{21} & (T_1)_{22} \end{pmatrix}, \tag{29}$$

where

$$t_0^{[1]} = \frac{1}{\Delta_1}\begin{pmatrix} \begin{vmatrix} \psi_{2,1} & \lambda_1\psi_{1,1} \\ \psi_{2,2} & \lambda_2\psi_{1,2} \end{vmatrix} & -\begin{vmatrix} \psi_{1,1} & \lambda_1\psi_{1,1} \\ \psi_{1,2} & \lambda_2\psi_{1,2} \end{vmatrix} \\ \begin{vmatrix} \psi_{2,1} & \lambda_1\psi_{2,1} \\ \psi_{2,2} & \lambda_2\psi_{2,2} \end{vmatrix} & -\begin{vmatrix} \psi_{1,1} & \lambda_1\psi_{2,1} \\ \psi_{1,2} & \lambda_2\psi_{2,2} \end{vmatrix} \end{pmatrix}, \quad \Delta_1 = \begin{vmatrix} \psi_{1,1} & \psi_{1,2} \\ \psi_{2,1} & \psi_{2,2} \end{vmatrix}, \tag{30}$$

$$(T_1)_{11} = \begin{vmatrix} 1 & 0 & \lambda \\ \psi_{1,1} & \psi_{2,1} & \lambda_1\psi_{1,1} \\ \psi_{1,2} & \psi_{2,2} & \lambda_2\psi_{1,2} \end{vmatrix}, \quad (T_1)_{12} = \begin{vmatrix} 0 & 1 & 0 \\ \psi_{1,1} & \psi_{2,1} & \lambda_1\psi_{1,1} \\ \psi_{1,2} & \psi_{2,2} & \lambda_2\psi_{1,2} \end{vmatrix}, \tag{31a}$$

$$(T_1)_{21} = \begin{vmatrix} 1 & 0 & 0 \\ \psi_{1,1} & \psi_{2,1} & \lambda_1\psi_{2,1} \\ \psi_{1,2} & \psi_{2,2} & \lambda_2\psi_{2,2} \end{vmatrix}, \quad (T_1)_{22} = \begin{vmatrix} 0 & 1 & \lambda \\ \psi_{1,1} & \psi_{2,1} & \lambda_1\psi_{2,1} \\ \psi_{1,2} & \psi_{2,2} & \lambda_2\psi_{2,2} \end{vmatrix}. \tag{31b}$$

T_1 satisfies the following equations

$$T_{1x} + T_1 A = A^{[1]} T_1, \tag{32}$$

$$T_{1t} + T_1 B = B^{[1]} T_1. \tag{33}$$

$$A_0^{[1]} = A_0 + [\sigma_3, t_0^{[1]}], \tag{34}$$

$$B_{-1}^{[1]} = T_1 \mid_{\lambda=-\mu} B_{-1} T_1^{-1} \mid_{\lambda=-\mu}. \tag{35}$$

Then the solutions of the system (1)-(5) are of the form

$$q^{[1]} = q - 2i\frac{(T_1)_{12}}{\Delta_1}, \tag{36}$$

$$\eta^{[1]} = \frac{\left(|\mu + (T_1)_{11}|^2 - |(T_1)_{12}|^2\right)\eta + p(T_1)_{21}(\mu + (T_1)_{11} - p^*(T_1)_{12}(\mu + (T_1)_{22})}{W}, \tag{37}$$

$$p^{[1]} = \frac{p\left[(\mu + (T_1)_{11})^2 - p^*(T_1)_{12}^2\right] + 2\eta(T_1)_{12}(\mu + (T_1)_{11})}{W}, \tag{38}$$

$$p*^{[1]} = \frac{p\left[(\mu + (T_1)_{22})^2 + p^*(T_1)_{21}^2\right] - 2\eta(T_1)_{21}(\mu + (T_1)_{22})}{W}, \tag{39}$$

where $W = (T_1)_{11}(T_1)_{22} - (T_1)_{12}(T_1)_{21}$.

The transformation T_1 has the following property

$$T_1(\lambda, \lambda_1, \lambda_2)\Big|_{\lambda=\lambda_i}\begin{pmatrix}\psi_{1,i}\\ \psi_{2,i}\end{pmatrix} = 0, i = 1,2. \tag{40}$$

Now we are ready to prove the theorem.

Proof of the Main theorem. From the expression (9), it follows that

$$M = \frac{1}{\Delta_1}\begin{pmatrix}\lambda_1\psi_{1,1}\psi_{2,2} - \lambda_2\psi_{1,2}\psi_{2,1} & (\lambda_2 - \lambda_1)\psi_{1,1}\psi_{1,2}\\ (\lambda_1 - \lambda_2)\psi_{2,1}\psi_{2,2} & \lambda_1\psi_{1,2}\psi_{2,1} + \lambda_2\psi_{1,1}\psi_{2,2}\end{pmatrix}. \tag{41}$$

From equation (29), we obtain

$$T_1(\lambda, \lambda_1, \lambda_2) = \lambda I - M = \frac{1}{\Delta_1}\begin{pmatrix}\lambda\Delta_1 - \begin{vmatrix}\psi_{2,1} & \lambda_1\psi_{1,1}\\ \psi_{2,2} & \lambda_2\psi_{1,2}\end{vmatrix} & -\begin{vmatrix}\psi_{1,1} & \lambda_1\psi_{1,1}\\ \psi_{1,2} & \lambda_2\psi_{1,2}\end{vmatrix}\\ \begin{vmatrix}\psi_{2,1} & \lambda_1\psi_{2,1}\\ \psi_{2,2} & \lambda_2\psi_{2,2}\end{vmatrix} & \lambda\Delta_1 + \begin{vmatrix}\psi_{1,1} & \lambda_1\psi_{2,1}\\ \psi_{1,2} & \lambda_2\psi_{2,2}\end{vmatrix}\end{pmatrix} \tag{42}$$

$$\lambda I + t_0^{[1]} = \lambda I - M = \frac{1}{\Delta_1}\begin{pmatrix}\lambda\Delta_1 - \begin{vmatrix}\psi_{2,1} & \lambda_1\psi_{1,1}\\ \psi_{2,2} & \lambda_2\psi_{1,2}\end{vmatrix} & -\begin{vmatrix}\psi_{1,1} & \lambda_1\psi_{1,1}\\ \psi_{1,2} & \lambda_2\psi_{1,2}\end{vmatrix}\\ \begin{vmatrix}\psi_{2,1} & \lambda_1\psi_{2,1}\\ \psi_{2,2} & \lambda_2\psi_{2,2}\end{vmatrix} & \lambda\Delta_1 + \begin{vmatrix}\psi_{1,1} & \lambda_1\psi_{2,1}\\ \psi_{1,2} & \lambda_2\psi_{2,2}\end{vmatrix}\end{pmatrix} \tag{43}$$

and the elements of the matrix T_1 are written as

$$(T_1)_{11} = \begin{vmatrix} \psi_{2,1} & \lambda_1\psi_{1,1} \\ \psi_{2,2} & \lambda_2\psi_{1,2} \end{vmatrix} - \lambda\Delta_1 = \begin{vmatrix} 1 & 0 & \lambda \\ \psi_{1,1} & \psi_{2,1} & \lambda_1\psi_{1,1} \\ \psi_{1,2} & \psi_{2,2} & \lambda_2\psi_{1,2} \end{vmatrix},$$

$$(T_1)_{12} = -\begin{vmatrix} \psi_{1,1} & \lambda_1\psi_{1,1} \\ \psi_{1,2} & \lambda_2\psi_{1,2} \end{vmatrix} = \begin{vmatrix} 0 & 1 & 0 \\ \psi_{1,1} & \psi_{2,1} & \lambda_1\psi_{1,1} \\ \psi_{1,2} & \psi_{2,2} & \lambda_2\psi_{1,2} \end{vmatrix},$$

$$(T_1)_{21} = \begin{vmatrix} \psi_{2,1} & \lambda_1\psi_{2,1} \\ \psi_{2,2} & \lambda_2\psi_{2,2} \end{vmatrix} = \begin{vmatrix} 1 & 0 & 0 \\ \psi_{1,1} & \psi_{2,1} & \lambda_1\psi_{2,1} \\ \psi_{1,2} & \psi_{2,2} & \lambda_2\psi_{2,2} \end{vmatrix},$$

$$(T_1)_{22} = -\begin{vmatrix} \psi_{1,1} & \lambda_1\psi_{2,1} \\ \psi_{1,2} & \lambda_2\psi_{2,2} \end{vmatrix} - \lambda\Delta_1 = \begin{vmatrix} 0 & 1 & \lambda \\ \psi_{1,1} & \psi_{2,1} & \lambda_1\psi_{2,1} \\ \psi_{1,2} & \psi_{2,2} & \lambda_2\psi_{2,2} \end{vmatrix},$$

$$t_{0x}^{[1]} + \lambda A_0 - i\lambda^2\sigma_3 + \lambda t_0^{[1]}\sigma_3 + t_0^{[1]}A_0 = -i\lambda^2\sigma_3 + \lambda A_0^{[1]} - i\lambda\sigma_3 t_0^{[1]} + A_0^{[1]}t_0^{[1]}. \quad (44)$$

Comparing the coefficients of λ^i of the two sides of (44) yields

$$\lambda^0: \quad t_{0x}^{[1]} + t_0^{[1]}A_0 = A_0^{[1]}t_0^{[1]},$$

$$\lambda^1: \quad A_0 - it_0^{[1]}\sigma_3 = A_0^{[1]} - i\sigma_3 t_0^{[1]},$$

$$\lambda^2: \quad i\sigma_3 = i\sigma_3$$

Analogous theorem 1 we can formulate the next theorem.

Theorem 2. The two-fold Darboux transformation of the nonlocal nonlinear Schrödinger and Maxwell – Bloch equation is

$$T_2(\lambda, \lambda_1, \lambda_2, \lambda_3, \lambda_4) = \\ = \lambda^2 I + \lambda t_1^{[2]} + t_0^{[2]} = \frac{1}{\Delta_2}\begin{pmatrix} (T_2)_{11} & (T_2)_{12} \\ (T_2)_{21} & (T_2)_{22} \end{pmatrix},$$

where

$$(T_2)_{11}=\begin{pmatrix} 1 & 0 & \lambda & 0 & \lambda^2 \\ \psi_{1,1} & \psi_{2,1} & \lambda_1\psi_{1,1} & \lambda_1\psi_{2,1} & \lambda_1^2\psi_{1,1} \\ \psi_{1,2} & \psi_{2,2} & \lambda_2\psi_{1,2} & \lambda_2\psi_{2,2} & \lambda_2^2\psi_{1,2} \\ \psi_{1,3} & \psi_{2,3} & \lambda_3\psi_{1,3} & \lambda_3\psi_{2,3} & \lambda_3^2\psi_{1,3} \\ \psi_{1,4} & \psi_{2,4} & \lambda_4\psi_{1,4} & \lambda_4\psi_{2,4} & \lambda_4^2\psi_{1,4} \end{pmatrix}, \quad (T_2)_{12}=\begin{pmatrix} 0 & 1 & 0 & \lambda & 0 \\ \psi_{1,1} & \psi_{2,1} & \lambda_1\psi_{1,1} & \lambda_1\psi_{2,1} & \lambda_1^2\psi_{1,1} \\ \psi_{1,2} & \psi_{2,2} & \lambda_2\psi_{1,2} & \lambda_2\psi_{2,2} & \lambda_2^2\psi_{1,2} \\ \psi_{1,3} & \psi_{2,3} & \lambda_3\psi_{1,3} & \lambda_3\psi_{2,3} & \lambda_3^2\psi_{1,3} \\ \psi_{1,4} & \psi_{2,4} & \lambda_4\psi_{1,4} & \lambda_4\psi_{2,4} & \lambda_4^2\psi_{1,4} \end{pmatrix},$$

$$(T_2)_{21}=\begin{pmatrix} 0 & 0 & 1 & 0 & \lambda \\ \psi_{1,1} & \psi_{2,1} & \lambda_1\psi_{1,1} & \lambda_1\psi_{2,1} & \lambda_1^2\psi_{2,1} \\ \psi_{1,2} & \psi_{2,2} & \lambda_2\psi_{1,2} & \lambda_2\psi_{2,2} & \lambda_2^2\psi_{2,2} \\ \psi_{1,3} & \psi_{2,3} & \lambda_3\psi_{1,3} & \lambda_3\psi_{2,3} & \lambda_3^2\psi_{2,3} \\ \psi_{1,4} & \psi_{2,4} & \lambda_4\psi_{1,4} & \lambda_4\psi_{2,4} & \lambda_4^2\psi_{2,4} \end{pmatrix}, \quad (T_2)_{22}=\begin{pmatrix} 0 & 0 & 1 & 0 & \lambda \\ \psi_{1,1} & \psi_{2,1} & \lambda_1\psi_{1,1} & \lambda_1\psi_{2,1} & \lambda_1^2\psi_{2,1} \\ \psi_{1,2} & \psi_{2,2} & \lambda_2\psi_{1,2} & \lambda_2\psi_{2,2} & \lambda_2^2\psi_{2,2} \\ \psi_{1,3} & \psi_{2,3} & \lambda_3\psi_{1,3} & \lambda_3\psi_{2,3} & \lambda_3^2\psi_{2,3} \\ \psi_{1,4} & \psi_{2,4} & \lambda_4\psi_{1,4} & \lambda_4\psi_{2,4} & \lambda_4^2\psi_{2,4} \end{pmatrix},$$

$$\Delta_2=\begin{pmatrix} \psi_{1,1} & \psi_{2,1} & \lambda_1\psi_{1,1} & \lambda_1\psi_{2,1} \\ \psi_{1,2} & \psi_{2,,2} & \lambda_2\psi_{1,2} & \lambda_2\psi_{2,2} \\ \psi_{1,3} & \psi_{2,3} & \lambda_3\psi_{1,3} & \lambda_3\psi_{2,3} \\ \psi_{1,4} & \psi_{2,4} & \lambda_4\psi_{1,4} & \lambda_4\psi_{2,4} \end{pmatrix}$$

T_2 satisfies the system

$$T_{2x}+T_2A=A^{[2]}T_2,$$

$$T_{2t}+T_2B=B^{[2]}T_1.$$

$$A_0^{[2]}=A_0+\left[\sigma_3,t_0^{[2]}\right],$$

$$B_{-1}^{[2]}=T_2\mid_{\lambda=-\mu} B_{-1}T_2^{-1}\mid_{\lambda=-\mu}.$$

Then the solutions of the system (1) – (5) are given by

$$q^{[2]}=q-2i\frac{(T_2)_{12}}{\Delta_2}$$

$$\eta^{[2]}=\frac{\left(\left|\mu+(T_2)_{11}\right|^2\left|(T_2)_{12}\right|^2\right)\eta+p(T_2)_{21}(\mu+(T_2)_{11})-p^*(T_2)_{12}(\mu+(T_2)_{22})}{W},$$

$$p^{[2]}=\frac{p\left[(\mu+(T_2)_{11})^2-p^*(T_2)_{12}^2\right]+2\eta(T_2)_{12}(\mu+(T_2)_{12}(\mu+(T_2)_{11})}{W},$$

$$p^{*[2]}=\frac{p^*\left((\mu+(T_2)_{22})^2+p(T_2)_{21}^2\right)-2\eta(T_2)_{21}(\mu+(T_2)_{22})}{W},$$

where $W=(T_2)_{11}(T_2)_{22}-(T_2)_{12}(T_2)_{21}$.

The transformation T_2 has the following property

$$T_2(\lambda,\lambda_1,\lambda_2,\lambda_3,\lambda_4)\Big|_{\lambda=\lambda_i}\begin{pmatrix}\psi_{1,i}\\ \psi_{2.i}\end{pmatrix}=0,\quad i=1,\ 2,\ 3,4.\ )$$

Conclusion

In this paper, we have obtained the DT for the nonlocal nonlinear Schrödinger and Maxwell – Bloch equation. Using the derived DT, some exact solutions including, the one-soliton solution are obtained. The determinant representations are given for one-fold, two-fold and n-fold DT for the onlocal nonlinear Schrödinger and Maxwell – Bloch equation. Using obtained results, one can also find the n-solitons, breathers and rogue wave solutions of the nonlocal nonlinear Schrödinger and Maxwell – Bloch equation. It is interesting to note that the rogue wave solutions of nonlinear equations are currently one of the most active topics in nonlinear physics and mathematics. The application of the obtained solutions in physics is an interesting subject. In particular, we hope that the presented solutions may be used in experiments or optical fibre communication. Also we will study some important generalizations of the nonlocal nonlinear Schrödinger and Maxwell – Bloch equation in future.

References

1. Zhunussova Zh. Kh., Yesmakhanova K. R., Tungushbaeva D. I., Mamyrbekova G. K., Nugmanova G. N., Myrzakulov R. Integrable Heisenberg Ferromagnet Equations with self-consistent potentials // [arXiv:1301.1649].

2. L.H. Wang, K. Porsezian, J.S. He. Breather and Rogue Wave solutions of a Generalized Nonlinear Schrödinger Equation// Phys. Rev. E. – 2013. – Vol.87. – P. 053202.

3. Jingsong He, Shuwei Xu, K. Porseizan. N-order bright and dark rogue waves in a Resonant erbium-doped Fibre system // Phys. Rev. E. – 2012. –Vol.86. – P.066603.

4. Shuwei Xu, Jingsong He. The Rogue Wave and breather solution of the Gerdjikov-Ivanov equation// arXiv: 1109.3283.

5. Jingsong He, Shuwei Xu, Yi Cheng. The rational solutions of the mixed nonlinear Schrödinger equation// arXiv: 1407.6917.

6. Ablowitz M.J., Musslimani Z.H. Integrable Nonlocal Nonlinear Schrödinger Equation. Physical Review Letters, – 2013. – Vol. 110, №6. – P. 064105.

7. Gadzhimuradov T. A., Agalarov A. M. Towards a gauge-equivalent magnetic structure of the nonlocal nonlinear Schrödinger equation // Physical Review A. – 2016. – Vol. 93. –P. 062124.

8. Gadzhimuradov T. A., Agalarov A. M. Gauge equivalence of nonlocal NLSE and PT-symmetric Heisenberg ferromagnetic equation. https://www.researchgate.net/publication/305721244.

9. Li-Yuan Ma, Zuo-Nong Zhu. Nonlocal nonlinear Schrödinger equation and its discrete version: Soliton solutions and gauge equivalence// Journal of Mathematical Physics. – 2016. – Vol.57. – P.083507; doi: http://dx.doi.org/10.1063/1.4960818.

10. El-Ganainy R., Makris K. G., Christodoulides D. N., Musslimani Z. H. Theory of coupled optical PT-symmetric structures // Optics Letters. – 2007. – Vol. 32, Issue 17. – P. 2632-2634.

11. Regensburger A., Bersch C., Miri M.A., Onishchukov G., Christodoulides D. N., Peschel U. Parity-time synthetic photonic lattices. Nature, (London). – 2012. – Vol. 488, – P. 167.

12. Li-Yuan Ma, Zuo-Nong Zhu. Nonlocal nonlinear Schrödinger equation and its discrete version: soliton solutions and gauge equivalence // DOI: 10.1063/1.4960818, arXiv: 1503.06909.

13. Chuanzhong Li, Jingsong He, K. Porsezian, Rogue waves of the Hirota and the Maxwell-Bloch equations // Physical Review E. – 2013. – Vol.87. – P.012913.

14. Jieming Yang, Chuanzhong Li, Tiantian Li, Zhaoneng Cheng, Darboux transformation and solutions of the two-component Hirota-Maxwell-Bloch system. Chin. Phys Lett. – 2013. – Vol.30, No. 10. – P. 104201.

15. Chuanzhong Li, Jingsong He. Darboux transformation and positons of the inhomogeneous Hirota and the Maxwell-Bloch equation. Commun. Theor. Phys. –2002. – Vol.38. –P. 493-496.

16. Jingsong He, Ling Zhang, Yi Cheng, Yishen Li. Determinant representation of Darboux transformation for the AKNS system// Science in China Series A: Mathematics. –2006. –Vol.49. – No. 12. – P. 1867-1878.

IRSTI 20.17.17

[1]G.T. Balakayeva, [1*]D.K. Darkenbayev, [2]Chris Phillips

[1]Faculty of Information Technologies, al-Farabi Kazakh National University, Almaty, Kazakhstan
[2]University of Newcastle upon Tyne, Newcastle, Great Britain
[*]e-mail: dauren.kadyrovich@gmail.com

Investigation of technologies of processing of big data

Abstract. An overview of the technologies and methods is presented, on the basis of which the authors of this article model the processing of a large amount of data, developing a web application. In particular, it is proposed to combine models to improve the efficiency of processing large amounts of data. Large data set before traditional storage systems and processing a new challenge. This article analyzes possible methods their decisions, limitations that do not allow to do it effectively, and also provides an overview of three modern approaches to working with large data: NoSQL and real-time event flow processing. Analysis of large data requires the use of technology and the means to implement highly productive computing. The main factors of the problem are, first of all, the complexity and the second physical volume of the information collection. It should be noted that the actual processing of data includes the construction of the algorithm and the time for its description and debugging. Unique data collections require the development of unique algorithms, which increases the total processing time by an order of magnitude.
Key words: BigData, DataMining, modeling of large data processing, NoSQL, data analysis, modeling, analysis.

Introduction

One of the topical tasks of many fields of science and technology is the task of processing large amounts of data, for example. The use of effective technologies of processing of large data allows enterprises to take a new level of work in such areas as: improving the quality of service, product development, risk management, security, cost optimization. The processing large amounts of data is relevant for geoinformatics, aerospace imagery obtained from remote sensing of the Earth, bioinformatics – analysis and ordering of genomic and proteomic information, etc.

The information value of large data is obvious, the proof of the topic is a set of tasks that can be solved by analyzing information flows of large data:

- forecast of the outflow of customers – based on analysis of data from call centers, technical support services and website traffic;
- creation of predictive models
- detection of fraud in real time
- risk analysis
- construction of situation rooms
- operative analytical processing, etc.

To solve the problem of large amounts of data, a special version of NoSQL databases was developed (http://www.nosql-database.org). A comparison of the properties of relational databases and NoSQL is presented in the table below [1,2].

Table 1 – Comparison of relational base data and NoSQL

Relational databases	NoSQL databases
Complex data relationships	Very simple relationship
Scalability	Arbitrary scheme; unstructured data
Static memory	Distributed Processing
Universal properties and functions	The memory is scaled together with the computing resources
	The system is application and developer oriented

NoSQL database features

There are not many common characteristics for all NoSQL, since many different systems are hidden under the NoSQL label. Many characteristics are peculiar only to certain NoSQL databases, this we will certainly mention in the listing.

1. Do not use SQL

This refers to ANSI SQL DML, since many databases try to use query languages similar to the well-known favorite syntax, but it was not possible to fully implement it, and it is unlikely to succeed. Although there are rumors that startups are trying to implement SQL, for example, in Hadup.

2. Unstructured (schemaless)

The sense is that in NoSQL databases, unlike relational databases, the data structure is not regulated (or poorly typed if analogies are made with programming languages) – you can add an arbitrary field in a separate line or document without first declaring the structure of the entire table. Thus, if there is a need to change the data model, the only sufficient action is to reflect the change in the application code.

For example, when renaming a field in MongoDB:

```
BasicDBObject order = newBasicDBObject();
order.put("date", orderDate); // this field was a long time ago
order.put("totalSum", total); // we used to simply "sum"
```

If we change the logic of the application, then we expect the new field also when reading. But because there is no data schema, the totalSum field is missing from other existing Order objects. In this situation, there are two options for further action. The first is to bypass all documents and update this field in all existing documents. Due to the amount of data, this process occurs without any locks (comparable to the alter table rename column), so during an update, existing data can be read by other processes during the update. Therefore, the second option – checking in the application code – is inevitable:

```
BasicDBObject order = newBasicDBObject();
Double totalSum = order.getDouble("sum"); // This is an old model
if (totalSum == null)
totalSum = order.getDouble("totalSum"); // This is an updated model
```
[3].

And already with the re-recording we will write this field into the database in a new format. A pleasant consequence of the lack of a scheme is the effectiveness of working with sparse data. If there is a date_published field in one document, and not in the second one, then no date_published field for the second field will be created. This is, In principle, logical, but less obvious example – the column-family NoSQL database, which uses familiar concepts of tables columns. However, due to the absence of the schema, the columns are not declared declaratively and can be changed added during the user session of working with the database. This makes it possible in particular to use dynamic columns to implement lists [4]. The unstructured scheme has its drawbacks – in addition to the above overhead in the application code when changing the data model – the absence of all possible restrictions from the database (not null, unique, check constraint, etc.), plus additional difficulties in understanding and controlling the structure data in parallel work with the database of different projects (there are no dictionaries on the side of the database). However, in a rapidly changing modern world such flexibility is still an advantage. An example is Twitter, which five years ago, together with a tweet, stored only a little extra information (time, Twitter handle and a few more meta information bytes), but now in addition to the message itself, a few more kilobytes of metadata are stored in the database [5].

Representation of data in the form of aggregates

Unlike the relational model, which preserves the logical business entity of the application in various physical tables for normalization purposes, the NoSQL repositories operate with these entities as with integral objects.

In this example, the aggregates for the standard conceptual relational model of e-commerce "order-order items-payments-product" are demonstrated. In both cases, the order is combined with the positions into one logical object, each position holding a reference to the product and some of its attributes, for example, the name (such a denormalization is necessary so as not to request the product object when retrieving the order – the main rule of distributed systems is the minimum "Joins" between objects). In one aggregate, payments are combined with an order and are an integral part of the object, in another aggregate they are placed in a separate object. This demonstrates the main rule of designing data structures in NoSQL databases – it must comply with the application requirements and be optimized to the most frequent requests. If payments are regularly

withdrawn along with the order – it makes sense to include them in a common object, but if many requests work only with payments – then it is better to put them in a separate entity. Many will argue that working with large, often denormalized, objects is fraught with numerous problems when trying to access arbitrary data requests, when the requests do not fit into the structure of the aggregates [6].

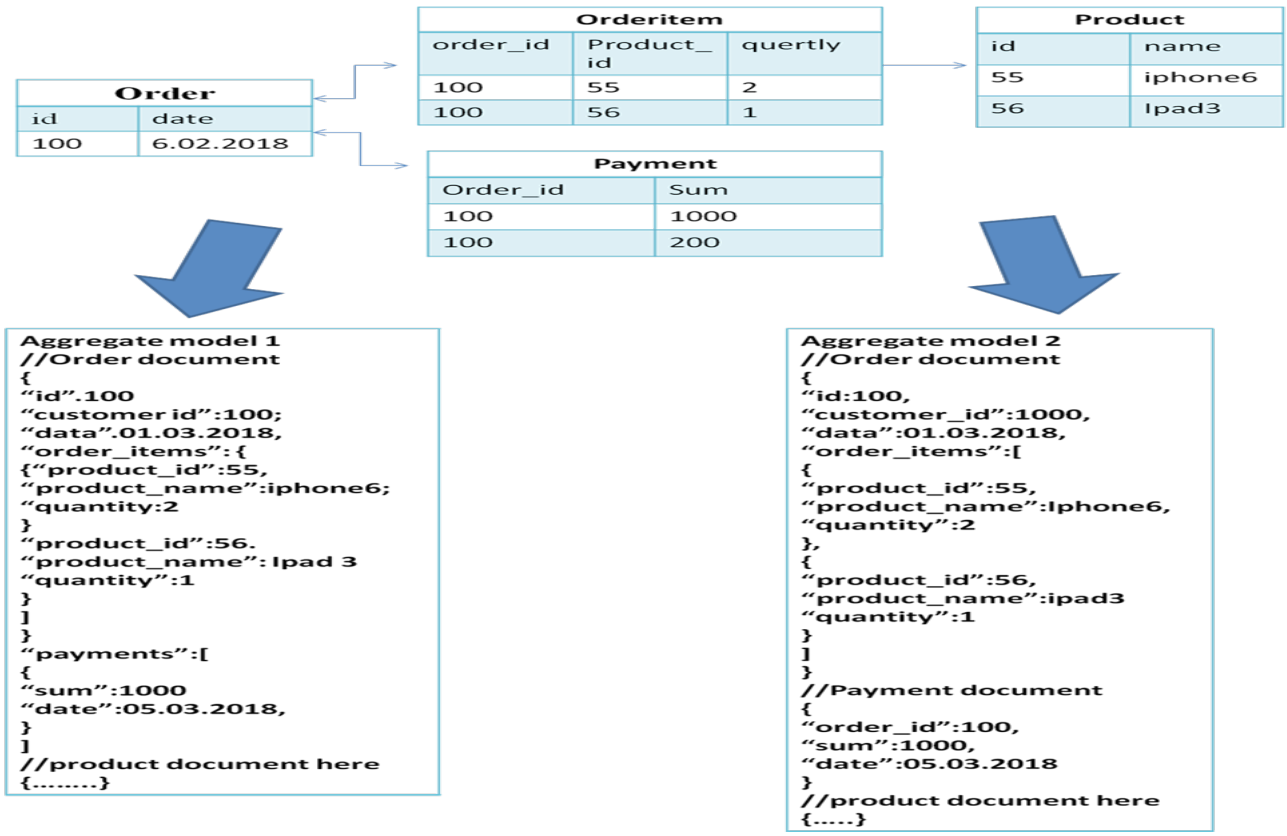

Distributed systems, without shared resources (share nothing)

Again, this does not apply to the database graph, whose structure by definition is poorly distributed over remote nodes. This, perhaps, is the main leitmotif of the development of NoSQL databases. With the avalanche-like growth of information in the world and the need to process it in a reasonable time, the problem of vertical scalability has risen – the speed of the processor has stopped at 3.5 GHz, the speed of reading from the disk is also growing at a slow pace, plus the price of a powerful server is always greater than the total price of several simple servers. In this situation, conventional relational databases, even clustered on an array of disks, can not solve the problem of speed, scalability, and bandwidth. The only way out of this situation is horizontal scaling, when several independent servers are connected by a fast network and each owns / processes only part of the data and / or only part of the read-update requests. In such an architecture, to increase the storage capacity (capacity, response time, bandwidth), you only need to add a new server to the cluster – that's all. The procedures of shading, replication, provision of fault tolerance (the result will be obtained even if one or more servers have ceased to respond), the NoSQL database itself handles the redistribution of data in case of adding a node. Briefly I will present the main properties of distributed NoSQL databases:

Replication – copy data to other nodes during the upgrade. Allows you both to achieve greater scalability, and increase the availability and security of data. It is accepted to subdivide into two types:

Master-slave:

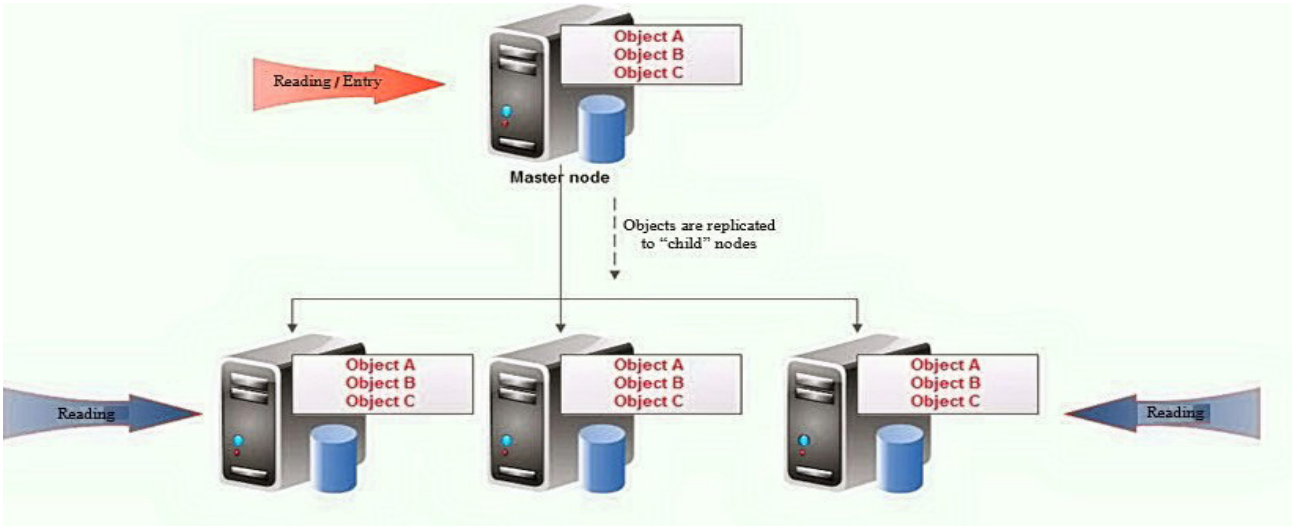

and peer-to-peer:

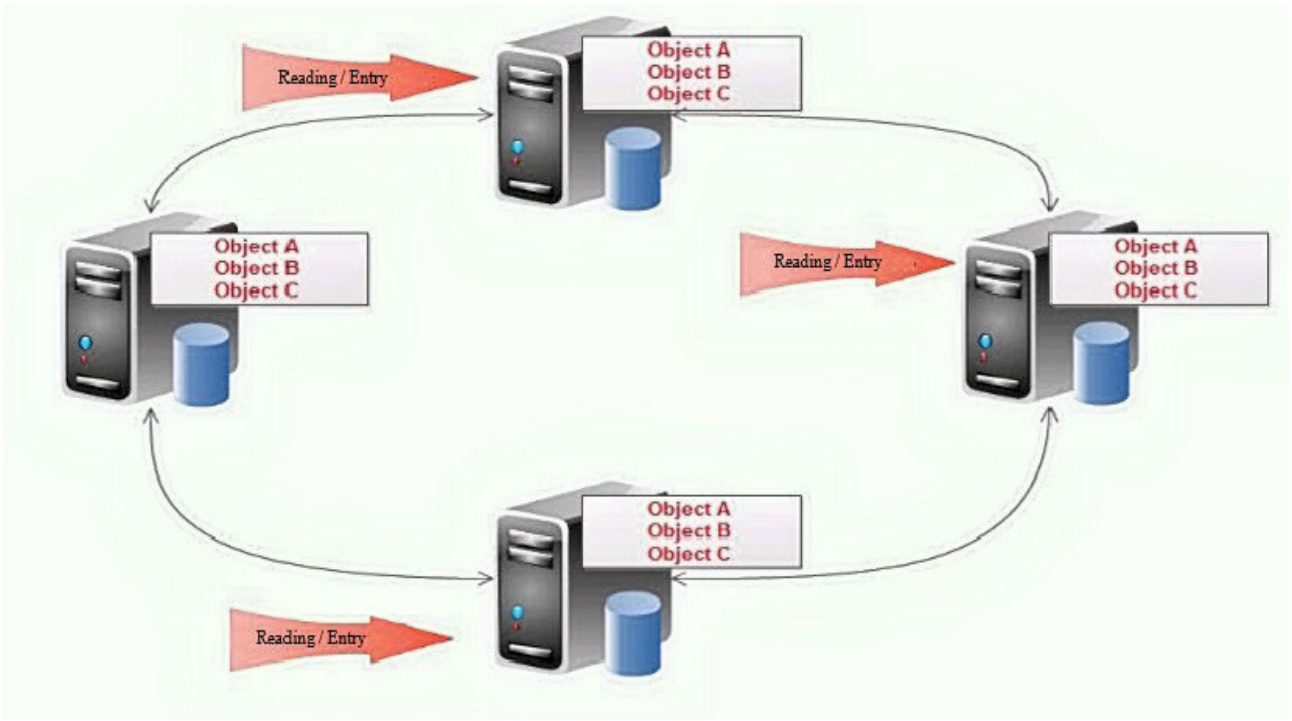

The first type assumes good read scalability (it can occur from any node), but an unscaled entry (only in the master node). Also there are subtleties with ensuring constant accessibility (in case of the master falling either manually or automatically in its place one of the remaining nodes is assigned). For the second type of replication, it is assumed that all nodes are equal and can serve both read and write requests.

Sharding – the division of data into nodes:

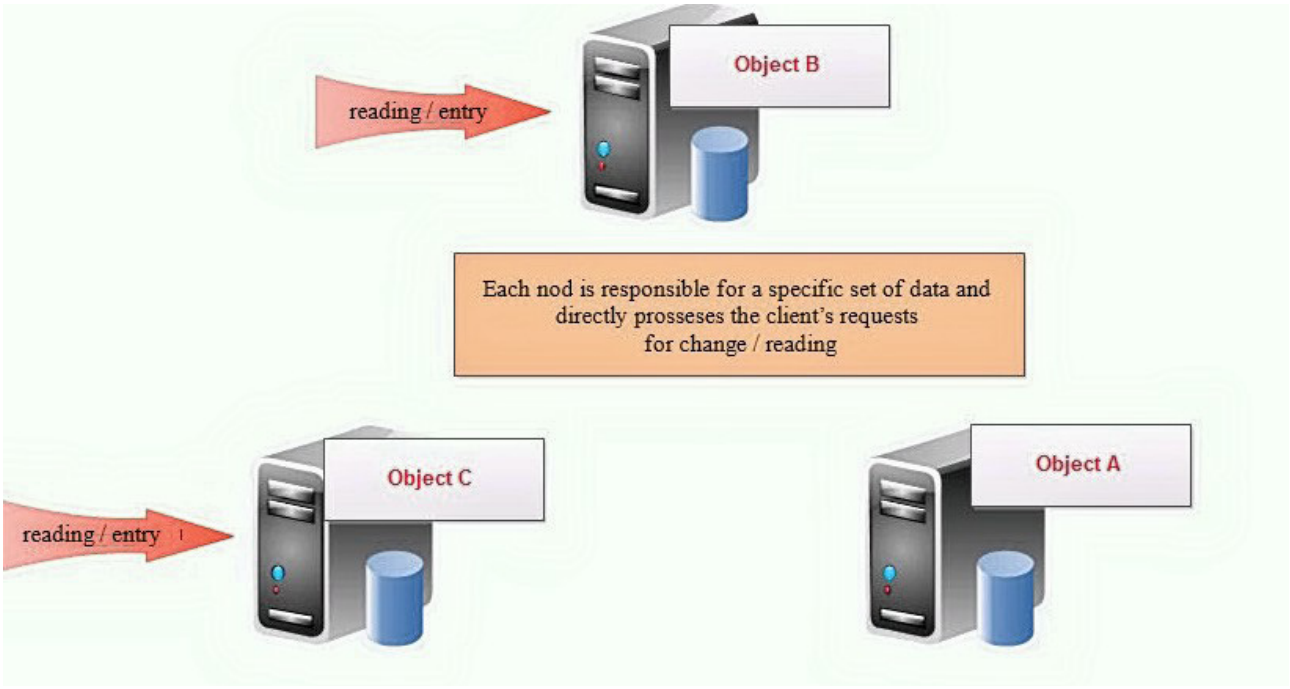

Sharding was often used as a "crutch" for relational databases in order to increase speed and throughput: a user application partitioned data into several independent databases and, when prompted by the user, accessed a specific database. In NoSQL databases, shading, like replication, is automatically produced by the database itself and the user application is separate from these complex mechanisms [7].

NoSQL databases technology

NoSQL databases technology (for example, Cassandra) is not intended to replace relational databases, but rather it helps to solve problems when the amount of data becomes too large. NoSQL often uses clusters of low-cost standard servers. This solution allows you to reduce the cost per gigabyte per second several times [8]. NoSQL databases continue to gain popularity. If five years ago they were not taken seriously , now the situation has radically changed. NoSQL databases become not just competitive, they are already leaders in projects requiring high performance. The state of the non-relational database technology has been investigated and several NoSQL databases have been categorized with respect to them: consistency, data models, replication and fulfillment of query capabilities. There are quite a few different models and functional systems for NoSQL databases [9]:

1. Warehouse key (usually store data in memory)

The key-value store works with key-value data, for example, as a dictionary. There is no place for structure or connections. After connecting to the server (for example, Redis), the application can set the key and its value, and subsequently receive these data on request. Such DBMSs are usually used to quickly store basic data, and sometimes not so basic, if you calculate the costs of the processor and memory. They are usually very fast, workable or easily scalable (it's good to use such databases for storing sessions, cache, counters, visits, etc.). As in the case of relational DBMSs, there are many open source products. Of the most popular we note memcached (and related memcachedb and membase), Voldemort, Redis and Riak .

2. Distributed storage (Column-oriented) – Cassandra, HBase, etc. (designed for very large amounts of data) . These databases work just fine by creating collections of one or more key-value pairs that in total correspond to one record. Unlike traditional tables in relational models, these databases do not require a preliminary description of the data structure. In general, distributed storage is nothing more than a two-dimensional array, where each key (record) contains one or more key-value pairs tied to it. Such a system allows you to store and use large amounts of unstructured data (one entry with a large amount of additional information). Such databases

are usually used when there are not enough simple key-value pairs, and you need to store a large amount of records with different information.

3. Document-oriented DBMS – MongoDB, Couchbase, etc. (designed to store hierarchical data structures – documents)

These databases allow much more nesting and complexity of the data structure. (for example, a document embedded in a document embedded in a document). Documents remove the nesting constraints of the first and second levels of the key-value type in distributed storages. In general, you can describe an arbitrarily complex data structure as a document and save it in such a database. Recently, in connection with the development of the Internet, search engines, social networks and highly loaded services are actively developing, which must handle large amounts of information and answer a huge number of requests. This requires not only a maximum consideration of the specifics of the information being processed, but also the transition to distributed computing. No server of any size is capable of providing the required performance [10].

Conclusion

The authors of this article in their work on the development of Web applications for processing large amounts of data take into account the above features of the functioning of databases. Including, there are three basic requirements for heavily loaded applications [11]:

• Lots of data: the largest of web applications handle data volumes of the order more than those intended for managing relational databases;

• Huge number of users: numbered in millions, access to systems simultaneously and constantly;

• Complex data: Typically, these applications are not simple processing of tabular data that can be found in many commercial and business applications.

The relational database technologies that have dominated the IT industry since 1980 began to show their weaknesses in the transition to web scales in these three aspects, so a growing number of people began to look for an alternative. Such an alternative became NoSQL database. In the advantages of using MongoDB, such as deep query capability, simple scalability, document-based storage, we made sure of the process of working on the web application “Electronic library for students, teachers and researchers” using MongoDB, NodeJS, PhpStorm [12]. The results of this research are used by the authors of this article to further simulate the processing of large amounts of data and develop a Web application.

References

1. From SQL to NoSQL and back [Electronic resource]. – Access mode: http://www.osp.ru/os/2012/02/13014127//, 2014. – P. 114-118.

2. Balakayeva G.T., Nurlybayeva K. Simulation of Large Data Processing for Smarter Decision Making. AWER Procedia Information Technology & Computer Science, 3rd World Conference on Information Technology (WCIT-2012). – 2013. – Vol. (03). – P.1253-1257

3. Redmont E., Uilson R. Seven Database in Seven Weeks: A Guid to Modern Databases and the NoSQL Movement. Publishing house “DMK Press”. – 2018. – P. 418-420. ISBN: 978-5-97028-455-2.

4. Pramod J., Sadalage, Martin Fowler. NoSQL Distilled. Publishing house “Moskva, Sankt-Peterburg-Kiev”. – 2013. – P. 135-140.

5. Gaurav Vaish .Getting Started with NoSQL. Packt books-Packt Publishing. – 2013. – P. 127-137. ISBN: 978-1849694988

6. Dan Sullivan. NoSQL for mere Mortals. Published by John Wiley&Sons, Inc.2014. – P. 321-324.

7. Adam Fowler. No SQL for Dummies. – 2015. – P. 231-237. ISBN-13: 978-1118905746

8. Guy Harisson. Next Generation Data bases. – 2016. – P. 245-247. ISBN-13: 978-1-48-42-1329-2.

9. Neal Leavitt. Will NoSQL Databases Live Up to Their Promise? Computer, 43:12–14, February 2010. – P. 128-132.

10. Gantz John, Reinsel David. The digital universe in 2020: Big Data, Bigger Digital Shadow s, and Biggest Grow th in the Far East. URL: http:// www.emc.com/collateral/analyst-reports/idc-the-digital-universe-in-2020.pdf (Date duration 10.07.2014)

11. Balakayeva G.T., Melisova A.E. Modeling large data with NoSQL. Nauka i Studia. – 2017. – Vol. 8(169). – P. 35-37.

12. Stefan Edlich. NoSQL Databases, Available at http://nosql-database. – 2011. – P.105-107.

IRSTI 50.03.05

* Z.M. Abdiakhmetova, B.K. Alimbayeva, P.T. Omarova

Faculty of Information Technology, al-Farabi Kazakh National University,
Almaty, Kazakhstan
*e-mail: zukhra.abdiakhmetova@gmail.com

Use of machine learning for early pre-clinical diagnostics of heart diseases

Abstract. The main cause of death in different countries are heart diseases. Therefore, the problem of early preclinical diagnosis of these diseases at the origin is acute. ECG analysis is widely used to diagnose many cardiac diseases. Since the majority of clinically useful information in the ECG is found in the intervals and amplitudes determined by its significant points (characteristic peaks and wave boundaries), the development of accurate and reliable methods for automatic ECG delineation is a matter of great importance, especially for the analysis of long records.

This article presents an intelligent system for the interpretation of electrocardiographic signals of cardiac valves based on the wavelet transform method. The model of the neural network of wavelet packets developed by us is used. The productivity of the developed system was estimated in 2000 samples. The test results showed that this system was effective when using wavelet transform methods. The correct rate of classification was about 91 percent for abnormal and normal subjects.

The aim of the study is to develop a neural network based on the wavelet transform method for early preclinical diagnosis of diseases, and paroxysmal atrial fibrillation of the heart.

At present, the problem of processing fuzzy data, short high-frequency low-amplitude signals is difficult to solve. Since, for example, if the ECG is visually monitored, the probability of obtaining a human error is high, every 10-result is interpreted with an error. In this connection, it became necessary to search for new methods for predicting signal propagation in various directions of science.

The problems of extracting information from the electrophysiological signal that can not be obtained by visual analysis of the record, as well as the problems of automation of traditional algorithms of medical analysis are relevant in connection with the lack of research in this field [1].

Key words: machine learning, neural networks, electrocardiogram, wavelet transformation.

Introduction

An artificial neural network is a mathematical model, as well as its software or hardware implementation, built on the principle of the organization and functioning of biological neural networks – nerve cell networks of a living organism. This concept arose when studying the processes occurring in the brain, and when trying to simulate these processes. The first such attempt was the neural networks of W. McCulloch and W. Pitts. After the development of learning algorithms, the resulting models began to be used for practical purposes: in forecasting problems, for pattern recognition, in control tasks, etc. An artificial neural network is a system of connected and interacting simple processors (artificial neurons). Such processors are usually quite simple (especially in comparison with processors used in personal computers). Each processor of such a network only deals with the signals it periodically receives, and the signals it periodically sends to other processors. And, nevertheless, being connected to a suficiently large network with controlled interaction, such separately simple processors together are able to perform rather complex tasks [2].

• From the point of view of machine learning, a neural network is a special case of methods for pattern recognition, discriminant analysis, clustering methods and so on.

• From the mathematical point of view, the training of neural networks is a multi parameter problem of nonlinear optimization.

 Printed in Kazakhstan

• From the point of view of cybernetics, the neural network is used in problems of adaptive control and as algorithms for robotics.

• From the point of view of the development of computer technology and programming, a neural network is a way of solving the problem of efiective parallelism.

And from the point of view of artificial intelligence, the artificial neural network is the basis of the philosophical trend of connectivism and the main direction in the structural approach to study the possibility of constructing (modeling) natural intelligence using computer algorithms. Neural networks are not programmed in the usual sense of the word, they are trained. The possibility of learning is one of the main advantages of neural networks over traditional algorithms. Technically, training is to find the coeficients of connections between neurons. In the process of learning, the neural network is able to detect complex dependencies between input data and output, and also perform generalization. This means that in case of successful learning the network will be able to return the correct result based on data that was not available in the training sample, as well as incomplete and / or "noisy partially distorted data [3].

Materials and methods

Most of the signals encountered in practice are represented in the time domain. And for most signal processing applications this view is not the best. In many cases, significant information is hidden in the frequency domain of the signal. To get the frequency representation, use the Fourier transform. The conversion formula is presented below [4-9]:

$$\widehat{f(\omega)} = \frac{1}{\sqrt{2\,\pi}} \int f(x) e^{-ixt} dx \qquad (1)$$

$i = \sqrt{-1}$

x – time

ω– frequency

f (x)– initial signal

$\widehat{f(x)}$– transformed signal

The method of wavelet transformation, in which the original discrete signal is decomposed into approximating and detailing values on different scales [10-14]. The wavelet transform method is based on the Fourier transform, but unlike it, thanks to this method, we were able to view the time-frequency representation of the signal.

The signal must be decomposed into sums of the product in the following form:

$$W(u,\alpha) = \frac{1}{\sqrt{\alpha}} \int f(t) \varphi \left(\frac{t-u}{\alpha}\right)^{*} dt \qquad (2)$$

$$\varphi(t) = \frac{1}{\sqrt{2\pi}\sigma} e^{-j\omega t} e^{-t/2\sigma^2} \qquad (3)$$

where φ(t) – mother Morlet wavelet,

W(u, α) – Wavelet transform,

α – scale coefficient,

u – shift coefficient,

f(t) – signal.

For example, if we consider the decomposition of the level 6 signal, medium values are discarded at each level and the detail values are remembered, at the very last level we have an average of level 6 and all the details of the previous levels [15].

For the experience, we studied the results of ECG images of 2000 patients from January 2017 to December 2017. P wave extension is associated with relapses of atrial fibrillation. Other studies have emphasized the importance of studying the morphology of P-waves, in predicting the recurrence of atrial fibrillation. Of these, 500 patients had the first episode, and 500 had a relapse episode of atrial fibrillation. Patients were observed for 12 months and classified into three groups, depending on the number of relapses of atrial fibrillation per year according Figure 1:

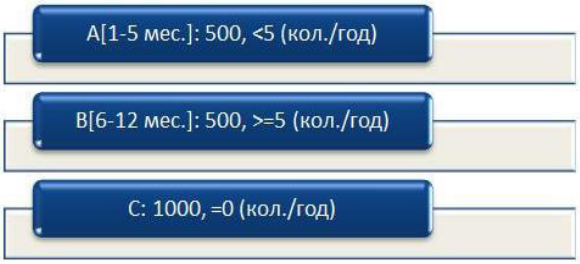

Figure 1 – Study groups

As a result of training, the neural network showed the following results – the network learned to recognize the disease, but in the early stages of its emergence to identify some signs was not able to. The application of the wavelet transform method distributed the group with early signs of the disease to the group of patients as in Figure 2:

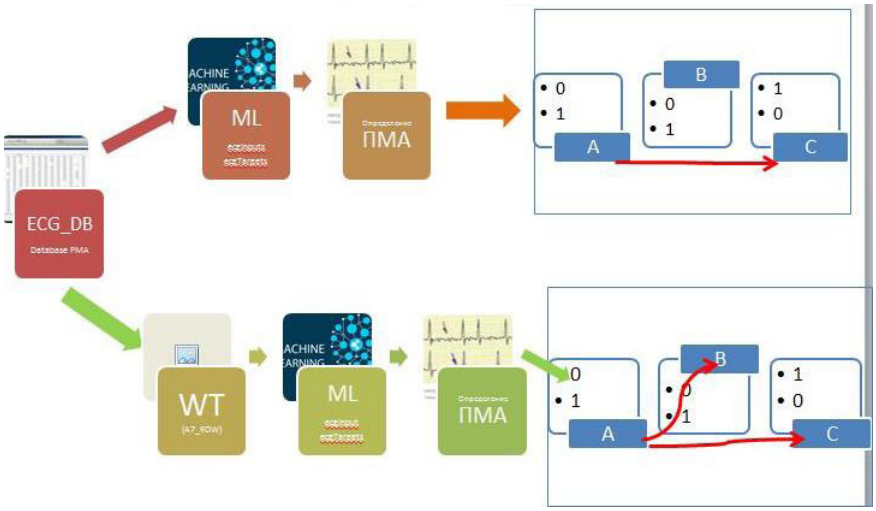

Figure 2 – Model of data processing

The neural network was trained based on 70 percent of the data from this database, 15 percent for validation, and the remaining 15 percent for network testing and the result of training on Figure 3:

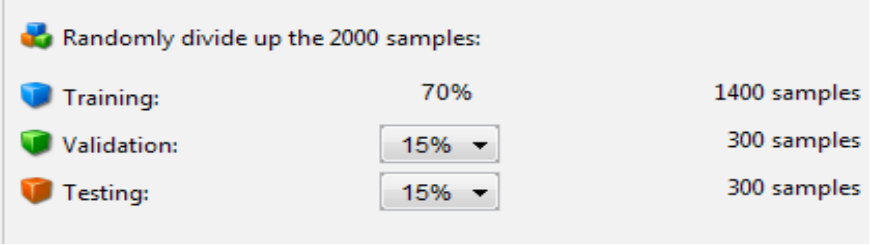

Figure 3 – Learning process

Main results

The accuracy of the algorithm is defined by the classical concept of confusion matrix [16-18] on Figure 4:

Figure 4 – Accuracy of the algorithm

TP – the experiment considers that the proof refers to class 0, and the algorithm also FP – experiment 1, algorithm 0. FN-experiment 0, algorithm 1. On the basis of this matrix, the precision was taken by 2000 data of ECG on the contiguity schedule, the accuracy was 0.85

Conclusion

An algorithm for digital data processing based on the wavelet transform method is developed;

Software modules have been developed for applying wavelet analysis to electrocardiogram (ECG) data;

A software module was developed and implemented to solve the main problems based on the built and trained neural network.

References

1. Chazov M. Guide to Cardiology in four volumes. Practice – 2014.

2. Dobesi I. Ten lectures on wavelets. Izhevsk. – 2001. – P.464.

3. www.wikipedia.org/wiki

4. Gautam Apoorv, Maninder Kaur ECG Analysis using Continuous Wavelet Transform (CWT). // IOSR Journal of Engineering. – 2012. – Vol. 2(4). – P. 632-635.

5. Grigoriev D.S., Spitsyn V.G. The application of a neural network and discrete wavelet transform for the analysis and classification of electrocardiograms // Proceedings of Tomsk Polytechnic University. – 2012. – Vol.321. – P. 57-61.

6. Hafizah H.,Lai L., Fatt Eficient ECG Signal Classification Using Sparsely Connected Radial basis Function Neural Network // 6th WSEAS International Conference on Circuits systems, Electorics,control and signal processing, Cairo, Egypt. – 2007. – P. 412-416.

7. Ivanko E.O., Ivanushkina N.G.,Synecop Yu.S. Multi-level analysis of electrocardiograms for the detection of late atrial potentials //Electronics and communications. – 2009. – Vol. 2. – P. 160-164.

8. Kamel Hussein Rahoum, Rabab Hamed Muhammad, Hesham Fathi Ali Hamed, Mona Abdel Baset Abo-Eldahaâ Heart.

9. Diseases Detection Based on Analysis and Diagnosis of Electrocardiogram Using Wavelet Transform and Prediction of Future Complications // Clinical Medicine Journal. – Vol. 3. – No. 3. – 2017. – P. 15-29.

10.Krug P.G. Neironnye seti i komputery // Moscow. fi MEI. – 2002. – P.176.

11.Monakhova O.A Chislennyy metod obrabotki elektrokardiosignalov na osnove veyvletnykh preobrazovaniy: dissertatsiya kandidata fiziko-matematicheskikh nauk: 05.13.18 – Saratov. – 2009. – P. 152.

12.Open MIT ECG Database 2012. – http:// www.physionet. org/cgi-bin/atm/ATM (date of the application 14.11.2017).

13.Rob MacLeod, Brian Birchler ECG Measurement and Analysis //Electronics and communications. – 2014.

14.Richard S. Sutton, Andrew G. Barto Reinforcement Learning: An Introduction The MIT Press Cambridge, Ìassachusetts London, England 2015.

15.Sasikala P., R.S.D. WahidaBanu Extraction of P wave and T wave in Electrocardiogram using Wavelet Transform // International Journal of Computer Science and Information Technologies. – 2011. – Vol. 2(1). – P. 489-493.

16.Silipo R., Marchesi C. Artificial neural networks for automatic ECG analysis //IEEE Transactions on signal processing. – 1995. – Vol. 46, Issue 5. – P.1417-1425.

17.K.Venkata Lakshmi Narayana Wavelet based QRS detection in ECG using MATLAB //Innovative Systems Design and Engineering. – 2011. – Vol.2. – P. 60-69.

18.Zaentsev I.V. Neironnye seti: osnovnye modeli // Voronezh. VGU, 1999.

IRSTI 28.17.23; 29.15.35

[1]F.F. Komarov, [2]A.I. Kupchishin, [3*]A.A. Kuatbayeva, [4]T.A. Shmygaleva,
[4]D.A. Katabas, [4]A. Yu. Ryabinin

[1]Belarusian State University, Minsk, Belarus
[2]Kazakh National Pedagogical University named after Abai, Almaty, Kazakhstan
[3]Sh.Ualikhanov Kokshetau State University,
[4]al-Farabi Kazakh National University, Almaty, Kazakhstan
[*]e-mail: ahamala2017@gmail.com

Mathematical modelling of radiation defect formation processes in the materials irradiated with protons and alpha particles

Abstract. Metals and alloys still remain constructional, instrumental and other materials basis. An important factor in their properties formation are the crystalline grid nano-defects arising, in particular, in case of radiation. By the ionic bombing receiving high-quality, dense metal films and coverings on substrates could be realized. Such materials search and development rely on clear understanding nano-defects radiation creation mechanisms. In the work process of interaction protons and alpha particles with substance and radiation defects formations is considered. For calculation the cascade and probabilistic functions, the primary beaten-out atoms (PBOA) ranges, radiation defects concentration needs to execute approximating expression selection and to find approximation coefficients for interaction section. Interaction section for protons and alpha particles is calculated by Rutherford's formula. Analytical expression on cascade and probabilistic function taking into account energy losses for protons and alpha particles from recurrence relations for transition probabilities is received. The cascade and probabilistic function calculation algorithm, primary beaten-out atoms range, radiation defects concentration is given.
Key words: Proton, alpha particle; approximation, cascade and probabilistic function, interaction section, a range of primary beaten-out atoms, concentration; radiation defects.

Introduction

When passing particles through substance quite difficult and diverse phenomena which have important theoretical and practical value for nuclear physics, solid body physics, other science and technology fields are observed. First of all, it belongs to physics of space beams [1-3], radiation physics of a solid body [4-7], and especially recently to radiation manufacturing techniques on materials with the set physical and chemical properties [8, 9].

For understanding and the description the specified phenomena, on the one hand, it is necessary to know what happens to particles (both primary, and secondary, generated in different impacts). One of the main objectives in this case is an establishment of spatial and power and temporary distributions on the falling and secondary particles in the environment. On the other hand, at the moment and also after particles passing through substance practically all properties on the substance change.

At the description these processes there is the choice problem on the research theoretical method. The most known and widely applied theoretical calculation methods is the Monte Carlo [10] method, the Boltzmann kinetic equations [11], Fokker-Planck's equation and various specialized methods and model [12].

Without belittling widely known numerical methods and models, apparently, one may say, at all that an undoubted advantage in comparison with them analytical methods possess even if with their help it is possible to describe any phenomenon only approximately. The analytical calculation method offered by us called cascade and probabilistic (CP) [13, 14] is developed by us in the course of long work in the field of elementary particles physics, physics of space beams, radiation physics of metals

and positron physics and also on the basis on the analysis and these researches generalization. Its correctness is checked on a large number on specific objectives from nuclear physics various fields and physics of a solid body [13-15]. The essence of this method consists in receiving and further usage the cascade and probabilistic functions. The received models allow to track all process in dynamics and further could be used in the industry for receiving materials with beforehand the set properties. Therefore researches in this direction are relevant.

Main results

For protons and alpha particles the approximating function dependence on penetration depth, is presented in the following form [13]:

$$\sigma(h) = \sigma_0\left(1 + \frac{1}{a(E_0 - kh)}\right), \qquad (1)$$

where σ_0, a, E_0, k – the approximation parameters calculated when comparing (1) with calculations of sections for Rutherford's formula.

From Kolmogorov-Chapman's equations we will receive recurrence relations for probabilities of transition:

$$\psi_n(h', h, E_0) = \int_{h'}^{h} \psi_{n-1}(h', h'', E_0)\frac{1}{\lambda_0}\left(1 + \frac{1}{a(E_0 - kh'')}\right)\psi_0(h'', h, E_0)dh''. \qquad (2)$$

From a ratio (2) we will receive CPF expression for protons and alpha particles in the following look:

$$\psi_n(h', h, E_0) = \frac{1}{n!\lambda_0^n}\left(\frac{E_0 - kh'}{E_0 - kh}\right)^{-l} \times$$
$$\times \exp\left(-\frac{h - h'}{\lambda_0}\right)\left(h - h' + \frac{\ln\left(\frac{E_0 - kh'}{E_0 - kh}\right)}{ak}\right)^n, \qquad (3)$$

where h',h – particle depths on generation and registration respectively, n – number of interactions, E_0 – initial energy of primary particle, σ_0, a, E_0, k – approximation coefficients, $\lambda_0 = 1/\sigma_0$, $l = 1/\lambda_0 ak$.

For CPF calculation for protons it is necessary to calculate interaction section by Rutherford's formula [16]. The sections transformed values calculated on this formula for protons and alpha particles depending on h have an appearance on the increasing curve. For great values of E_1 of section slowly increase, with reduction of E_1 - it is very sharp. Results of selection of approximations are presented in the figure 1. Approximating parameters for alpha particles in molybdenum at various values of initial energy are specified in table 1.

We receive depths of observations for protons, using tables of run and brake abilities for easy ions [17]. The values of sections found on Rutherford's formula are approximated by expression (1). Coefficients σ_0, a, E_0, k are by the smallest squares method, and E_0 here isn't initial energy of primary particle, and there is an approximation coefficient. The theoretical correlation relations fluctuate in an interval 0,97 ÷ 0,9999.

Table 1 – Approximating parameters for alpha particles in molybdenum

E_0	σ_0	α	E_0	k	η
50	13801.11158	89.00812	0.05837	1.60874	0.99786
40	14208.86517	21.31636	0.17366	6.93237	0.99837
29	16103.96377	0.00684	375.16828	25333.17	0.99876
20	19288.56287	0.10035	17.66345	2158.797	0.99931

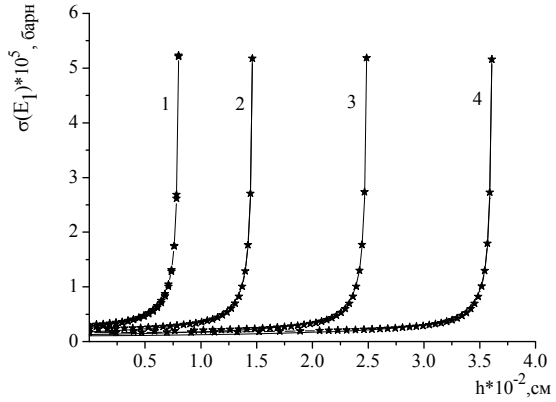

Figure 1 – Dependence σ(h) for alpha particles in wolfram (tungsten) at E_0: 1-20; 2-30;3-40;4-50 (MeV) (1-4)

Using expression (3) for CPF, calculations were made on a formula:

$$\psi_n(h',h,E_0) = \exp\left(-n\lambda_0 - \ln n! - \frac{1}{\lambda_0 ak}\ln\left(\frac{E_0-kh'}{E_0-kh}\right) - \frac{h-h'}{\lambda_0} + n\ln\left(h-h'+\frac{1}{ak}\ln\left(\frac{E_0-kh'}{E_0-kh}\right)\right)\right). \quad (4)$$

CPF calculations results depending on interactions number are presented in the figure 2, from penetration depth in the figure 3. Calculations results shows that CPF for protons behave as follows: at values n=0,1 CPF depending on h decrease, with increase in n CPF increase, reaching a maximum and begin to decrease; at the others n increase. With increase of E_0 the number of the decreasing curves increases, the curves number with a maximum also grows, and the increasing curves number decreases [15, 18]. At small E_0 curves with increase in h already have a maximum, at small h curves have no maximum, at h, approaching to h_{max}, curves increase. At great values of E_0 curves have a maximum already at small h which is displaced with increase in n and h to the right and then disappears. For alpha particles the CPF behavior is similar to CPF behavior for protons except that at the same E_0 values the number of the decreasing curves and curves with maximum increases, but the number on the increasing curves decreases. CPF depending on interactions number for protons and alpha particles behave as follows: at small values of depths CPF decrease, with increase in CPF penetration depth the CPF increase, reaching a maximum, then decrease. With increase E_0 the number of the decreasing curves increases [20-22].

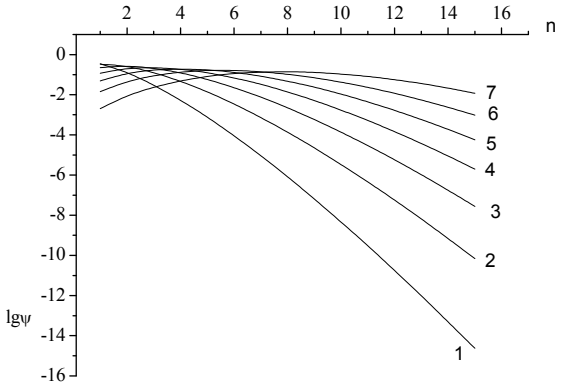

Figure 2 – Dependence $\psi_n(h',h,E_0)$ for protons in copper at E0=5 MeV from number of interactions for h =0,001; 0,002; 0,003; 0,004; 0,005; 0,006; 0,007 cm (1-7)

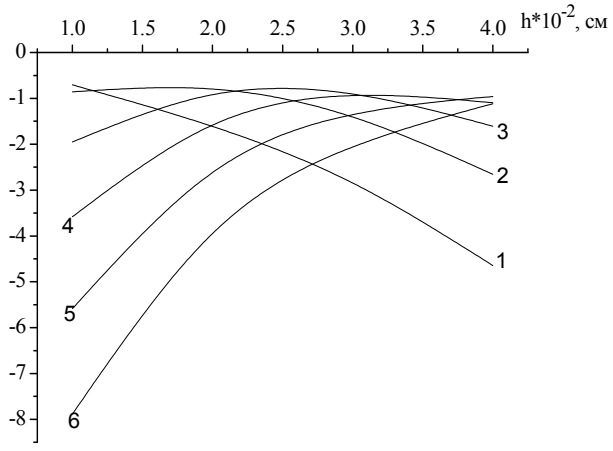

Figure 3 – Dependence $\psi_n(h',h,E_0)$ for protons in copper at E_0=15 MeV from penetration depth for n=1, 4, 7, 10, 13, 16 (1-6)

In the solid bodies irradiated with protons and alpha particles it is necessary for calculation radiation defects concentration in PBOA range $W(E_0,E_2,h)$ to integrate on E_2 to E_c up to E_{2max} [14, 15]. Then:

$$C_k(E_0,h)=\int_{E_c}^{E_{2\max}} W(E_0,E_2,h)dE_2\,, \qquad (5)$$

$$E_{2\max}=\frac{4m_1c^2m_2c^2}{(m_1c^2+m_2c^2)^2}E_1\,,$$

E_2 – energy of primary beaten-out atom, E_c – threshold energy, E_{2max} – the maximum energy transferred to atom, m_1c^2 – energy of rest of a proton or alpha particle, m_2c^2 – energy of rest of a target, E_1 – energy of a particle after losses.

PBOA range $W(E_0,E_2,h)$ is defined by a formula:

$$W(E_0,E_2,h)=$$
$$=\sum_{n=0}^{n_1}\int_{h-k\lambda_2}^{h}\psi_n(h')\exp\left(-\frac{h-h'}{\lambda_2}\right)\frac{\omega(E_1,E_2,h')}{\lambda_1(h')}\frac{dh'}{\lambda_2}\,, \quad (6)$$

where n_1 – maximum number of elastic collisions, $\psi_n(h')$ – cascade and probabilistic function taking into account losses of energy for protons and alpha particles later for n-number interactions at generation depth h'.

$$\lambda_1(h')=\frac{1}{\sigma_0 n\left(1+\frac{1}{a(E_0-kh')}\right)}*10^{24}\,(\text{cm}). \quad (7)$$

For λ_2 calculations on σ_2 on Rutherford's formula at z_1=1 for protons, z_1=2 for alpha particles, z_2=z (z – atomic number of the considered element). A PBOA range in the elementary act $\omega(E_1,E_2,h')$ at h' depth is defined as the relation of differential Rutherford section $\frac{d\sigma(E_1,E_2,h)}{dE_2}$ to integrated [14,15]. Calculations results are presented in the Figure 4.

From results of calculations it is visible that concentration distributions curves defects on depth increase, reaching a maximum, then decrease to zero. With increase in initial energy on a particle curves are displaced to the right and defects concentration values decrease. With increase in threshold energy on the E_c concentration value decrease, and curves pass much below, transition through a maximum is carried out more smoothly.

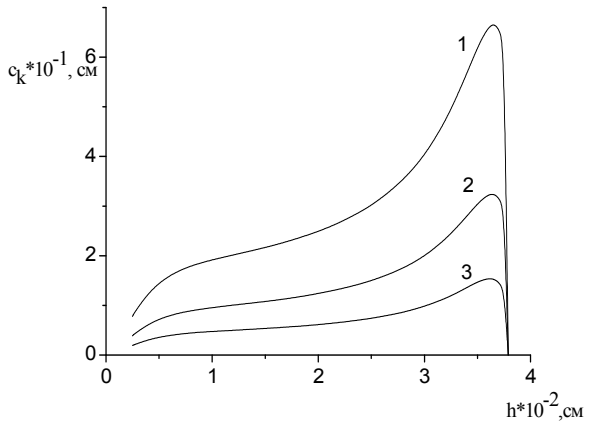

Figure 4 – Dependence of radiation defects concentration on depth at radiation by aluminum alpha particles at E_0=30 MeV E_c=50 KeV(1), E_c=100 KeV(2), E_c=200 KeV(3)

Conclusion

Thus, mathematical models of cascade and probabilistic functions taking into account energy losses for protons and alpha particles are received. With usage the received models, the calculation models of primary beaten-out atoms ranges and radiation defects concentration are received. The CPF calculation algorithm depending on interactions number and particles penetration depth is presented. Approximating expression selection is made for protons and alpha particles, approximation coefficients for various targets are found. CPF Calculations depending on interactions number and particles penetration depth , concentration of radiation defects in the materials irradiated with protons and alpha particles are made. Results of the received researches can be used by experts in the area to radiation physics of a solid body, space physics.

References

1. Yanossi L. Space beams. – M.: Foreign literature, 1949. – P. 463.

2. Rossi B., Greisen K. Interaction of space beams with substance. – M.: Foreign literature, 1948. – P. 132.

3. Dobrotin N.A. Space beams. – M.: Gostekhizdat, 1954. – P. 320.

4. Dins J., Vinyard J. Radiation effects in solid bodies. – M.: Foreign literature, 1960. – P. 243.

5. Damask A., Dins J. Dot defects in metals. – M.: World, 1966. – P. 291.

6. Czarnacka, K., Komarov, F.F., Romanov, I.A., Zukowski, P., Parkhomenko, I.N. AC measurements and dielectric properties of nitrogen-rich silicon nitride thin films. // Proceedings of the 2017 IEEE 7th International Conference on Nanomaterials: Applications and Properties, NAP 2017. – No. 5. – P. 657-669.

7. Komarov, F.F., Milchanin, O.V., Parfimovich, I.D., Tkachev, A.G., Bychanok, D.S. Absorption and Reflectance Spectra of Microwave Radiation by an Epoxy Resin Composite with Multi-Walled Carbon Nanotubes. //Journal of Applied Spectroscopy. – 2017. – Vol. 84. – No. 4. – P. 570-577.

8. Komarov F.F. Nano- and microstructuring of solids by swift heavy ions//Physics-Uspekhi. -2017. – Vol. 187. – No. 5. –P. 465-504.

9. Komarov, F.F., Romanov, I.A., Vlasukova, L.A., Mudryi, A.V., Wendler, E. Optical and Structural Properties of Silicon with Ion-Beam Synthesized InSb Nanocrystals.// Spectroscopy.-2017. – Vol. 120. – No. 1. –P. 204-207.

10. Komarov, F.F., Konstantinov, S.V., Strel'nitskij, V.E., Pilko, V.V. Effect of Helium ion irradiation on the structure, the phase stability, and the microhardness of TiN, TiAlN, and TiAlYN nanostructured coatings. //Technical Physics. – 2016. – Vol. 61. – No. 5. – P. 696-702.

11. Al'zhanova, A., Dauletbekova, A., Komarov, F., Akilbekov, A., Zdorovets, M. Peculiarities of latent track etching in SiO2/Si structures irradiated with Ar, Kr and Xe ions.-2016. – Vol. 374. – No. 1. –P. 121-124.// Nuclear Instruments and Methods in Physics Research, Section B: Beam Interactions with Materials and Atoms.-2016. – Vol. 426. – No. 1. – P. 1-56.

12. Komarov, F.F., Zayats, G.M., Komarov, A.F.,Michailov, V.V., Komsta, H.Simulation of radiation effects in SiO2/Si Structures.// Acta Physica Polonica A. –2015. – Vol. 3. – No. 1. – P. 854-860.

13. Komarov, F., Uglov, V., Vlasukova, L., Zlotski, S., Yuvchenko, V.Drastic structure changes in pre-damaged GaAs crystals irradiated with swift heavy ions.// Nuclear Instruments and Methods in Physics Research, Section B: Beam Interactions with Materials and Atoms. – 2015. – Vol. 360. – No. 4. – P. 150-155.

14. E.G. Boos, A.A. Kupchishin, A.I. Kupchishin, E.V. Shmygalev, T.A. Shmygaleva. Cascade and probabilistic method, solution of radiation and physical tasks, Boltzmann's equations. Communication with Markov's chains. -Monograph. Almaty: KazNPU after Abay, Scientific Research Institute for New Chemical Technologies and Materials under al-Farabi KazNU, 2015. – P. 388.

15. Kodanova, S.K., Ramazanov, T.S., Issanova, M.K., Golyatina, R.I., Maiorov, S.A Calculation of ion stopping in dense plasma by the Monte-Carlo method.// Journal of Physics: Conference Series. – 2018. – Vol. 946. – No. 1. – P. 148-154.

16. Smyrnova, K.V., Pogrebnjak, A.D., Beresnev, V.M., Kravchenko, Y.O., Bondar, O.V. Microstructure and Physical–Mechanical Properties of (TiAlSiY)N Nanostructured Coatings Under Different Energy Conditions.// Metals and Materials International. – 2018. – Vol. 24. – No. 2. – P. 241-439.

17. Kozhamkulov, B.A., Kupchishin, A.I., Bitibaeva, Z.M., Tamuzs, V.P. Radiation-Induced Defect Formation in Composite Materials and Their Destruction Under Electron Irradiation // Mechanics of Composite Materials. – 2017. – Vol. 53. – No. 1. – P. 59-64.

18. Kupchishin, A.I. On positrons irradiation in the defects of vacancy type.// IOP Conference Series: Materials Science and Engineering. – 2017. – Vol. 184. – No. 1. – P. 234-248.

19. Kupchishin, A.I., Niyazov, M.N., Voronova, N.A., Kirdiashkin, V.I., Abdukhairova, A.T.The effect of temperature, static load and electron beam irradiation on the deformation of linear polymers.// IOP Conference Series: Materials Science and Engineering. – 2017. – Vol. 168. – No. 1. – P. 229-274.

20. Kupchishin, A.I., Kupchishin, A.A., Voronova, N.A. Cascade-probabilistic methods and solution of Boltzman type of equations for particle flow// IOP Conference Series: Materials Science and Engineering. -2016. – Vol. 110. – No. 1. – P. 123-129.

21. Kupchishin, A.I., Kupchishin, A.A., Voronova, N.A., Kirdyashkin, V.I.Positron sensing of distribution of defects in depth materials. // IOP Conference Series: Materials Science and Engineering. – 2016. – Vol. 110. – No. 4. – P. 248-258.

IRSTI 27.31.44

[1*]A. Altybay, [2]M. Ruzhansky, [1]N. Tokmagambetov

[1]Al-Farabi Kazakh National University, department of Mechanics and Mathematics, Almaty, Kazakhstan
[2]Imperial College London, London, United Kingdom
[*]e-mail: arshyn.altybay@gmail.com

On numerical simulations of the 1d wave equation with a distributional coefficient and source term

Abstract. In this note, we illustrate numerical experiments for the one-dimensional wave equation with δ-like (delta like) terms. Our research is connecting the theory with the numerical realisations. By using results on very weak solutions introduced by Michael Ruzhansky with his co-authors, we investigate a corresponding regularized problem. In contrast to our expectations, the experiments show that the solution of the regularized problem has a "good" behaviour. Indeed, numerical experiments show that approximation methods work well in situations where a rigorous mathematical formulation of the problem is difficult in the framework of the classical theory of distributions. The concept of very weak solutions eliminates this difficulty, giving results of correctness for equations with singular coefficients. In the framework of this approach (very weak solutions), the expected physical properties of the equation can be reconstructed, for example, the distribution profile and the decay of the solutions for large times. Finally, we give a number of illustrations.
Key words: wave equation, numerical experiment, very weak solutions, distributional coefficient, singular source term, regularized problem, decay of solutions.

Introduction

In this paper, we follow the results of the paper [4] and study the Cauchy-Dirichlet problem for the 1D-Wave Equation

$$\begin{cases} \partial_{tt}^2 u(t,x) - a(t)\partial_{xx}^2 u(t,x) = f(t,x),\ (t,x) \in [0,T] \times [0,1], \\ u(t,0) = 0, t \in [0,T], \\ u(t,1) = 0, t \in [0,T], \\ u(0,x) = u_0(x), x \in [0,1], \\ \partial_t u(0,x) = u_1(x), x \in [0,1]. \end{cases} \tag{1}$$

The notion of very weak solutions has been introduced in [GR15] to analyse second order hyperbolic equations. In [3] and [5] Ruzhansky and Tokmagambetov applied it to show the well-posedness of the Landau Hamiltonian wave equations in distributional electro-magnetic fields. Also, in [2] were investigated very weak solutions for an acoustic problem of wave propagation through a discontinuous medium.

In this paper, we allow the coefficient $a(t)$ and the source term $f(t,x)$ to be distributional in t. One of the interesting cases is when $a(t) = 1 + \delta(t - t_0)$ and $f(t,x) = \delta(t - t_1)$ for some, in general, different t_0 and t_1. For more motivation, we refer to [6] – [11].

Numerical experiments

We start by regularizing $a(t)$ and $f(t,x)$ by the parameter ε, that is,

$$a_\varepsilon(t) = (a * \varphi_\varepsilon)(t),\ f(t) = (f * \varphi_\varepsilon)(t),$$

by the convolution with the mollifier $\varphi_\varepsilon(t) = {}^1\!/_\varepsilon\, \varphi({}^t\!/_\varepsilon)$, where

$$\varphi(t) = \begin{cases} \frac{1}{C} e^{\frac{1}{(t^2-1)}}, |t| \le 1, \\ 0, \quad |t| > 1. \end{cases}$$

Here C = 0.443994 so that $\int_{-1}^{1} \varphi(t)dt = 1$. Instead of (1) consider a regularized problem

$$(2) \quad \begin{cases} \partial_{tt}^2 u_\varepsilon(t,x) - a_\varepsilon(t)\partial_{xx}^2 u_\varepsilon(t,x) = f_\varepsilon(t,x),\ (t,x) \in [0,T] \times [0,1], \\ u_\varepsilon(t,0) = 0, t \in [0,T], \\ u_\varepsilon(t,1) = 0, t \in [0,T], \\ u_\varepsilon(0,x) = u_0(x), x \in [0,1], \\ \partial_t u_\varepsilon(0,x) = u_1(x), x \in [0,1]. \end{cases}$$

From [4] it follows that the problem (1) has a unique very weak solution. It is given by a family of functions $\{u_\varepsilon(t,x)\}_{0<\varepsilon\le 1}$. For each positive $\varepsilon \le 1$, the function $u_\varepsilon(t,x)$ is a solution of the regularized problem (2) controlled by the estimate

$$||\partial_t^\alpha \partial_x^\beta u_\varepsilon(t,x)||_{L^2} \le C\varepsilon^{-L-\alpha-\beta},$$

for some $C>0$ and $L \ge 0$, for all $\alpha, \beta \in \mathbb{Z}_+$.

We put $u_0(x) \equiv 0, u_1(x) \equiv 0$, $a(t) = 1 + \delta(t-t_0)$ and $f(t,x) = \delta(t-t_1)$. Then we get $a_\varepsilon(t) = 1 + \varphi_\varepsilon(t-t_0)$, $f_\varepsilon(t,x) = \varphi_\varepsilon(t-t_1)$. Finally, we have the following problem to solve numerically

$$(3) \quad \begin{cases} \partial_{tt}^2 u_\varepsilon(t,x) - \big(1 + \varphi_\varepsilon(t-t_0)\big)\partial_{xx}^2 u_\varepsilon(t,x) = \varphi_\varepsilon(t-t_1),\ (t,x) \in [0,T] \times [0,1], \\ u_\varepsilon(t,0) = 0, t \in [0,T], \\ u_\varepsilon(t,1) = 0, t \in [0,T], \\ u_\varepsilon(0,x) = 0, x \in [0,1], \\ \partial_t u_\varepsilon(0,x) = 0, x \in [0,1]. \end{cases}$$

In the following, we demonstrate numerical simulations. All calculations are made in C++ by using the sweep method. For all simulations $\Delta t = \Delta x = 0.01$. In all computer simulations, we use Matlab R2017b. At first, we consider the case when $t_0 = t_1 = 0.2$. In Figure 1 and Figure 2, we see the decay of the solution $u_\varepsilon(t,x)$ with respect to the time t of the regularised problem (3), for $\varepsilon = 0.8$.

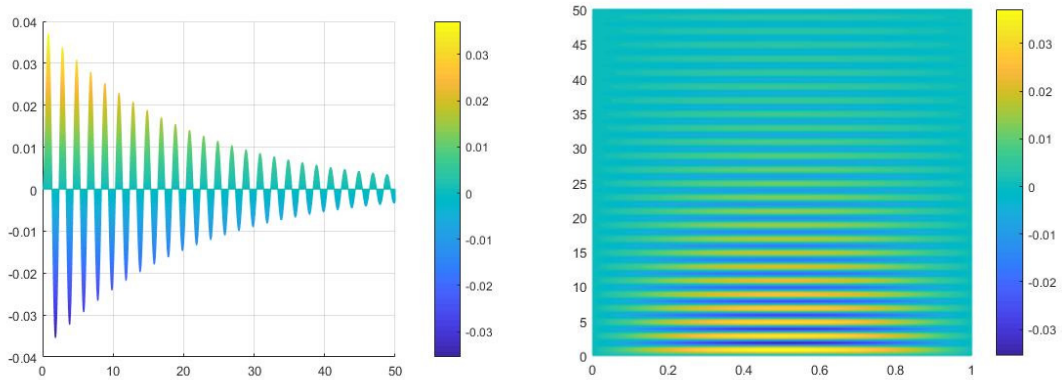

Figure 1 – In these plots, we can see the decay of the solution $u_\varepsilon(t,x)$ with respect to the time t of the regularised problem (3), for $\varepsilon = 0.8$ when $t_0 = t_1 = 0.2$. In the first plot, the time t is given by the horizontal axe, and the graphic of $\max_{x\in[0,1]} u_\varepsilon(t,x)$ is drawn. Here, we use colours to indicate the value of the solution $u_\varepsilon(t,x)$.

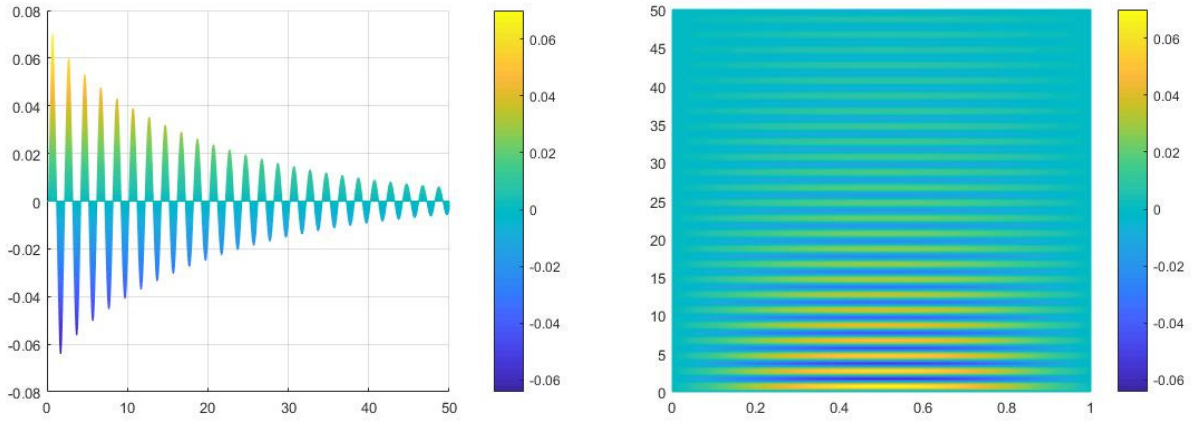

Figure 2 – In these pictures, we see the decay of the solution $u_\varepsilon(t,x)$ with respect to the time t of the regularised problem (3), for $\varepsilon = 0.01$ when $t_0 = t_1 = 0.2$.

Now, compare the solution $u_\varepsilon(t,x)$ at $t = 100$ of the regularized problem (3), for several values of ε. In Figure 3, there is given a comparison of the solution $u_\varepsilon(t,x)$ at time $t = 100$ of the regularized problem (3), for the parameter ε at $\varepsilon = 0.8, 0.5, 0.3, 0.1, 0.08, 0.05, 0.03, 0.01$.

Consider the case when t_0 and t_1 are different. Let us start with the case $t_0 < t_1$. Let $t_0 = 0.2$ and $t_1 = 10$ for $\varepsilon = 0.01$. Then for the illustrations we have Figure 4.

Now, we consider the case $t_1 < t_0$. Let $t_0 = 30$ and $t_1 = 0.2$ for $\varepsilon = 0.01$. Then for the illustrations we obtain Figure 5.

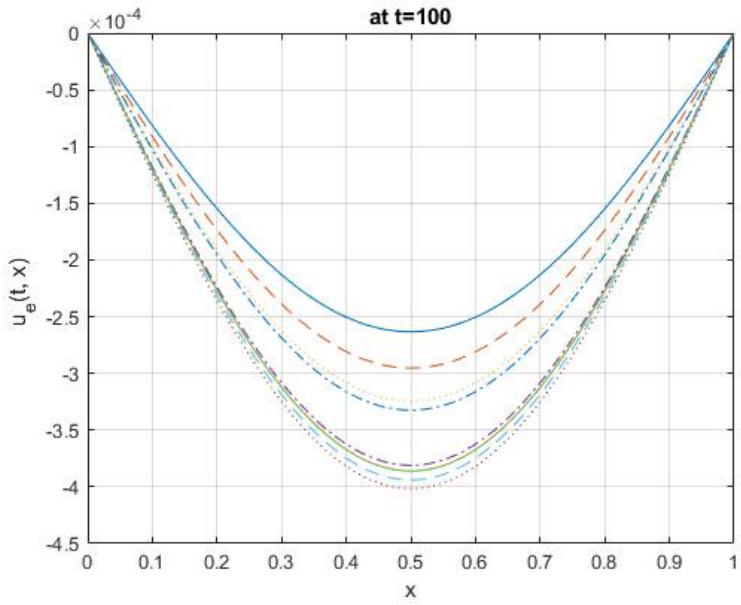

Figure 3 – Comparison of the solution $u_\varepsilon(t,x)$ at time $t = 100$ of the regularized problem (3), for the parameter ε. The graphics correspond to $u_\varepsilon(t,x)$ at $\varepsilon = 0.8, 0.5, 0.3, 0.1, 0.08, 0.05, 0.03, 0.01$ from top to bottom, respectively.

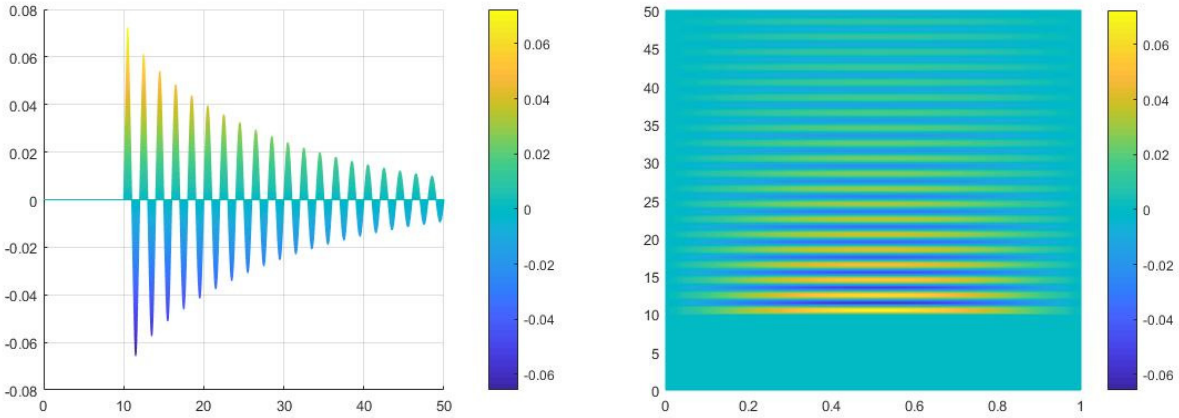

Figure 4 – In these plots, we see the decay of the solution $u_\varepsilon(t,x)$ with respect to the time t of the regularised problem (1.3), for $\varepsilon = 0.01$ when $t_0 = 0.2$ and $t_1 = 10$.

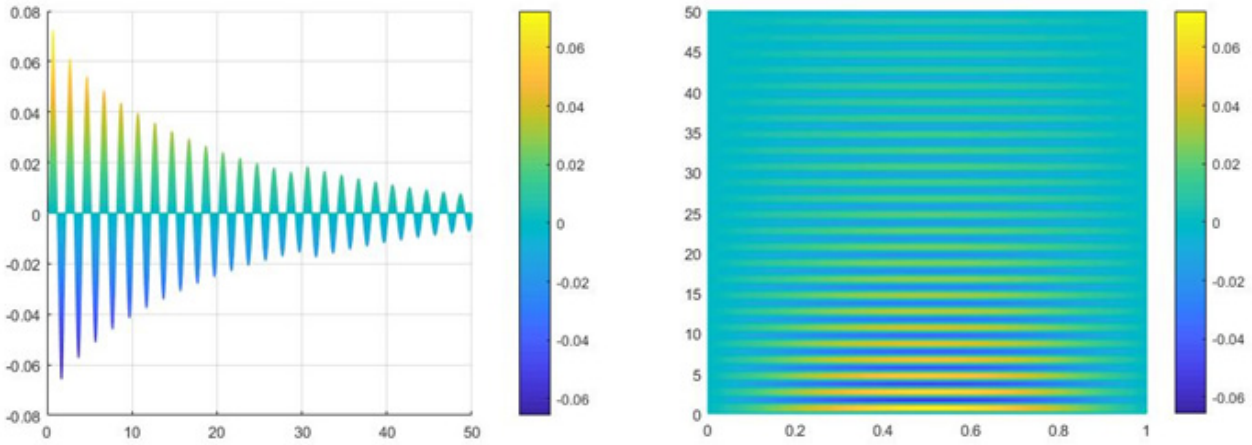

Figure 5 – In the plots, we can see the decay of the solution $u_\varepsilon(t,x)$ with respect to the time t of the regularised problem (3), for $\varepsilon = 0.01$ when $t_0 = 30$ and $t_1 = 0.2$.

Conclusion

Numerical experiments show that approximation methods work well in situations where a rigorous mathematical formulation of the problem is difficult in the framework of the classical theory of distributions. The concept of very weak solutions eliminates this difficulty, giving results of correctness for equations with singular coefficients. In the framework of this approach (very weak solutions), the expected physical properties of the equation can be reconstructed, for example, the distribution profile and the decay of the solutions for large times.

References

1. C. Garetto, M. Ruzhansky. Hyperbolic second order equations with non-regular time dependent coefficients. Archive for Rational Mechanics and Analysis. – Vol. 217 (2015). – No. 1. – P. 113-154.

2. J. C. Munoz, M. Ruzhansky, and N. Tokmagambetov. Wave propagation with irregular dissipation and applications to acoustic problems and shallow waters. https://arXiv:1705.01401

3. M. Ruzhansky, N. Tokmagambetov. Very weak solutions of wave equation for Landau Hamiltonian with irregular electromagnetic field. Letters in Mathematical Physics. – Vol. 107. – No 4. – 2017. – P. 591–618.

4. M. Ruzhansky, N. Tokmagambetov. Wave Equation for Operators with Discrete Spectrum and Irregular Propagation Speed. Archive for Rational Mechanics and Analysis. – Vol. 226. – No 3, 2017. – P. 1161–1207.

5. M. Ruzhansky, N. Tokmagambetov. On very weak solutions to the wave equations for the Hamiltonian in singular electromagnetic field. To appear in Mathematical Notes.

6. Cicognani, M., Colombini, F.: Awell-posed Cauchy problem for an evolution equation with coefficients of low regularity. J. Differ. Equ., 254(8). – 2013. – P. 3573–3595.

7. Colombini, F., De Giorgi, E., Spagnolo, S.: Sur les équations hyperboliques avec des coefficients qui ne dépendent que du temps. Ann. Scuola Norm. Sup. Pisa Cl. Sci. (4), 6(3). – 1979. – P.511–559.

8. Colombini, F., Del Santo, D., Reissig, M.: On the optimal regularity of coefficients in hyperbolic Cauchy problems. Bull. Sci. Math., 127(4). – 2003. – P.328–347.

9. Colombini, F., Jannelli, E., Spagnolo, S.: Nonuniqueness in hyperbolic Cauchy problems. Ann. Math. (2), 126(3). – 1987. – P. 495–524.

10. Hörmann, G., de Hoop,M.V.: Microlocal analysis and global solutions of some hyperbolic equations with discontinuous coefficients. Acta Appl.Math., 67(2). – 2001. – P.173–224.

11. Hörmann, G., de Hoop, M.V.: Detection ofwave front set perturbations via correlation: foundation for wave-equation tomography. Appl. Anal., 81(6). – 2002. – P. 1443–1465.

IRSTI 28.17.23; 29.15.35

[1]F.F. Komarov, [2]A.I. Kupchishin, [3*]A.A. Kuatbayeva, [4]T.A.Shmygaleva,
[4]K.A.Kabi, [4]D.A. Katabas

[1]Belarusian state university, Minsk, Belarus
[2]Kazakh National Pedagogical University named after Abai, Almaty, Kazakhstan
[3]Sh.Ualikhanov Kokshetau State university, Kokshetay, Kazakhstan
[4]al-Farabi Kazakh National University, Almaty, Kazakhstan
[*]e-mail: ahamala2017@gmail.com

Computer modelling of distributions processes on vacancy nanoclusters depth in the heavy targets irradiated with ions

Abstract. Creation new materials with unique properties is one of priority researches areas, both in physics, and in technique. The study of small metal particles properties from atoms hundreds and thousands is of great interest by their possible usage as materials or surface nanostructures. The fact that nanomaterial properties considerably depend on the particles properties making them is undoubted. The free clusters internal structure research could play a key role in an explanation of their physical or chemical features. Work is assigned to obtaining the regularities arising when modeling radiation processes in the heavy ions irradiated with various ions. The regularities arising when calculating cascade and probabilistic functions depending on particles penetration depth, interactions number are found. Real areas finding the radiation defects concentration result are defined, calculations for various flying particles and heavy targets in the energy range 100 - 1000 keV are made. Calculations results are presented in the schedules and tables form.
Key words: Modeling, ion, heavy target, vacancy nanoclusters, radiation defects concentration, area.

Introduction

Particles interaction problems with substance and radiation defects generation at substance radiation ions have devoted many works [1-5]. Application of the cascade and probabilistic method (CPM) in various fields of physics with usage the simplest cascade and probabilistic function (CPF) is described in works [6, 7]. CPF usage taking into account energy losses of for various charged particles within CPM is shown in work [8]. This work is performed within CPM which essence consists in receiving and further CPM usage. In this work CPF it is used for receiving calculation models on primary beaten-out atoms ranges and vacancy type nanoclusters concentration. Passing ions through substance is a difficult task as during creation physical, and mathematical models. A set of the flying particles types and targets of Mendeleev's Periodic system represents a huge elements number [9-14]. At the same time it is possible to consider various situations when the flying particles mass number are less than a target atomic number, it is commensurable with a target atomic number and a case when the flying particle atomic weight is more or much more target atomic number. Elements are classified by us on easy and heavy by element density. In work interaction process of the flying ions, various on density, with heavy ions is considered [15, 18].

Main results

For receiving calculation models of primary beaten-out atoms ranges and radiation defects concentration it is necessary to receive analytical expression of the cascade and probabilistic functions (CPF) making sense to probability that the particle generated at h' depth, will reach h depth after n impacts number. We have used CPF taking into account energy losses for ions, has the following appearance [8]:

$$\psi_n\left(h',h,E_0\right)=\frac{1}{n!\lambda_0^n}\left(\frac{E_0-kh'}{E_0-kh}\right)^{-l}exp\left(-\frac{h-h'}{\lambda_0}\right)*\left[\frac{\ln\left(\frac{E_0-kh'}{E_0-kh}\right)}{ak}-\left(h-h'\right)\right]^n, \quad (1)$$

where h',h – generation and registration depths of a particle respectively, n– interactions number, E_0 – primary particle initial energy, $l=1/\lambda_0 ak$, λ_0, a, k, E_0 – the approximation parameters entering the following recurrence relation [12-18]:

$$\sigma(h)=\sigma_0\left(\frac{1}{a(E_0-kh)}-1\right), \quad (2)$$

Approximating coefficients selection results are presented in tables 1, 2. Approximations selection results are presented in the figure 1.

Table 1 – Approximating parameters for silicon in silver

E_0	σ_0*10^8	a	E_0`	k	η
1000	0,00084229	0,00028854	1,1432	2440,1	0,999
800	0,28096	0,089117	1,0067	2653,6	0,999
500	0,014611	0,0034919	0,85506	3574,9	0,999
200	0,036748	0,0084184	0,34591	3755,6	0,999
100	0,11412	0,02743	0,16292	3757	0,999

Table 2 – Approximating parameters for silver in silver

E_0	σ_0*10^{10}	a	E_0`	k	η
1000	0,21185	0,16977	1,0087	7528,6	0,998
800	0,59507	0,47916	0,71531	6677,5	0,997
500	0,76419	0,37929	0,7438	11227	0,997
200	2,5751	2,4126	0,13503	4694,8	0,999
100	6,533	10,542	0,035424	2140,5	0,999

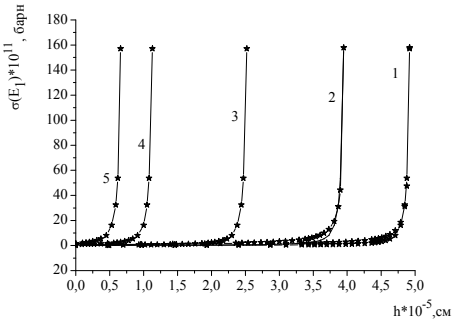

Figure 1 – Approximation of the cascade and probabilistic function modified section for Indian in gold:E_0=1000(1), 800(2), 500(3), 200(4), 100(5) keV. Points – settlement the dependences of section on depth, continuous lines – approximation

CPF Calculations are executed on the following formula:

$$\psi_n(h',h,E_0)=$$
$$=\exp\left[-\ln(n!)-n*\ln(\lambda_0)-\frac{1}{\lambda_0 ak}\ln\left(\frac{E_0-kh'}{E_0-kh}\right)+\frac{h-h'}{\lambda_0}+\right. \quad (3)$$
$$\left.+n*\ln\left(\frac{\ln\left(\frac{E_0-kh'}{E_0-kh}\right)}{ak}-(h-h')\right)\right.$$

CPF calculations results depending on interactions number and particles penetration depth are presented in figures 2,3.

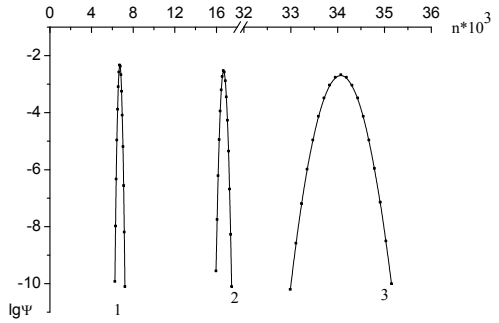

Figure 2 – CPF dependence on interactions number for the titan in iron for E_0=1000 keV h=0,0001; 0,0002; 0,0003 cm (1-3)

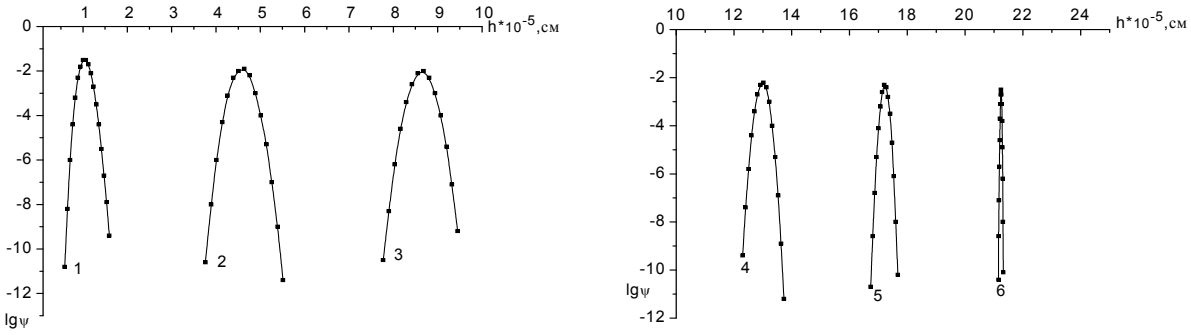

Figure 3 – CPF dependence for aluminum in tungsten from interactions number at E_0= 1000 keV and n=153, 787, 1804, 3496, 6548, 17108 (1-6)

When calculating CPF depending on interactions number and particles penetration depth and also vacancy type nanoclusters concentration needs to find real result finding area. We will note the main regularities when calculating CPF depending on interactions number arising when result finding area for various flying particles and heavy targets [11-15].

1. With initial energy reduction (the flying particle and a target same) with the same penetration depth the area of result is displaced to the small depths area.

2. For heavy targets the area of result is displaced to the small depths area, the area left border decreases more slowly, the right border sharply decreases.

3. With increase in observation depth the area of result is narrowed and displaced to the small depths area.

The regularities arising when calculating CPF depending on penetration depth following [18-21]:

1. With increase in atomic weight of the flying particle the step for calculation increases, reaching several hundred and even thousands.

2. With a big atomic weight of the flying particle and target the counting duration considerably increases and selection of borders becomes complicated.

3. With increase in observation depth the area of result is displaced to the big depths area and narrowed.

4. With initial particle energy reduction the area of result is displaced to the big depths area and narrowed.

Radiation defects concentration at ionic radiation is calculated on the following formula [8]:

$$c_k(E_0,h)=\frac{E_d}{E_c}\frac{(E_{2\max}-E_c)}{(E_{2\max}-E_d)}\sum_{n=n_0}^{n_1}\int_{h-k\lambda_2}^{h}\psi_n(h')\exp\left(-\frac{h-h'}{\lambda_2}\right)\frac{dh'}{\lambda_1(h')\lambda_2}\ , \qquad (4)$$

where E_0 – initial energy of the flying ion, E_d – threshold energy of shift, E_c– energy of the primary beaten-out atom (PBOA) at which the amount of the displaced atoms equals to atoms number N_d, being in a spontaneous recombination zone, E_{2max}– the greatest possible energy acquired by atom, $\psi_n(h')$ – CPF function in modified type, $\lambda_1(h')$ and λ_2 – shift run an ion – and atom - atomic shifts [15, 22].

Calculations results on distributions at the vacancy nanoclusters depth are presented in figures 4-6.

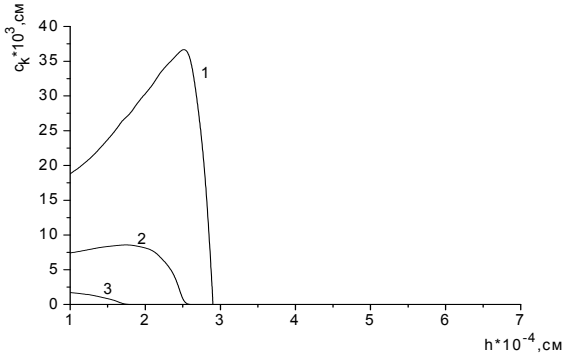

Figure 4 – Dependence on concentration of cascade areas on depth at copper radiation by aluminum ions: E_0= 500 keV, E_c= 50 (1), 100 (2), 200 (3) eV

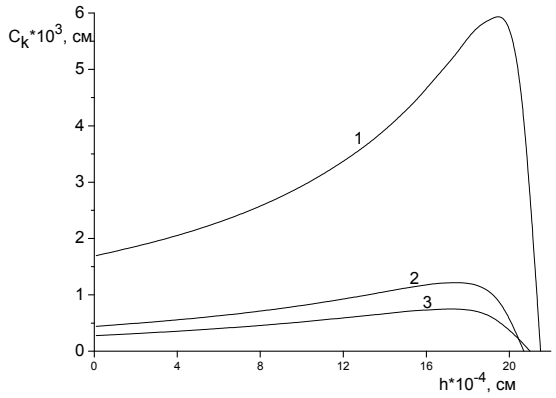

Figure 5 – Dependence of radiation defects concentration on depth at ionic radiation for carbon in Germanium (1), boron in Germanium (2) and fluorine in Germanium (3); E_c=50 keV; E_0= 1000 keV

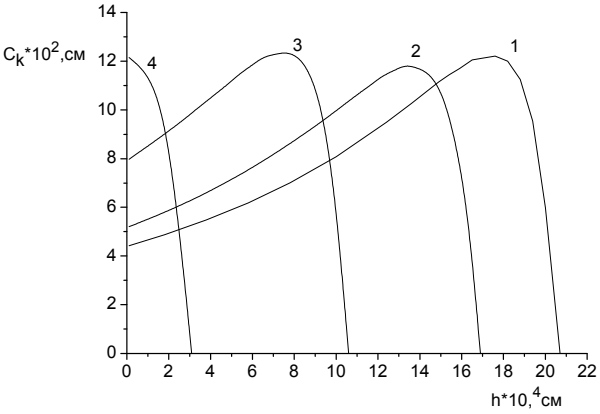

Figure 6 – Dependence of the radiation defects concentration on the depth at ion irradiation for nitrogen in germanium at E_c=50 keV; E_0= 1000 (1), 800 (2), 500 (3) keV

Conclusion

Thus, in the work an approximation expression for the interaction cross-section is selected and the approximation coefficients are found. Cascade-probability functions are calculated as a function of the interactions number and the particles penetration depth, the defects concentration in heavy targets. The regularities in the result domain behavior for calculating cascade-probability functions, the spectrum on primary-knocked-out atoms, and the radiation defects concentration of in heavy targets irradiated by ions are obtained. It could be seen that as the atomic number of the target increases for the same incident particle, the value of the function at the maximum point increases insignificantly, the depth values decrease, that is, in the heavier target of the vacancy clusters, more is formed, especially in the near-surface region.

References

1. Caro A. Molecular dynamic approach to heavy ion impast // Radiation Effects and Defects in Solids.-M: 1993. – Vol. 126. – P. 15-20.

2. Zou Y., Waya Y.A., Kambara T., Kanai Y., Oivra M. Ardo K., Hitashi A., Kravis S. Foil target element and incident energy dependence of multiple inner shell vacancy production of projectile ar ions // Radiation Effects and Defects in Solids. – 1993. – Vol. 126. – P. 87-90.

3. Audouard A., Balanzar E., Jousset J.C., Lesueur D., Thome L. Anisotropy of the atomic movements induced in amorphous metallic alloys by swift heavy ion irradiation // Radiation Effects and Defects in Solids. – 1993. – Vol. 126. – P. 93-96.

4. Fink D., Chadderton L.T., Cruz S.A., Fahrner W.R. Hnatowir V., E.H. te Kaat, Melnikov A.A., Varichenko V.S., Zaitsev A.M. Ion Tracks in condensed carbonaceus matter // Radiation Effects and Defects in Solids. – 1993. – Vol. 126. – P. 247-250.

5. Bogdanski P., Carin R., Cruege F., Hairie A., Madelon R., Metzner M.N. Study of an anderson negative – u system by means of hall mobility measurements in silicon // Radiation Effects and Defects in Solids. – 1993. – Vol. 126. – P. 261-264.

6. Boss E. G., Kupchishin A.I. Solution of physical tasks by a cascade and probabilistic method. - Alma-Ata: Science. – 1988. – P. 112.

7. Boss E. G., Kupchishin A.I. Solution of physical tasks by a cascade and probabilistic method. - Alma-Ata: Science. – 1998. – P. 144.

8. E.G. Boos, A.A. Kupchishin, A.I. Kupchishin, E.V. Shmygalev, T.A. Shmygaleva. Cascade and probabilistic method, solution of radiation and physical tasks, Boltzmann's equations. Communication with Markov's chains. – Monograph. Almaty.: KazNPU after Abay, Scientific Research Institute for New Chemical Technologies and Materials under al-Farabi KazNU. – 2015 – P. 388.

9. Komarov F.F. Nano- and microstructuring of solids by swift heavy ions//Physics-Uspekhi. -2017. – Vol. 187. – No. 5. – P. 465-504.

10. Komarov, F.F., Romanov, I.A., Vlasukova, L.A., Mudryi, A.V., Wendler, E. Optical and Structural Properties of Silicon with Ion-Beam Synthesized InSb Nanocrystals.// Spectroscopy. – 2017. – Vol. 120. – No. 1. – P. 204-207.

11. Komarov, F.F., Konstantinov, S.V., Strel'nitskij, V.E., Pilko, V.V. Effect of Helium ion irradiation on the structure, the phase stability, and the microhardness of TiN, TiAlN, and TiAlYN nanostructured coatings. //Technical Physics. – 2016. – Vol. 61. – No. 5. – P. 696-702.

12. Al'zhanova, A., Dauletbekova, A., Komarov, F., Akilbekov, A., Zdorovets, M. Peculiarities of latent track etching in SiO2/Si structures irradiated with Ar, Kr and Xe ions. – 2016. – Vol. 374. – No. 1. – P. 121-124.

13. Al'zhanova, A., Dauletbekova, A., Komarov, F., Akilbekov, A., Zdorovets, M. Nuclear Instruments and Methods in Physics Research, Section B: Beam Interactions with Materials and Atoms. – 2016. – Vol. 426. – No. 1. – P. 1-56.

14. Komarov, F.F., Zayats, G.M., Komarov, A.F.,Michailov, V.V., Komsta, H.Simulation of radiation effects in SiO2/Si Structures.// Acta Physica Polonica A. – 2015 . – Vol. 3. – No. 1. –P. 854-860.

15. Komarov, F., Uglov, V., Vlasukova, L., Zlotski, S., Yuvchenko, V.Drastic structure changes in pre-damaged GaAs crystals irradiated with swift heavy ions. // Nuclear Instruments and Methods in Physics Research, Section B: Beam Interactions with Materials and Atoms. – 2015. – Vol. 360. – No. 4. – P. 150-155.

16. Smyrnova, K.V., Pogrebnjak, A.D., Beresnev, V.M., Kravchenko, Y.O., Bondar, O.V. Microstructure and Physical–Mechanical Properties of (TiAlSiY) N Nanostructured Coatings Under Different Energy Conditions.// Metals and Materials International. – 2018. – Vol. 24. – No. 2. – P. 241-439.

17. Kupchishin, A.I., Kupchishin, A.A., Voronova, N.A. Cascade-probabilistic methods and solution of Boltzman type of equations for particle flow// IOP Conference Series: Materials Science and Engineering. – 2016. – Vol. 110. – No. 1. – P. 123-129.

18. Kupchishin, A.I., Kupchishin, A.A., Voronova, N.A., Kirdyashkin, V.I.Positron sensing of distribution of defects in depth materials. // IOP Conference Series: Materials Science and Engineering. – 2016. – Vol. 110. – No. 4. – P. 248-258.

19. Nowak, S.H., Bjeoumikhov, A., von Borany, J., Wedell, R., Ziegenrücker, R. Examples of XRF and PIXE imaging with few microns resolution using SLcam® a color X-ray camera //X-Ray Spectrometry. – 2015. – Vol. 44. – No. 3. – P. 135-140.

20. Bjeoumikhov, A., Buzanich, G., Langhoff, N., Soltau, H., (...), Wedell, R. The SLcam: A full-field energy dispersive X-ray camera.// Journal of Instrumentation. – 2012. – Vol. 7. – No. 5. – P. 248-252.

21. Bock, M., Skibina, J., Fischer, D., (...), Beloglazov, V., Steinmeyer, G.Nanostructured fibers for sub-10 fs optical pulse delivery. // Laser and Photonics Reviews. – 2013. – Vol. 7. – No. 3. – P. 566-570.

22. Dubovichenko, S., Burtebayev, N., Dzhazairov-Kakhramanov, A., (...), Kliczewski, S., Sadykov, T. New measurements and phase shift analysis of p16O elastic scattering at astrophysical energies.// Chinese Physics C. – 2017. – Vol. 41. – No. 1. – P. 485-495.

23. Kupchishin, A.I., Shmygalev, E.V., Shmygaleva, T.A., Jorabayev, A.B.Relationship between markov chains and radiation defect formation processes by ion irradiation.// Modern Applied Science. – 2015. – Vol. 9. – No. 3. – P. 59-70.

24. Kupchishin, A.I., Kupchishin, A.A., Shmygalev, E.V., Shmygaleva, T.A., Tlebaev, K.B.Calculation of the spatial distribution of defects and cascade- Probability functions in the materials.// Journal of Physics: Conference Series. – 2014. – Vol. 552. – No. 2. –P. 89-96.

IRSTI 29.31.27; 29.31.15

*G.B. Kussainova, Ye.S. Mukhametkarimov, N.R. Guseinov, O.Yu. Prikhodko

al-Farabi Kazakh National University, Almaty, Kazakhstan
*e-mail: gulden.kusainova@gmail.com

Optical properties of a-As_2Se_3 thin films

Abstract. Chalcogenide glassy semiconductors currently have found widely applications in the opto- and microelectronics devices. On this work we studied the optical properties of amorphous a-As_2Se_3 thin films which were produced on the quartz substrate by thermal evaporation method with different thickness: 500 nm, 1000 nm, 2000 nm. The transmission spectra were measured by spectrophotometer in the spectral range 250 -1000 nm. It is known that Swanepoel method can be used to determine the frequency dependent refractive index of thin films via interference fringes of transmission spectra. Using the obtained transmission spectrum and Swanepoel's method we calculated the optical constants of a-As_2Se_3 thin films in the 700 – 900 nm wavelength range. The found optical constants of a-As_2Se_3 films were used to theoretically determine the transmission spectrum by the matrix transfer method (TMM). The comparison of theoretical and experimental values of transmittance was made and proved the practical usage of these methods.
Key words: a-As_2Se_3 thin films, transmission spectrum, refractive index, Swanepoel's method, transfer matrix method.

Introduction

During the last several years the interest in chalcogenide glassy semiconductors grew remarkably. Chalcogenide glasses thin films are produced by various methods such as thermal evaporation, sputtering, chemical vapor deposition etc [1]. Many attractive materials have been selected up to now. One of them is As_2Se_3 which was prepared by direct fusion of high-purity As and Se and has excellent infrared transmission characteristics [2]. They are useful material for optical elements [3], optical memory disks [4], functional elements in integral-optic systems [5], IR-fibres [6] that show high flexibility and chemical durability [7] etc.

Chalcogenide glasses based on Se have good thermal, mechanical and chemical properties and they are used as materials for electronic and optoelectronic devices [8]. The fundamental issue of amorphous semiconductors is to analyze the difference in characteristics between the crystalline and the amorphous phase [9].

The optical properties of the material depend on the optical band gap, refractive index and extinction coefficient. It is quite essential to know the material's atomic structure, electronic band structure and electrical properties [10]. We can easily calculate the optical constants of materials using transmittance and reflectance spectra. During the experimental work, we determined the optical properties of As_2Se_3 by using a variety of thin films of different thickness.

Experiment

As_2Se_3 thin films were produced by thermal evaporation method in VUP-5 equipment. The spectra of optical transmittance and reflectance of the obtained thin films were measured using Shimadzu UV-Vis spectrophotometer. The transmittance and reflectance spectra of As_2Se_3 thin films with different thickness 500 nm, 1000 nm and 2000 nm are represented on Fig. 1. The thickness of films was determined by Scanning Electron Microscope, Quanta 3D 200i.

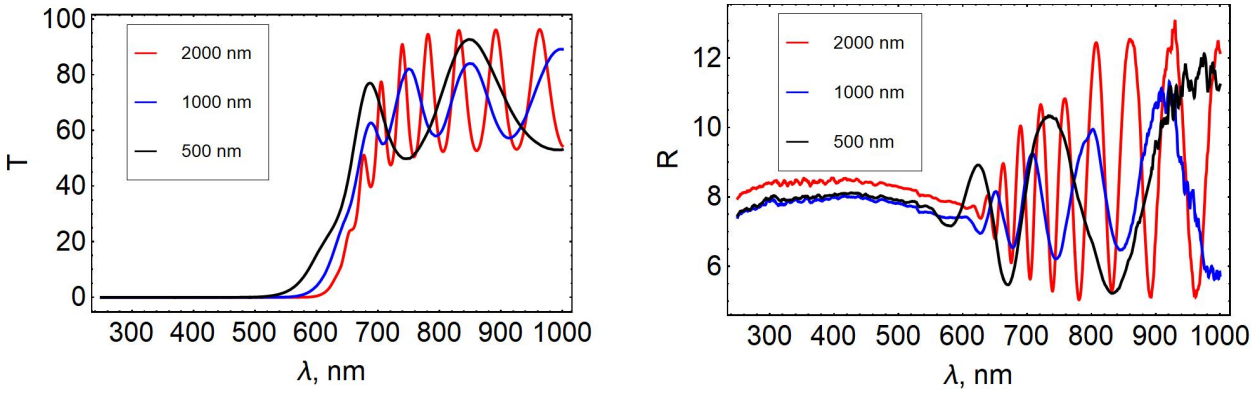

Figure 1 – The transmission (a) and reflection (b) spectra of a-As_2Se_3 films obtained by thermal evaporation

Swanepoel's method for determination of optical constants

The optical transmission measurement of film-on-substrate system which is shown in Fig. 2 has semitransparent or transparent films and the finite thickness of the substrate d_s which is several orders of magnitude larger than the film thickness d [11].

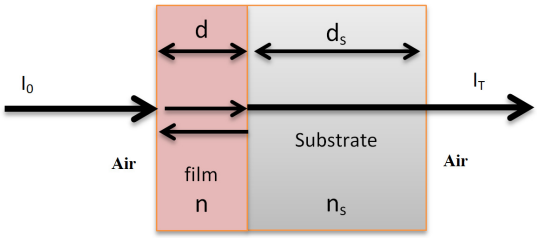

Figure 2 – Schematic illustration of light transmission through a film-substrate system

The total transmission $T(\lambda)$ by Swanepoel's method:

$$T(\lambda) = \frac{Ax}{B - Cx\cos\varphi + Dx^2}. \qquad (1)$$

Optical constants of thin films described with complex refractive index $n_c = n + i\,k$, n – the refractive index, k- the extinction coefficient which can be found as

$$k = \alpha\lambda/4\pi, \qquad (2)$$

where α denotes absorption coefficient of As_2Se_3 films.

The absorption coefficient α can be calculated in the strong absorption region by taking into account measured values of R and T:

$$\alpha = \frac{1}{d}\ln\left(\frac{(1-R)^2 + \left[(1-R)^4 + 4R^2T^2\right]^{\frac{1}{2}}}{2T}\right). \qquad (3)$$

The refractive index $n(\lambda)$ can be found using Swanepoel's method:

$$n = [N + (N^2 - s^2)^{1/2}]^{1/2}, \qquad (4)$$

where

$$N = 2s\frac{T_M - T_m}{T_M T_m} + \frac{s^2+1}{2}. \qquad (5)$$

Those equations are enough to calculate optical constants of the thin films. The T_m and T_M were obtained by transmittance spectra and presented with puncture lines on Fig. 3, s – is a refractive index of quartz substrate, s=1.55. The Fig.4 shows the refractive index and extinction coefficient of As_2Se_3 which are found using (2) and (4) for thickness of 2000 nm.

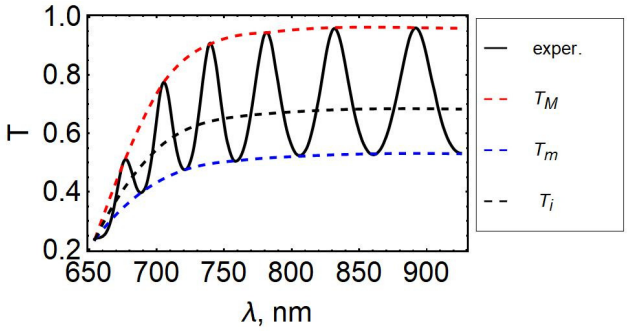

Figure 3 – The reflection spectrum of a-As_2Se_3 films obtained by thermal evaporation

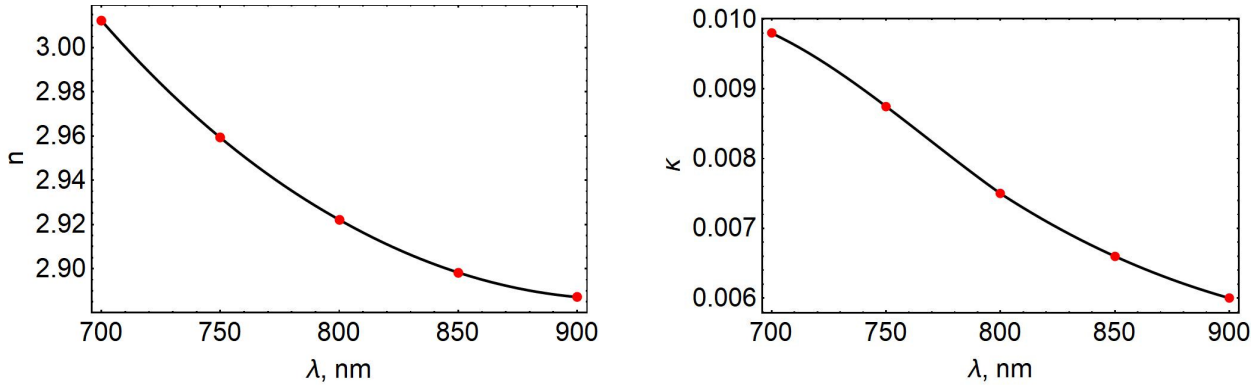

Figure 4 – The refractive index (a) and extinction coefficient (b) of a-As_2Se_3 films determined according to the Swanepoel's method

Transfer Matrix Method

Using Transfer Matrix Method and values of refractive coefficient it is possible to calculate transmittance on layered structures. The basic formula for wave propagation on layered systems has the following form:

$$\begin{bmatrix} E_1^+ \\ E_1^- \end{bmatrix} = T \begin{bmatrix} E_{N-1}^+ \\ E_{N-1}^- \end{bmatrix}, \quad (6)$$

where E_1^-, E_1^+ – backward and forward amplitudes of incidence wave, E_{N-1}^+ – transmitted wave amplitude and T is the transfer matrix which is obtained by multiplying: the transition matrix $T_{i\to j}$ through the interface, and the propagation matrix in a dielectric medium $P_i(d)$. In our case, T is determined as

$$T = T_{0\to 1} P_1(d) T_{1\to 2}. \quad (7)$$

The transition matrix $T_{i\to j}$ defined as follows:

$$T_{i\to j} = \frac{1}{ti,j} \begin{bmatrix} 1 & r_{i,j} \\ r_{i,j} & 1 \end{bmatrix}. \quad (8)$$

For TE-polarization:

$$r_{ij} = \frac{n_j cos\theta_i - n_j cos\theta_j}{n_j cos\theta_i + n_i cos\theta_j}, \quad (9)$$

$$t_{ij} = 1 + r_{ij} = \frac{2n_i cos\theta_i}{n_j cos\theta_j + n_i cos\theta_j}, \quad (10)$$

and for TM-polarization:

$$r_{ij} = \frac{n_j cos\theta_i - n_i cos\theta_j}{n_j cos\theta_i + n_i cos\theta_j}, \quad (11)$$

$$t_{ij} = \frac{n_i}{n_j}\left(1 + r_{ij}\right) = \frac{2n_i cos\theta_i}{n_j cos\theta_j + n_i cos\theta_j}. \quad (12)$$

Propagation matrix in As_2Se_3 layer is written by following form

$$P_i = \begin{bmatrix} e^{-k_{x,i}d_i} & 0 \\ 0 & e^{k_{x,i}d_i} \end{bmatrix}. \quad (13)$$

The transmission coefficient Tr at normal incidence of wave can be obtained by using simple relation:

$$Tr = \left|\frac{1}{T_{11}}\right|^2. \quad (14)$$

Figure 5 represents the comparison of transmission coefficient of 1000 nm thick As_2Se_3 film determined by numerical results based on TMM with experimental measurements. The small difference in the spectra in Fig. 5 is probably due to the inhomogeneity of the film thickness in which interference is observed.

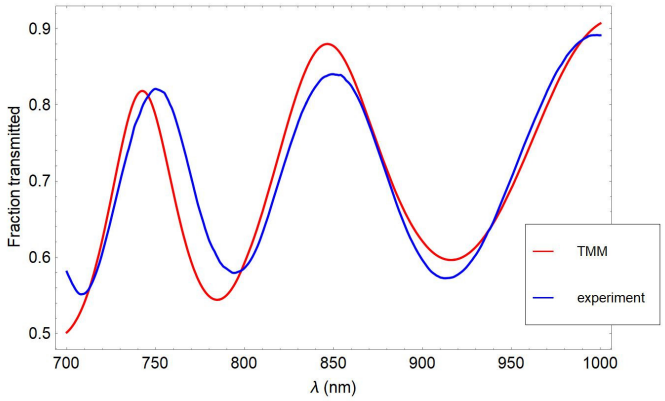

Figure 5 – Comparison of theoretical and experimental results of transmission spectrum of As_2Se_3 thin films

Conclusion

Thin As_2Se_3 films were produced by thermal evaporation method with different thickness 500nm, 1000nm, 2000nm. Swanepoel's method is used to evaluate the values of refractive index and extinction coefficient which are in a good agreement with the results of other authors. The refractive index and extinction coefficient were found in the range of 700 nm - 900 nm. The found coefficients were used to theoretically determine the transmission spectrum by the matrix transfer method. The theoretical and experimental results have some slight difference due to non-uniform thickness of thin films. According to the result, it can be concluded that the transfer matrix method gives adequate results and can be used to predict the optical characteristics of thin films and their layered structures.

References

1. Zakery, S.R. Elliott. Optical properties and applications of chalcogenide glasses: a review // J. Non-Cryst. Solids. – 2003. – Vol. 330. – P.1–12.

2. Adler D. Physics of Desordered Materials // Springer Science & Business Media, –2012. – Vol.396. – P.105-155.

3. Cerquar-ichardson K. A., Mckinley J. M., Lawrence B., Joshi S., Villeneuve A. Comparison of nonlinear optical properties of sulfide glasses in bulk and thin film form // Optical Materials. –2001. – Vol.10. – P. 155-159.

4. Andriesh A., Chumash V., Nonlinear optical phenomena in chalcogenide glasses // Pure & Applied Optics. – 2005. – Vol.7. – P.351-361.

5. Petkov P., Vassilev V., Petkova T., Monchev B., Aljihmani L. Optical properties of ternary chalcogenide thin films with SnTe // Journal of Optoelectronics and Advanced Materials. –2005. – Vol. 7. – P. 1965-1969.

6. Cheng J., W. Chen, D. Ye. Zinc porphyrins with a pyridine-ring-anchoring group for dye-sensitized solar cells // J. Non-Cryst. Sol. – 2013. – Vol.330. – P.184, 124.

7. Boycheva S.V., Vassilev V.S., Petkovic P., Y. Nedevac. Optical characteristics of thermally evaporated GeSe2–Sb2Se3–ZnSe amorphous thin films // Materials Letters. – 2005. – Vol. 59. –P. 1521-1525.

8. Li L., Lin H., Qiao S., Zou Y., Danto S., K. Richardson, J.D. Musgraves, N. Lu, J. Hu. Integrated flexible chalcogenide glass photonic devices // Nat. Photonics. – 2014. – Vol.8 – P. 643-649.

9. Sati D.C., Kumar R.,Mehra R.M. Influence of Thickness on Optical Properties of a: As2Se3 Thin Films // Turkish J. Phys. – 2016. – Vol.30. – P. 519 - 527.

10. Sarsembinov Sh., Prikhodko O.Yu., Ryaguzov A.P., Maksimova S. Ya., Ushanov V. Zh. Local structure and electronic properties of amorphous As2S3 films prepared by different methods // Semiconductor science and technology. – 2004. – Vol.7. – P.787.

11. Pimpabute N., Burinprakhon T., Somkhunthot W. Determination of optical constants and thickness of amorphous GaP thin film // Optica Applicata. – 2011. –Vol. 41. – P.1-12.

12. Swanepoel R., J. Phps. Determination of the thickness and optical constants of amorphous silicon // E: Sci. Instrum. – 1983. – Vol. 16. – P.5.

13. Sarsembinov Sh., Prikhodko O. Yu., Ryaguzov A.P., Maksimova S. Ya., Ushanov V. Zh. Atomic structure and short-and medium-range order parameters in amorphous chalcogenide films prepared by different methods // Journal of non-crystalline solids. – 2007. – Vol.18. – P.2057-2061.

IRSTI 30.17.02

*A. Issakhov, A. Abylkassymova, M. Sakypbekova

Faculty of Mechanics and Mathematics, al-Farabi Kazakh National University,
Almaty, Kazakhstan
*e-mail: alibek.issakhov@gmail.com

Applications of parallel computing technologies for modeling the mixed convection in backward-facing step flows with the vertical buoyancy forces

Abstract. This paper presents numerical solutions of the mixed convection in backward-facing step flows with the vertical buoyancy forces. A two-dimensional incompressible Navier-Stokes equation is used to describe this process. This system is approximated by the control volume method and solved numerically by the projection method. The two-dimensional Poisson equation satisfying the discrete continuity equation that is solved by the Jacobi iterative method at each time step. The numerical solutions of the laminar flow behind the backward-facing step with the vertical buoyancy forces are compared with the numerical results of other authors. This numerical algorithm is completely parallelized using various geometric domain decompositions (1D, 2D and 3D). Preliminary theoretical analysis of the various decomposition methods effectiveness of the computational domain and real computational experiments for this problem were made and the best domain decomposition method was determined. In the future, a proven mathematical model and parallelized numerical algorithm with the best domain decomposition method can be applied for various complex flows with the vertical buoyancy forces.

Key words: domain decomposition method, backward-facing step flow, projection method, vertical buoyancy forces, mixed convection.

Introduction

In many technical flows of practical interest, like flow divisions, with the sudden expansion of geometry or with subsequent re-joining, are a common occurrence. The existence of a flow separation and recirculation area has a significant effect on the performance of heat transfer devices, for example, cooling equipment in electrical engineering, cooling channels of turbine blades, combustion chambers and many other heat exchanger surfaces that appear in the equipment.

Many papers are devoted to the motion of a fluid with separation and reconnection of flows without taking into account the buoyancy forces. The importance of this process is indicative of the number of papers where special attention was paid to building equipment [1-3] and developing experimental and theoretical methods for detailed study of flows with separation regions [4-6]. An extensive survey of isothermal flows in fluid flows is given in papers [10-12]. Heat transfer in the flows has been investigated by many authors, like Aung [13, 14], Aung et al. [15], Aung and Worku [16], Sparrow et al. [17, 18] and Sparrow and Chuck [19]. However, published papers on this topic do not take into account the strength of buoyancy force on the flow stream or the characteristics of heat transfer. These effects become significant in the laminar flow regime, where the velocity is relatively low, and when the temperature difference is relatively high. Ngo and Byon [26] studied the location effect of the heater and the size of the heater in a two-dimensional square cavity using the finite element method. Oztop and Abu-Nada [27] numerically investigated natural convection in rectangular shells, partially heated from the side wall by the finite volume method.

In this paper considered the influence of buoyancy forces on the flow and heat transfer

characteristics in individual flows. Numerical solutions for a laminar mixed convective airflow (Pr=0.7) in a vertical two-dimensional channel with a backward-facing step to maintain the buoyancy effect are shown in Figure 1. Numerical results of interest, such as velocity and temperature distributions, re-binding lengths and friction coefficients are presented for the purpose of illustrating the effect of buoyancy forces on these parameters.

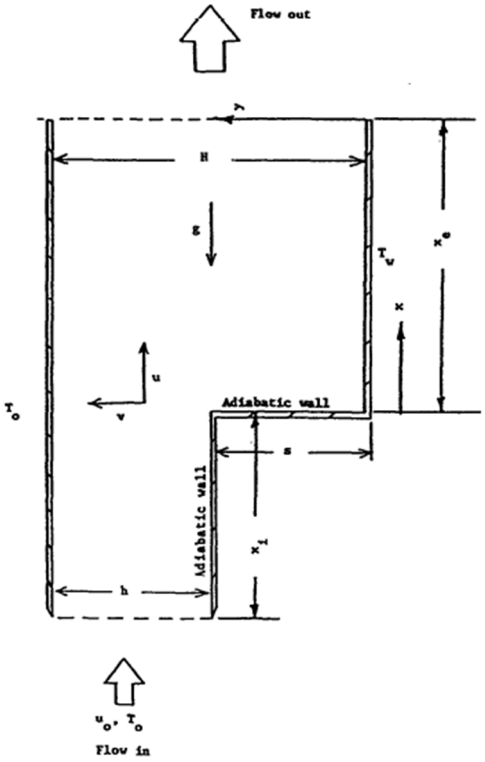

Figure 1 – Schematic representation of the backward-facing step flows

Mathematical formulation of the problem

Consider a two-dimensional laminar convective flow in a vertical channel with a sudden expansion behind the inverse step of height s, as shown in Fig. 1. The straight wall of the channel is maintained at a uniform temperature equal to the temperature of the inlet air T_0. The stepped wall below the stage is heated to a uniform temperature, which can be adjusted to any desired value T_w. The upper part of the stepped wall and the reverse side is installed as an adiabatic surface. The inlet length of the channel x_i and the outlet lower length x_e of the channel are appropriate dimensions. These lengths are assumed to be infinite, but the simulation domain is limited by the length $L_e = x_e + x_i$. The smaller section of the channel before the projection has a height, and the large section below the stage has a height $H = h + s$. Air flows up the channel with mean velocity u_0 and uniform temperature T_0. The gravitational force g in this problem is considered to act vertically downwards.

To describe this physical problem, was used assumption about constant properties, and was used the Boussinesq approximation. This system of equations in an immense form can be written in the form:

1) $$\frac{\partial U}{\partial X}+\frac{\partial U}{\partial Y}=0. \qquad (1)$$

2) $$\frac{\partial U}{\partial t}+U\frac{\partial U}{\partial X}+V\frac{\partial U}{\partial Y}= =-\frac{\partial P}{\partial X}+\frac{1}{\mathrm{Re}}\left(\frac{\partial^2 U}{\partial X^2}+\frac{\partial^2 U}{\partial Y^2}\right)+\frac{Gr}{\mathrm{Re}^2}\theta \qquad (2)$$

3) $$\frac{\partial V}{\partial t}+U\frac{\partial V}{\partial X}+V\frac{\partial V}{\partial Y}= =-\frac{\partial P}{\partial Y}+\frac{1}{\mathrm{Re}}\left(\frac{\partial^2 V}{\partial X^2}+\frac{\partial^2 V}{\partial Y^2}\right) \qquad (3)$$

4) $$\frac{\partial \theta}{\partial t}+U\frac{\partial \theta}{\partial X}+V\frac{\partial \theta}{\partial Y}= =\frac{1}{\mathrm{Pr}\,\mathrm{Re}}\left(\frac{\partial^2 \theta}{\partial X^2}+\frac{\partial^2 \theta}{\partial Y^2}\right) \qquad (4)$$

The dimensionless parameters in the equations given above are defined by the formula:

$$U=u/u_0\,, \qquad V=\upsilon/u_0\,,$$
$$X=x/s\,, \qquad Y=y/s\,,$$
$$\theta=\left(T-T_0\right)/\left(T_w-T_0\right), \qquad P=p/\rho_0 u_0^2\,,$$
$$\mathrm{Pr}=\nu/\alpha\,, \qquad \mathrm{Re}=u_0 s/\nu\,,$$
$$Gr=g\beta\left(T_w-T_0\right)s^3/\nu^2\,.$$

where α – the temperature diffusion, ν – the kinematic viscosity, and β – the thermal expansion coefficient are estimated at the film temperature $T_f=\left(T_0+T_w\right)/2$.

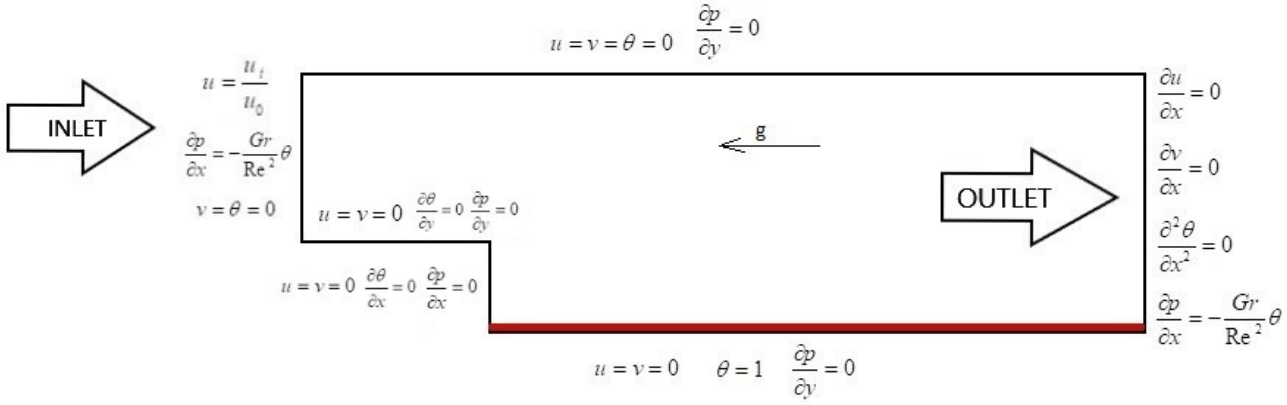

Figure 2 – Boundary conditions

Boundary conditions:

(a) Inlet conditions: At the point $X = -X_i$ and $1 \le Y \le H/s$: $U = u_i/u_0$, $V = 0$, $\theta = 0$, $\frac{\partial p}{\partial x} = -\frac{Gr}{\mathrm{Re}^2}\theta$.
where u_i is the local distribution of velocities at the inlet, which is assumed to have a parabolic profile and u_i/u_0 an average inlet velocity, that is, given by formula

$$u_i/u_0 = 6\left[-y^2 + (H+s)y - Hs\right]/(H-s)^2$$

(b) Outlet conditions: At the point $X = X_e$ and $0 \le Y \le H/s$: $\partial U/\partial X = 0$, $\partial^2\theta/\partial X^2 = 0$, $\partial V/\partial X = 0$, $\frac{\partial p}{\partial x} = -\frac{Gr}{\mathrm{Re}^2}\theta$.

(c) on the top wall: At the point $Y = H/s$ and $-X_i \le X \le X_e$: $U = 0$, $V = 0$, $\theta = 0$, $\frac{\partial p}{\partial y} = 0$.

(d) on the wall of the upper stage: At the point $Y = 1$ and $-X_i \le X < 0$: $U = 0$, $V = 0$, $\partial\theta/\partial Y = 0$, $\frac{\partial p}{\partial y} = 0$.

(e) on the wall of the lower stage: At point $X = 0$ and $0 \le Y \le 1$: $U = 0$, $V = 0$, $\partial\theta/\partial X = 0$, $\frac{\partial p}{\partial x} = 0$.

(f) on the wall below the stage: At the point $Y = 0$ and $0 \le X \le X_e$: $U = 0$, $V = 0$, $\theta = 1$, $\frac{\partial p}{\partial y} = 0$.

The last term on the right-hand side of equation (2) is the contribution of the buoyancy force. The length of the downstream flow from the simulation area was chosen to be 70 steps ($X_e = 70$). The upper length of the design area was chosen to be 5 steps (i.e. $X_i = 5$), and the velocity profile at the input area was set as parabolic profile, like $u_i/u_0 = 6\left[-y^2 + (H+s)y - Hs\right]/(H-s)^2$, and temperature was chosen as uniform T_0.

The numerical algorithm

For a numerical solution of this system of equations, the projection method is used [20-23]. The equations are approximated by the finite volume method [20, 24]. At the first stage it is assumed that the transfer of momentum is carried out only through convection and diffusion, and an intermediate velocity field is calculated by the fourth-order Runge-Kutta method [21, 22]. At the second stage, according to the found intermediate velocity field, there is a pressure field. The Poisson equation for the pressure field is solved by the Jacobi method. At the third stage it is assumed that the transfer is carried out only due to the pressure gradient. At the fourth stage, the equations for the temperature are calculated by the fourth-order Runge-Kutta method [21, 22].

I. $$\int_{\Omega}\frac{\vec{u}^{*}-\vec{u}^{n}}{\Delta t}d\Omega = -\oint_{\partial\Omega}(\vec{u}^{n}\,\vec{u}^{*}-\frac{1}{\mathrm{Re}}\nabla\vec{u}^{*})n_i d\Gamma-\int_{\Omega}\frac{Gr}{\mathrm{Re}^2}\theta d\Omega,$$

II. $$\oint_{\partial\Omega}(\nabla p)d\Gamma=\int_{\Omega}\frac{\nabla\vec{u}^{*}}{\Delta t}d\Omega,$$

III. $$\frac{\vec{u}^{n+1}-\vec{u}^{*}}{\Delta t}=-\nabla p,$$

IV. $$\int_{\Omega}\frac{\theta^{*}-\theta^{n}}{\Delta t}d\Omega=-\oint_{\partial\Omega}(\vec{u}^{n}\,\theta^{*}-\frac{1}{\mathrm{Re}\,\mathrm{Pr}}\nabla\theta^{*})n_i d\Gamma,$$

Parallelization algorithm

For numerical simulation was constructed a computational mesh by using the PointWise software. The problem was launched on the ITFS-MKM software using a high-performance computing. This numerical algorithm is completely parallelized using various geometric domain decompositions (1D, 2D and 3D). Geometric partitioning of the computational grid is chosen as the main approach of parallelization. In this case, there are three different ways of exchanging the values of the grid function on the computational nodes of a one-dimensional, two-dimensional, and three-dimensional mesh. After the domain decomposition stage, when parallel algorithms are built on separate blocks, a transition is made to the relationships between the blocks, the simulations on which will be executed in parallel on each processor. For this purpose, a numerical solution of the equation system was used for an explicit scheme, since this scheme is very efficiently parallelized. In order to use the domain decomposition method as a parallelization method, this algorithm uses the boundary nodes of each subdomain in which it is necessary to know the value of the grid function that borders on the neighboring elements of the processor. To achieve this goal, at each compute node, ghost points store values from neighboring computational nodes, and organize the transfer of these boundary values necessary to ensure homogeneity of calculations for explicit formulas.

Data transmission is performed using the procedures of the MPI library [25]. By doing preliminary theoretical analysis of the effectiveness of various domain decomposition methods of the computational domain for this problem, which will estimate the time of the parallel program as the time T_{calc} of the sequential program divided by the number of processors plus the transmission time $T_p = T_{calc} / p + T_{com}$. While transmissions for various domain decomposition methods can be approximately expressed through capacity:

$$T_{com}^{1D} = t_{send}\,2N^2x2$$

$$T_{com}^{2D} = t_{send}\,2N^2x4p^{1/2} \qquad (5)$$

$$T_{com}^{3D} = t_{send}\,2N^2x6p^{2/3}$$

where N^3 – the number of nodes in the computational mesh, p – the number of processors (cores), t_{send} – the time of sending one element (number).

It should be noted that for different decomposition methods, the data transmission cost can be represented as $T_{com}^{1D} = t_{send}\,2N^2xk(p)$ in accordance with the formula (5), where $k(p)$ is the proportionality coefficient, which depends on the domain decomposition method and the number of processing elements used.

At the first stage, one common program was used, the size of the array from start to run did not change, and each element of the processor was numbered by an array of elements, starting from zero. For the test simulation is used well known problem – 3D cavity flow. Despite the fact that according to the theoretical analysis of 3D decomposition is the best option for parallelization (Figure 3), computational experiments showed that the best results were achieved using 2D decomposition, when the number of processes varies from 25 to 144 (Figure 3).

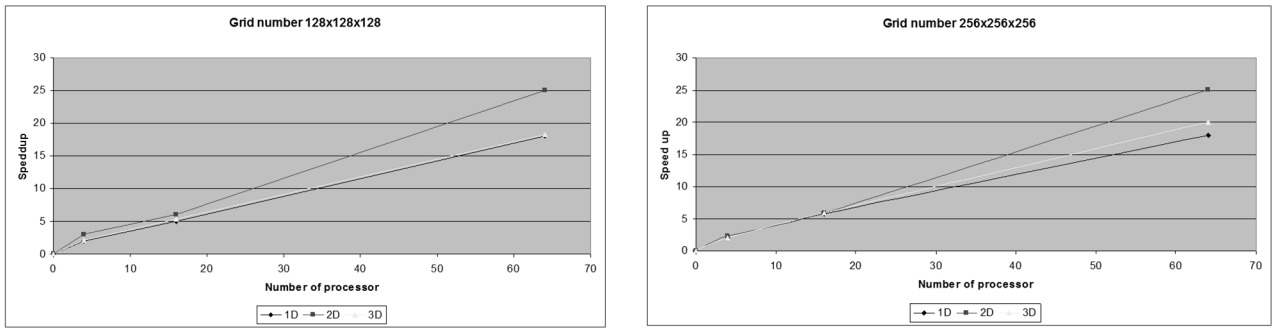

Figure 3 – Speed-up for various domain decomposition methods of the computational domain.

Based on the preliminary theoretical analysis of the graphs, the following character can be noted. The simulation time without the interprocessor communications cost with different domain decomposition methods should be approximately the same for the same number of processors and be reduced by T_{calc}/p. In fact, the calculated data show that when using 2D decomposition on different computational grids, the minimal cost for simulation and the cost graphs are much higher, depending on the simulation time, on several processors taken T_{calc}/p.

To explain these results, it is necessary to pay attention to the assumptions made in the preliminary theoretical analysis of efficiency for this task. First, it was assumed that regardless of the distribution of data per processor element, the same amount of computational load was done, which should lead to the same time expenditure. Secondly, it was assumed that the time spent on interprocessor sending's of any degree of the same amount of data is not dependent on their memory choices. In order to understand what is really happening, the following sets of computational simulations test were carried out. For evaluation, the sequence of the first approach was considered when the program is run in a single-processor version, and thus simulates various geometric domain decomposition methods of data for the same amount of computation performed by each processor.

Numerical results

Geometric parameters are indicated in Figure 1: channel length L = 75, channel height H = 2, step height S = 1. Numerical results were obtained for the dimensionless numbers Re = 50, Pr = 0.7 and Gr = 19.1 [9].

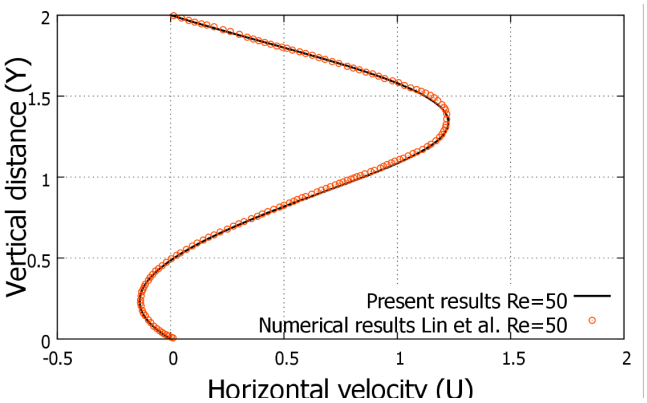

Figure 4 – Velocity profile with vertical buoyancy forces for dimensionless number Re=50, $\Delta T = 1°C$, $x/x_f = 0.5$, where $x_f = 2.91$.

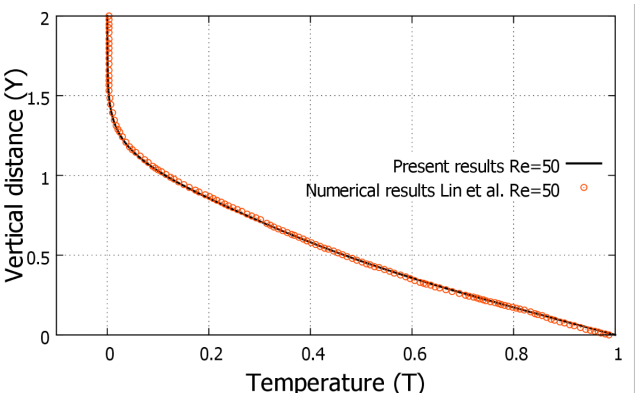

Figure 5 – Temperature profile with vertical buoyancy forces for dimensionless number Re=50, $\Delta T = 1°C$, $x/x_f = 0.5$, where $x_f = 2.91$.

Figure 4 shows the comparison of the longitudinal velocity profile with the numerical data of Lin et al. [9] at the point x/x_f = 0.5,

where $x_f = 2.91$. Figure 5 shows the comparison of temperature profiles with the numerical data of Lin et al. [9] at the point $x/x_f = 0.5$, where $x_f = 2.91$. It can be seen from the figures that the mathematical model and the numerical algorithm which is used in this paper is coincided with the numerical results obtained by Lin et al. [9]. Figure 6 shows the streamlines and the horizontal velocity contour for dimensionless numbers Re = 50, Pr = 0.7 and Gr = 19.1. Figure 7 shows the vertical velocity contour for dimensionless numbers Re = 50, Pr = 0.7 and Gr = 19.1. Figure 8 shows the temperature profile for dimensionless numbers Re = 50, Pr = 0.7 and Gr = 19.1. For a better understanding of this process from figures 6-8 can be seen the development of the backward-facing step flow with vertical buoyancy force: the initiation and process of the development of the region of flows reconnection with taking into account the buoyancy forces.

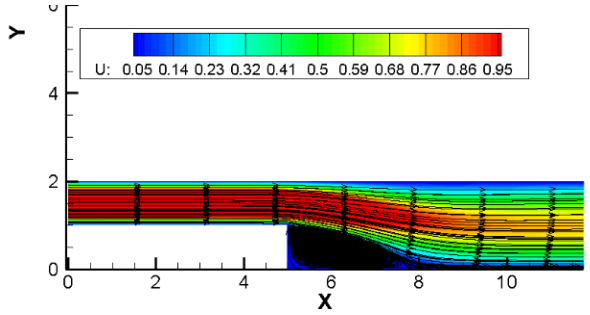

Figure 6 – The contour of the horizontal velocity component with streamlines for dimensionless numbers Re=50, Pr=0.7 and Gr=19.1.

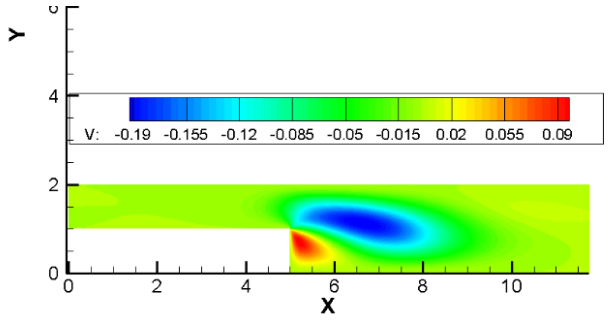

Figure 7 – The contour of the vertical velocity component for dimensionless numbers Re=50, Pr=0.7 and Gr=19.1.

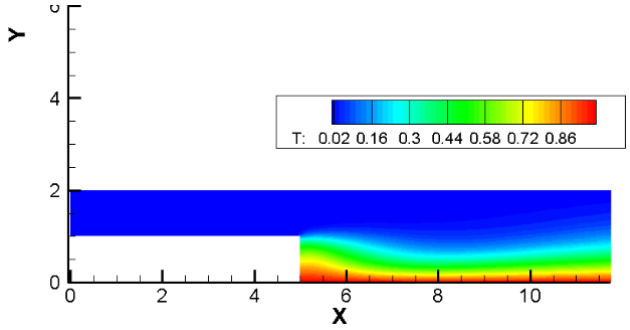

Figure 8 – Temperature contour for dimensionless numbers Re=50, Pr=0.7 and Gr=19.1.

Conclusion

Numerical studies of the laminar flow were carried out by the zone of joining the flows behind the backward-facing step with taking into account the buoyancy forces. This gave a deeper insight into the internal flow behind the backward-facing step and the processes of flows reconnection under the influence of temperature effects, which in turn gave an idea of the further appearance of secondary zones. The distance from the ledge to the canal boundary is 4 times the channel height, for a more detailed study of the backward-facing step flows with taking into account the buoyancy forces [9]. The numerical data of the velocity distribution showed the formation of a primary reattachment zone of backward-facing step flows. To numerically solve the system of Navier-Stokes equations, the projection method was used. From numerical results can be seen that the realized numerical method gives a small error in comparison with the numerical results of other authors [9] for the dimensionless numbers Re = 50, Pr = 0.7 and Gr = 19.1.

Also in this paper is used a parallel algorithm to obtain fast numerical results. This parallel algorithm is based on one-dimensional, two-dimensional and three-dimensional domain decomposition method. The numerical results from the 3D cavity flow test problem, which used 1D, 2D and 3D domain decomposition method showed that 3D domain decomposition is not time-consuming compared to 2D domain decomposition, for the number of processors that does not exceed 250,

and 3D domain decomposition has more time-consuming software implementation and the use of 2D domain decomposition is sufficient for the scope of the problem. That's why for backward-facing step flow with vertical buoyancy force is used 2D domain decomposition. It should also be noted that setting the boundary conditions is an important process. In the future, this mathematical model and a parallel numerical algorithm can be applied to various complex flows taking into account the buoyancy forces.

References

1. Abbott D.E., Kline S.J. Experimental investigations of subsonic turbulent flow over single and double backward-facing steps // J. Basic Engng. – 1962. – Vol.84. – P. 317.

2. Sebanr A. Heat transfer to the turbulent separated flows of air downstream of a step in the surface of a plate // J. Heat Transfer. – 1964. – Vol.86. – P. 259.

3. Goldsteinr J., Eriksenv L., Olsonr M., Eckerte R.G. Laminar separation, reattachment and transition of flow over a downstream-facing step // J. Basic Engng. – 1970. – Vol.92. – P. 732.

4. Durst F., Whitelawj H. Aerodynamic properties of separated gas flows: existing measurements techniques and new optical geometry for the laser-Doppler anemometer // Prog. Heat Mass Transfer. – 1971. – Vol.4. – P. 311.

5. Gosmana D., Punw M. Lecture notes for course entitled: 'Calculation of recirculating flow' // Heat Transfer Rep. – 1974. – Vol.74. – P. 2.

6. Kumara, Yajnikk S. Internal separated flows at large Reynolds number // J. Fluid Mech. – 1980. – Vol.97. – P. 27.

7. Chiang T.P., Tony W.H., Sheu, Fang C.C. Numerical investigation of vortical evolution in backward-facing step expansion flow // Appl. Math. – 1999. – Vol.23. – P. 915-932.

8. Fletcher C.A.J. Computational techniques for fluid dynamics 2 // Springer-Verlag New York. – 1988. – Vol.1. – P. 387.

9. J.T. Lin, B.F. Armaly, T.S. Chen. Mixed convection in buoyancy-assisting, vertical backward-facing step flows. // International Journal of Heat and Mass Transfer. – 1990. – Vol. 33, Issue 10. – P. 2121-2132.

10. B. F. Armaly and F. Durst, Reattachment length and recirculation regions downstream of two dimensional single backward facing step. In Momentum and Hear Transfer Process in Recirculating Flows, ASME HTD. – 1980. – Vol. 13. – P. l-7.

11. J. K. Eaton and J. P. Johnson, A review of research on subsonic turbulent flow reattachment, AfAA J. – 1981. – Vol. 19. – P. 1093-1100.

12. R. L. Simpson. A review of some phenomena in turbulent flow separation, J. Fluid Engng. – 1981. – Vol.103. – P. 52-530.

13. W. Aung, An experimental study of laminar heat transfer downstream of backsteps, J. Heat Transfer. – 1983. – Vol.105. – P. 823-829.

14. W. Aung, Separated forced convection, Proc. ASMEIJSME Thermal Enana Joint Con/ ASME. New York. – 1983. – Vol. 2. – P. 499-515.

15. W. Aung, A. Baron and F. K. Tsou, Wall independency and effect of initial shear-layer thickness in separated flow and heat transfer, Int. J. Hear Muss Transfer. – 1985. – Vol. 28. – P. 1757-1771.

16. W. Aung and G. Worku, Theory of fully developed. Combined convection including flow reversal, J. Hear Transfer. – 1986. – Vol. 108. – P. 485-488.

17. E. M. Sparrow, G. M. Chrysler and L. F. Azevedo. Observed flow reversals and measured-predicted Nusselt numbers for natural convection in a one-sided heated vertical channel, J. Heat Transfer. – 1984. – Vol. 106. – P. 325-332.

18. E. M. Sparrow, S. S. Kang and W. Chuck. Relation between the points of flow reattachment and maximum heat transfer for regions of flow separation. Inr. J. Hear Mass Transfer. – 1987. – Vol. 30. – P. 1237-1246.

19. E. M. Sparrow and W. Chuck, PC solutions for heat transfer and fluid flow downstream of an abrupt, asymmetric enlargement in a channel, Numer. Hear Transfer. – 1987. – Vol. 12. – P. 1940.

20. Chung T.J. Computational fluid dynamics. – 2002. – P. 1034.

21. Issakhov A., Mathematical modeling of the discharged heat water effect on the aquatic environment from thermal power plant // International Journal of Nonlinear Science and Numerical Simulation, – 2015. – Vol. 16(5). – P. 229–238, doi:10.1515/ijnsns-2015-0047.

22. Issakhov A., Mathematical modeling of the discharged heat water effect on the aquatic environment from thermal power plant under various operational capacities // Applied Mathematical Modelling, – 2016. – Vol. 40, Issue 2. – P. 1082–1096,

http://dx.doi.org/10.1016/j.apm.2015.06.024.

23. Issakhov A. Large eddy simulation of turbulent mixing by using 3D decomposition method // *J. Phys.: Conf. Ser.* – 2011. – Vol. 318(4). – P. 1282-1288, doi:10.1088/1742-6596/318/4/042051.

24. Chorin A.J. Numerical solution of the Navier-Stokes equations // Math. Comp. – 1968. – Vol. 22. – P. 745-762.

25. Karniadakis G. E., Kirby II R. M. Parallel Scientific Computing in C++ and MPI: A Seamless Approach to Parallel Algorithms and their Implementation. Cambridge University Press. – 2000. – P. 630.

26. Ngo I., Byon C., Effects of heater location and heater size on the natural convection heat transfer in a square cavity using finite element method, J. Mech. Sci. Technol. – 2015. – Vol. 29 (7). – P. 2995.

27. Oztop H. F., Abu-Nada E. Numerical study of natural convection in partially heated rectangular enclosures filled with nanofluids, Int. J. Heat. Fluid Fl. – 2008. – Vol. 29 (5). – P. 1326-1336.

IRSTI 30.51.23; 30.17.35; 28.17.23

[1*]A.S. Askarova, [1]S.A. Bolegenova, [1]S. A. Bolegenova,
[1]V.U. Maximov, [1]A.O. Nugymanova, [2]P. Safarik

[1]Faculty of physics and technology, al-Farabi Kazakh National University, Almaty, Kazakhstan
[2]Faculty of mechanical engineering, Technical University in Prague, Prague, Greece
[*]e-mail: aizhana0708@mail.ru

Combustion processes in furnace chambers of Kazakhstan TPPs using high-ash coal

Abstract. In this article, carried out computational experiments to study the aerodynamic, thermal and concentration characteristics in combustion chamber of the boiler BKZ-420 Almaty TPP-2. Combustion chamber BKZ-420 has a significant drawback, which is that of a jet of hot air hitting the wall that is opposite the burners. This leads to her firing and a further violation of integrity. On the Almaty CHP-2 in the basic mode using this wall served cold the air mass flow 5 kg/s. In this paper, we proposed a new flow mode, which allows you to protect the wall from overheating, to reduce the temperature of the incoming flow more cold air. Carried out researches have allowed to conclude that the proposed regime provides not only protection against overheating of the boiler walls, but also reduces the concentration of harmful emissions. As a result of computer experiments were obtained fields of velocity, temperature, concentrations of harmful dust and gas emissions (CO, CO2, NO2) formed in combustion of solid fuels for different layout options holes and speed boost-extra air (5kg/s and 10 kg/s).
Key words: numerical simulation, combustion chamber, temperature, air velocity, carbon dioxide, nitrogen dioxide.

Introduction

The main consumer of primary energy resources in Kazakhstan is the electricity and heat generation sector (about 50% of consumed fuel). The total capacity of power generating sources in the RK is more than 18 thousand MW. The basis of generating capacity is thermal power plants – about 87%. The main type of fuel and energy resources in Kazakhstan is coal, the supply of which is mainly from the Ekibastuz field. Burning fossil fuels to produce electrical energy and heat, especially the power industry, with its huge centralized power plants, is one of the foundations of the functioning of a modern society and economy. On the other hand, fuel-burning installations consume large amounts of fossil fuel of different types, converting them into useful energy. The functioning of these enterprises leads to the formation of a variety of waste and delivery of large quantities of contaminants in all natural environments.

In recent decades, the rapid growth in computing power and the continuous improvement of numerical algorithms has led to the extension of the range of applications available for study by computational methods. This increases the requirements to the mathematical models describing a certain class of application tasks, and accuracy of numerical methods for their implementation.

Relevant in the present time is the study of heat and mass transfer processes in industrial power plants, in particular, heating devices, thermal power plants operating on solid fuel. The goal of environmentally sound and efficient use of coal fuel to nominate important issues for research in this area. The solution to the problem of reducing harmful emissions of thermal power plants requires the development of new designs and optimization of operating modes of furnaces, and in General – development of scientific bases of creating ecologically clean thermal power plants for solid fuels. At the same time, physical modeling of real combustion processes or full-scale tests on boilers is characterized by extremely high cost. Consideration of modern thermal and environmental requirements in solving problems of development of perspective and modernization of existing designs of

 Printed in Kazakhstan

furnace facilities and optimization of their operating modes requires at present the attraction of numerical simulation methods for the comprehensive study of furnace processes.

However, the formation of complexes (packages) computer programs, sufficiently accurate and versatile to conduct serial numerical experiment on modeling of the totality of the combustion process, remains an urgent task.

Experimental part

As object of research was selected combustion chamber of the boiler BKZ-420, with steam capacity 420 t/h, located at the Almaty CHP-2. The boiler BKZ-420-140-7 designed to work on the Ekibastuz coal for generation of superheated steam in thermal power plants with cogeneration turbines with high steam parameters. Scheme of the combustion chamber of the boiler and its breakdown into control volumes is shown in figure 1, and the input data used in conducting computational experiments are summarized in table 1.

The combustion chamber of the boiler (figure 2) is equipped with six-vortex flow of the two pulverized coal burners arranged in two levels with three burners on the front wall of the boiler. Extreme burner is turned to the center of the furnace by 8 degrees. The capacity of one burner is 12 t/h of Ekibastuz coal. In the furnace burned dust low-grade high-ash Ekibastuz coal ash content 40%, a volatiles 24%, moisture 5% and the highest calorific value of 16.750 kJ/kg. Fineness of grinding of coal was equal to R90 = 15 %. All numerical calculations were performed on the above-mentioned technique [1-7].

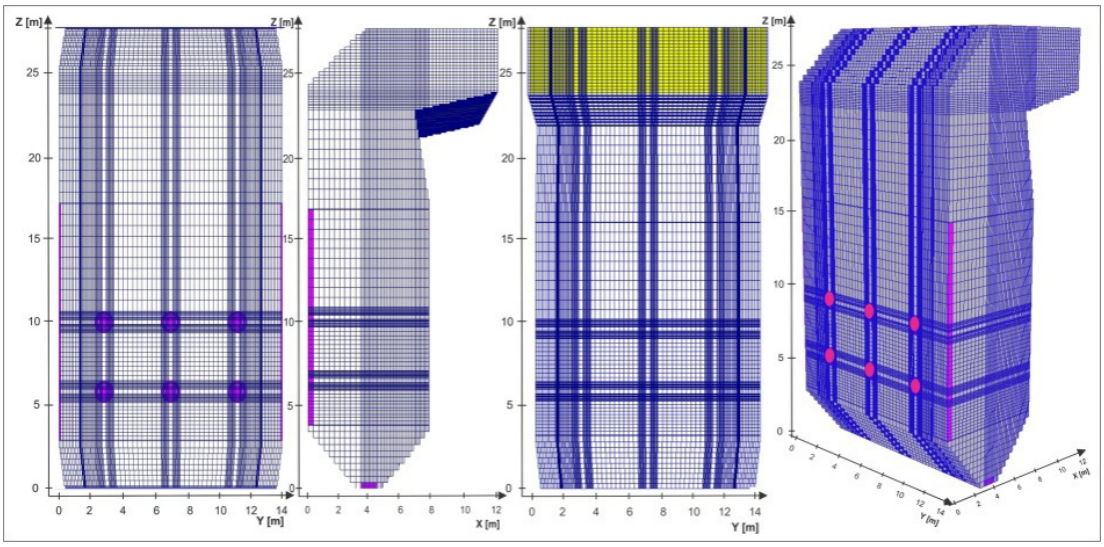

Figure 1 – General view of the combustion chamber of the boiler BKZ-420 Almaty TPP-2 and its breakdown into control volumes

Table 1 – Technical characteristics of the boiler BKZ-420 and input data for numerical simulation

№	Name	Designation	Size	Meaning
	Humidity	W_r	%	5
	Ash	A_r	%	40.0
	The lowest calorific value	Q_r	kcal/kg	4000
	Devolatilization	V_{daf}	%	24-28
	Sulfur	S_t	%	0.4-0.7
The elemental composition of the fuel mass				
	Carbon	C_{daf}	%	82.0
	Hydrogen	H_{daf}	%	5.0

Continuation of Table 1

	Nitrogen	N_{daf}	%	1.5
	Oxygen	O_{daf}	%	11.5
	The number of boilers at thermal power plants	N_B	pieces	7
	One of the kindling according to the regulations	t	hour	3.5÷4
	Fuel consumption for the boiler (at full load)	B	t/h	72
Type burners		Vortex dual stream		
	The number of burners in the boiler	N_B	pieces	6
	The performance of one of the burner fuel	B_B	t/h	12
	The temperature of Aero mixture after mills	t_a/cm	℃	90÷130
	The primary air flow per burner (two separate channels)	$V_{P.B.}$	$Nm^3/h *10^3$	13860 (17879.4 kg/h)
	The flow of secondary air to the burner (two channels)	$V_{S.B}$	$Nm^3/h *10^3$	52140 (67260.6 kg/h)
	The temperature of hot air	$T_{H.A.}$	°C	280÷340
	The coefficient of excess air for furnace	α_F		1.1÷1.4

Results and discussion

This paper presents results of 3-D modeling of Ekibastuz coal burning in furnace of boiler BKZ-420 Almaty TPP-2 for two variants of the flow of additional air through the holes located on the opposite wall burners and is shown in figure 2.

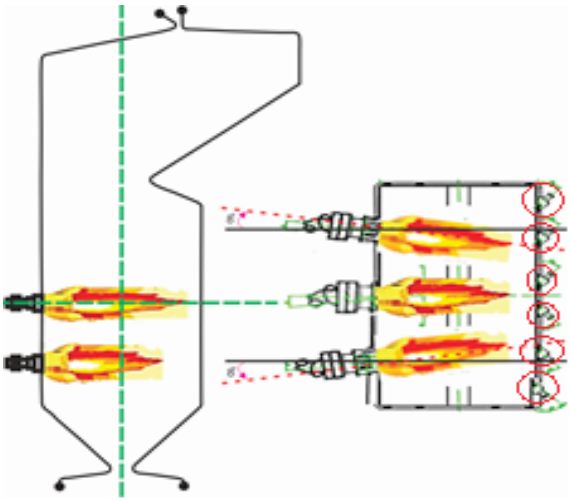

Figure 2 – General view of the industrial boiler BKZ-420 Almaty TPP-2

The burning of fuel at the Almaty TPP -2 is carried out when the value of the mass air flow 5 kg/s through the holes in the wall of the combustion chamber located opposite the burner (see Fig. 2). In the course of research work we have proposed a new mode of operation for CHP-2, when the flow rate is doubled, and the holes are located at an angle of 45° to the wall of the boiler. The choice of angle of 45° creates the condition for the formation of the arc stream, which protects the walls from overheating and helps to reduce the temperature of the return flow.

As a result of computational experiments on the aerodynamics of the process was constructed of the distribution of the vector full speed, which are shown in figures 3-5.

Figure 3 shows the distribution of the vector of full speed in the longitudinal section (y=7.18 m) of the boiler BKZ-420 at a mass flow equal to 5 kg/s (figure 3 a) and 10 kg/s (figure 3 b) and directed from the wall opposite the burners.

Analyzing figure 3, we see that the flows from the lower burners, colliding with the opposite wall, forming a return current. Part of the flow towards the cold region of the funnel forms the bottom of the vortex. Another part is directed upward to the region of the upper burners and openings for secondary air, which also generated turbulence. Maximum values of velocity is in the region of the pulverized coal burner secondary air.

Comparing figures 3 (a) and 3 (b), we note that with increasing mass flow of air from the anti-burners, increases the turbulence as well as maximum, average and minimum speed values. The maximum speed value for the first case is equal to 36.6 m/s, and the second 38 m/s When the mass flow rate of air is 10 kg/s flow of Aero mixture and air create turbulence above and below the upper burners. The formation of the turbulent eddies creates the best conditions for complete combustion of pulverized coal.

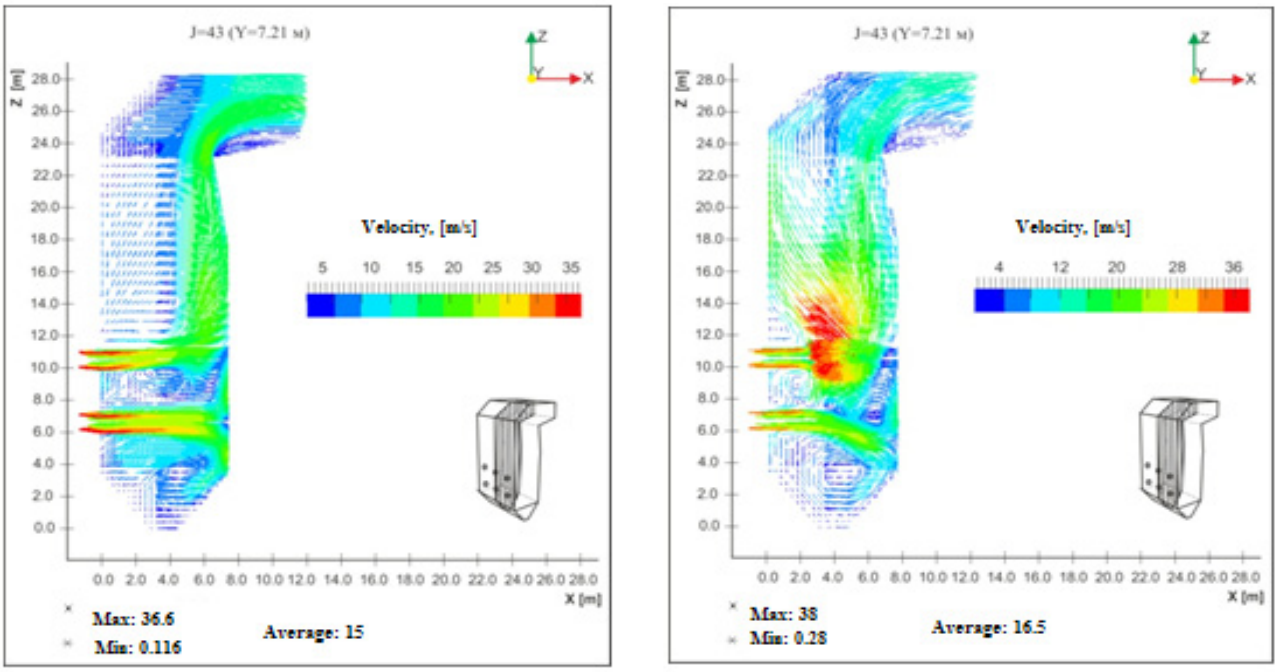

a) 5 kg / s b) 10 kg / s

Figure 3 – Distribution of the vector of full speed in the Central longitudinal section (y=7.18 m) of the combustion chamber of the boiler BKZ-420 Almaty TPP-2

Figure 4 (a and b) shows the distribution of the vector of full speed in the longitudinal section of the combustion chamber (X=4m), located closer to the burners, for different values of the mass flow of air (5kg and 10kg). From the drawings it is seen that in each case at equal speeds of expiry of Aero mixture (coal dust+primary air) from the burner devices, counter flows collide and, due to the presence of the suction cups through the bottom hole in the lower part of the furnace and to form in the area of two longitudinal cold funnel of the vortex.

Formed in this region, the vortices create the conditions for uniform heating of the walls of the combustion chamber and solve the problem of slagging of furnace screens, which prolongs the service life of individual elements of the boiler plant and increases the surface of heat removal.

A large swirling flow in the Central region of the combustion chamber is beneficial to the combustion process of pulverized coal due to the turbulent nature of the flow, there is an intensive mixing of the propellant with the oxidant, and thus provides a more complete burnout of coal dust, and this in turn has to use larger fractions of coal particles.

The use of large fractions of the particles of pulverized coal reduces the cost of dust-preparation of coal, transportation and feeding it into the combustion chamber that is more cost-effective. In addition, such an arrangement of furnace processes (figures 3-4) eliminates the need for the installation of devices for the introduction of secondary air to assist combustion of the coal particles, which undoubtedly would have led to an increase in heat losses and increased formation of harmful dust and gas emissions from the combustion chamber into the atmosphere.

5-the figure shows the distribution of the full velocity at 6 m from the burner along the X axis or on the opposite wall from the area burners on 2 m. one Can notice that the velocity values in figure 5 in comparison with its values in figure 4. This is because of the holes on the burners on the opposite wall serves an additional stream of air with high velocity. Figure 5 (b), we see that the maximum speed is 80 m/s. This value 2 times greater than the rate in figure 5 (a).

5-the figure shows the distribution of the full velocity at 6 m from the burner along the X axis or on the opposite wall from the area burners on 2 m. one Can notice that the velocity values in figure 5 in comparison with its values in figure 4. This is because of the holes on the burners on the opposite wall serves an additional stream of air with high velocity. Figure 5 (b), we see that the maximum speed is 80 m/s. This value 2 times greater than the rate in figure 5 (a).

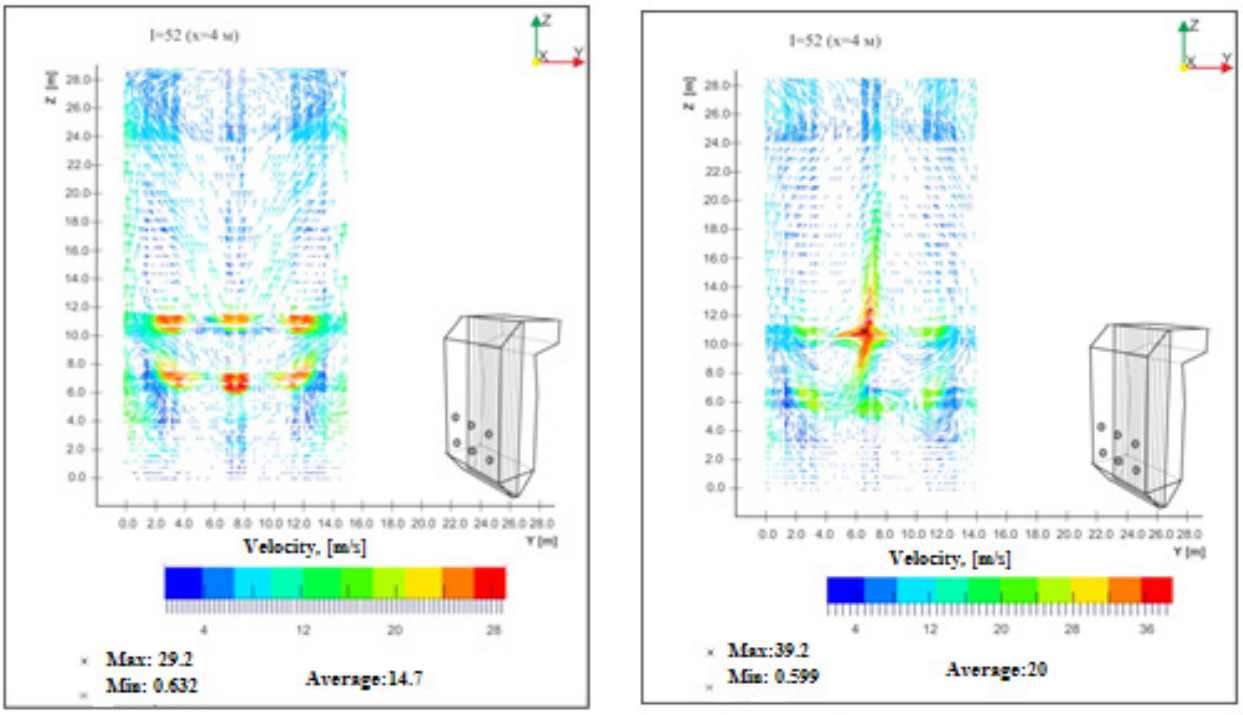

a) 5 kg / s b) 10 kg / s

Figure 4 – Distribution of the vector of full speed in the center of the longitudinal sections of the combustion chamber (X=4 m)

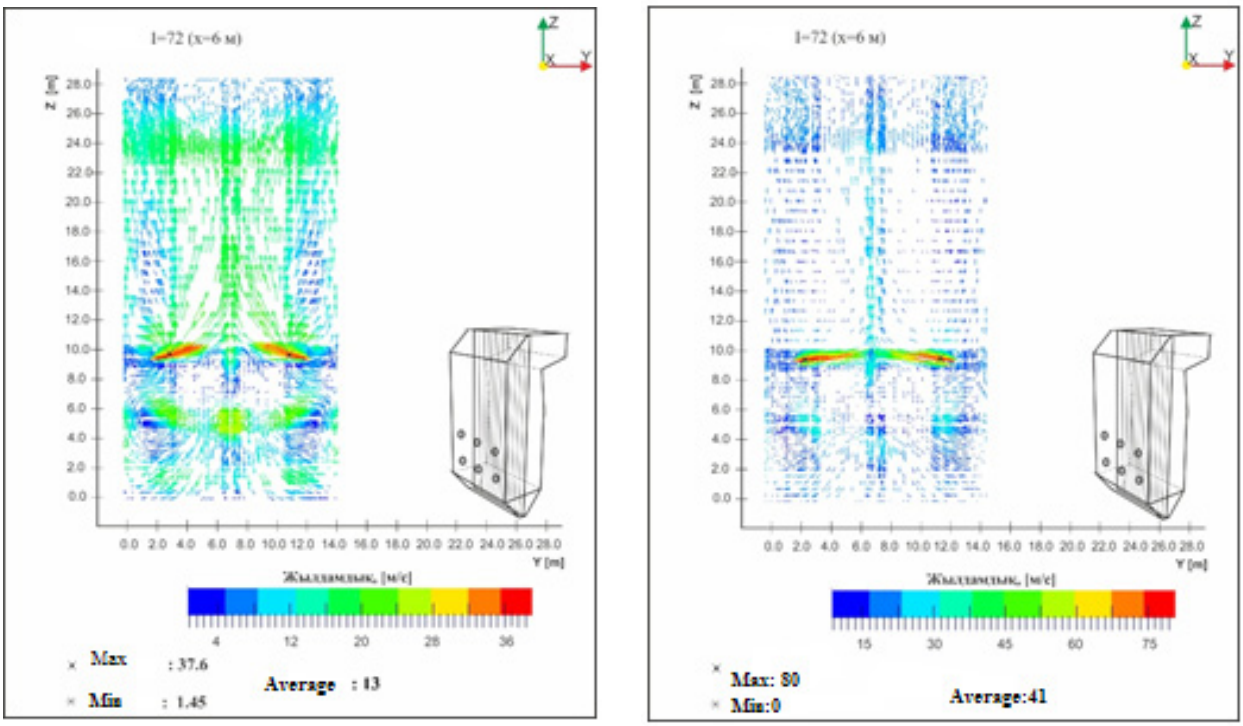

a) 5 kg / s b) 10 kg / s

Figure 5 – Distribution of the vector full speed in the center of the longitudinal sections of the combustion chamber (X=6 m)

Figure 6 shows a three-dimensional field of temperature distribution in two longitudinal sections (Y1 = 2.95 m and Y3 = 11.4775 m) of the combustion chamber located in areas of extreme burners of the upper and lower tiers. We see that the flow of additional air, equal to 5 kg/s maximum temperature is observed at the wall located opposite to the burners and is equal to 1740°C in the lower arusu burner (Z = 6.82 m). And at an air flow of 10 kg/s (figure 6b) one can notice that the temperature at the wall has significantly decreased to about 350°C.

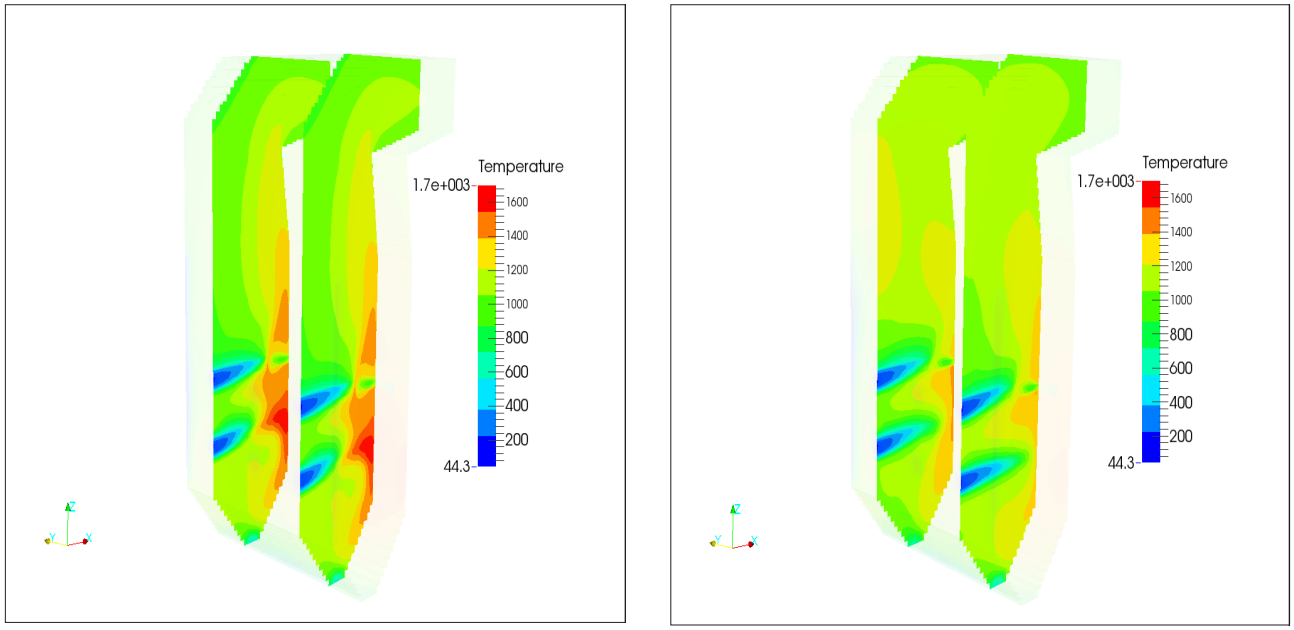

a) 5 kg / s

b) 10 kg / s

Figure 6 – Three-dimensional distribution of the temperature field in longitudinal cross-section Y1 = 2.95 m and Y3 = m 11.4775 of the combustion chamber

Figure 7 shows the temperature distribution in the longitudinal section along the X-axis (X = 4.01 m). From the analysis of figure shows that at low mass flow rate of air (5kg/s) of counter burners torch is formed in a region between the burners (figure 7a), while at higher flow rate (10 kg/s) temperature field (figure 7 b), as it were, in the sky, height of the furnace.

Figure 8 shows the temperature field at the outlet of the combustion space for the two values of the air flow from holes: 5 kg/s and 10 kg/s. As can be seen from the drawings, in the second case (figure 8 b) the area of high temperatures is less than in the first case (figure 8 a).

Since the burner and the holes for secondary air is installed on the opposite walls and directed towards each other, in the center of the furnace in the zone of contact flows, as mentioned earlier, the cut. Part of the flow goes into the area of the cold funnel, forming two longitudinal vortex at a height of below 10.8 m and the part formed by thrust, heading for the exit. Next, as you move to the exit of the furnace and chemical processes weaken (figure 6), the temperature falls and the output of its average value is ~1045°C for flow rates of 5 kg/s (figure 6 a) and 987°C – flow rate 10 kg/s (figure 6 b).

The above is confirmed by two-dimensional graphs of the temperature distribution along the height of combustion chamber for two different mass flows of additional air through the opening shown in figure 9. The analysis of the figure shows that at a height of z_1=6.82 and z_2=10.8 meters burner is pumped through the cold hole, there are minima in the temperature distribution. The output of the camera when the mass air flow 5 kg/s temperature value higher than the supply at 10 kg/s.

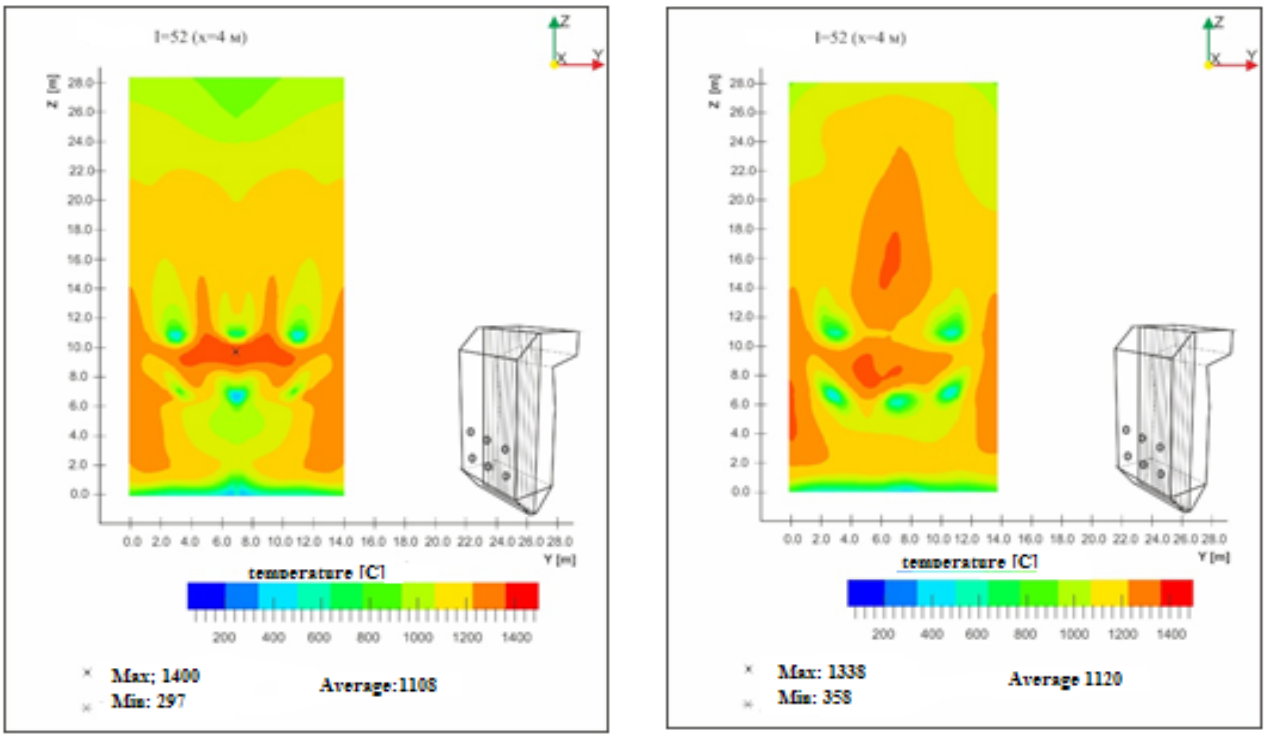

a) 5 kg / s b) 10 kg / s

Figure 7 – Temperature field in longitudinal section of X=4.01 m for different values of mass air flow

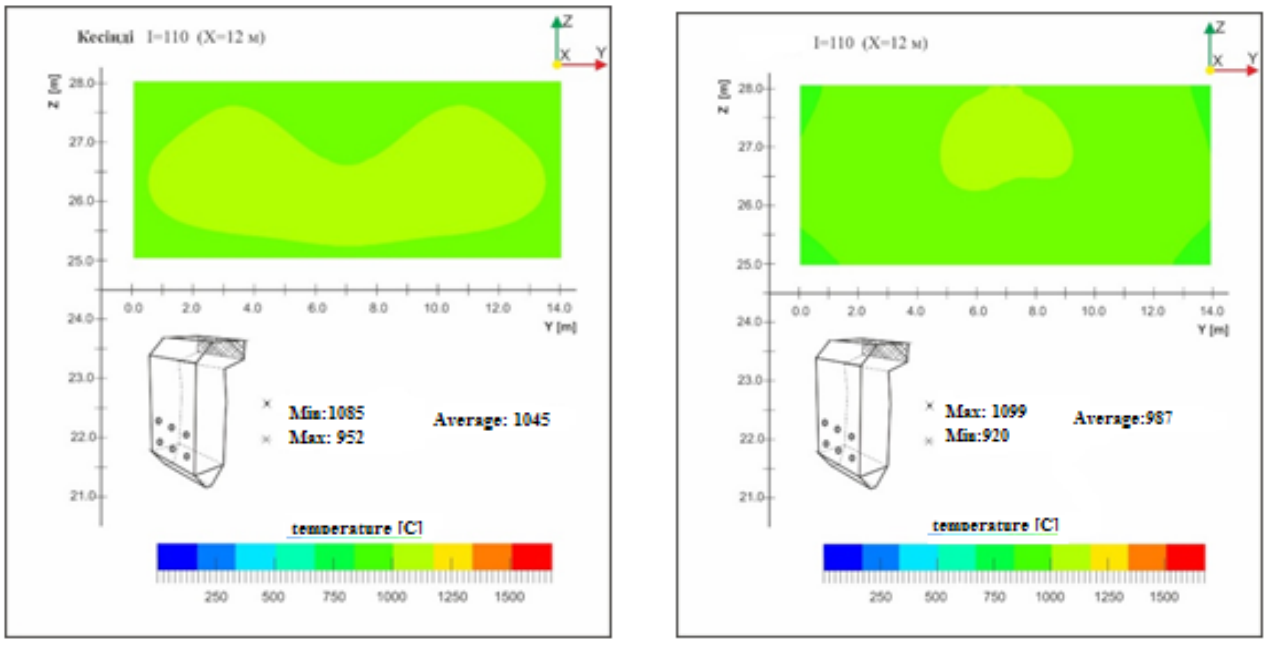

a) 5 kg/s b) 10 kg/s

Figure 8 – Temperature field at the exit of combustion chamber (X=12 m)

This is because in this area are located the burner through which pulverized coal is supplied fuel and oxidizer at a temperature lower than the temperature of the camera. In the region of the belt burners are observed and the maximum temperature, because here is the core of the torch.

The outlet temperature of the furnace is supported by its experimental value (T=1171 °C), obtained directly in the CHP, are given in [8-10] and numerical [11]. Comparing these values, we can conclude: conducted a computational experiment to determine temperature in volume of the combustion chamber, with sufficient accuracy consistent with the measured values of temperature (figure 9). This allows you to judge the reliability of the obtained results and the applicability of physical, mathematical and numerical models to further study the thermal and concentration characteristics of combustion chamber BKZ 420 Almaty TPP-2 [12]. For more references, see [13] – [21].

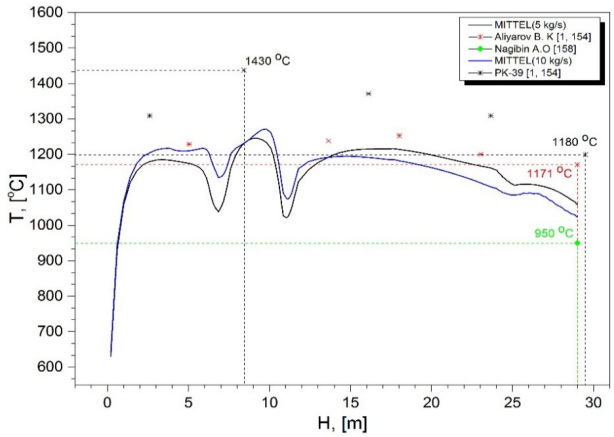

Figure 9 – Average temperature in the height of the boiler furnace

Figure 10 shows the distribution of average values of concentrations of carbon monoxide CO at the height of the furnace for two different values of the mass flow of additional air through the holes located on the opposite burner wall. We see that as a three-dimensional color graph of the temperature field at the exit of the combustion chamber at a mass flow equal to 5 kg/s, the concentration value of carbon monoxide CO higher in comparison with the case where the flow rate is 10kg/s.

Analysis figure 10 shows that the maximum of both curves reach the region of the burners. This is because the largest concentrations coming into this part of the furnace carbon fuel and oxygen oxidizer, the intensity of physic-chemical interaction between them, causing here a strong increase in temperature and large heat release due to chemical reactions between the propellants and oxidizer.

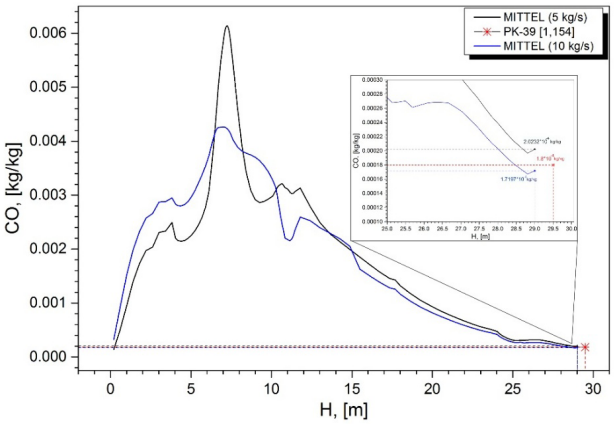

Figure 10 – distribution of the concentration of carbon monoxide CO at the height of the combustion chamber

Figure 11 shows a comparative graph of the distribution of average values of carbon dioxide CO_2 the height of the combustion chamber for the two values of mass air flow 5 kg/s and 10 kg/s.

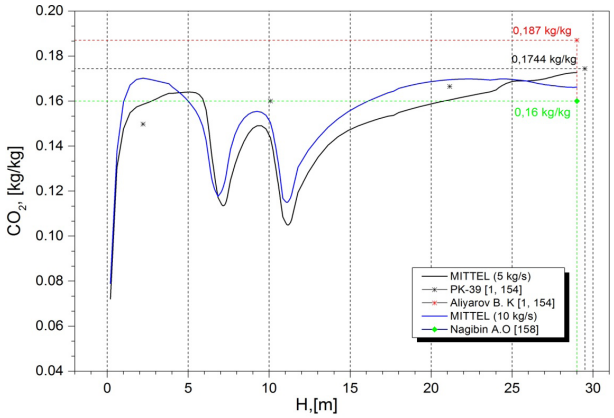

Figure 11 – distribution graph of mean values of carbon dioxide CO_2 the height of the combustion chamber for different values of the mass flow of the additional air

By analyzing this chart you can see that in the location field of burners, and above them, the concentrations of carbon dioxide for the case when the flow of additional air through openings in the wall of the combustion chamber located opposite the burner units equal to 10 kg/s higher than for the air flow 5 kg/s.

Figure 12 shows the comparative distribution of the mean concentrations of NO_2 at the height of the furnace. Analyzing the picture, you will notice that as you move to the exit of the combustion chamber, the concentration of nitrogen dioxide decreases. It is primarily associated with the destruction of nitrogen dioxide NO_2 and its interaction with hydrocarbons, carbon, oxygen, etc., with the decrease of temperature in the upper layers of the gas mixture and of course a decrease in these areas, nitrate concentrations of fuel and oxidant, which is already chemically reacted in the bottom region of the burners.

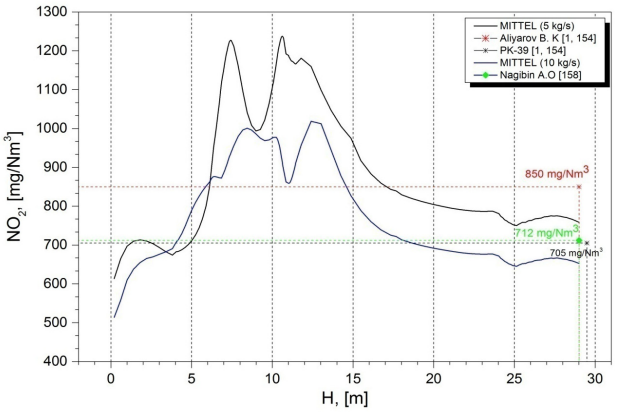

Figure 12 – Graph of the distribution of average values of nitrogen dioxide NO_2 at the height of the furnace for different values of the mass flow of the additional air

Conclusion

By results of researches, we can draw the following conclusions

Computational experiments on the study of aerodynamic, thermal and concentration characteristics in combustion chamber of the boiler BKZ-420 Almaty TPP and the resulting velocity field, temperature, concentrations of harmful dust and gas emissions (CO, CO_2, NO_2) from the combustion of pulverized coal for different layout options holes and speed boost-extra air (5kg/s and 10 kg/s).

Developed by optimum technology for burning high-ash fuel and energy and the best structural parameters of the combustion chamber of the boiler BKZ-420 Almaty TPP, which allows increasing the wear resistance of power and reducing the emission of harmful substances into the atmosphere. The proposed incineration of Ekibastuz coal lowers the temperature of the walls of the furnace located opposite to the burners at 3000□, i.e., by 17.24%, and reduces average concentrations of carbon monoxide at the outlet of the furnace by 15%, carbon dioxide CO_2 by 4.65% and nitrogen dioxide NO_2 by 14% .

References

1. Askarova A., Bolegenova S., Bekmukhamet A., Maximov Yu.V., Beketayeva M., Ospanova Sh. Gabitova Z.K. Investigation of turbulence characteristics of burning process of the solid fuel in BKZ 420 combustion chamber // WSEAS Transactions on Heat and Mass Transfer. –2014. – Vol. 9. –P. 39-50.

2. Askarova A.S., Bekmukhamet A., Bolegenova S.A., Beketayeva M.T., Maximov Yu.V., Ospanova Sh.S., Gabitova Z.K. Numerical modeling of turbulence characteristics of burning process of the solid fuel in BKZ-420-140-7c combustion chamber // International Journal of Mechanics. – ISSN: 1998-4448. – 2014. – Vol. 8. – P. 112-122.

3. Askarova, A. S., Messerle, V. E., Ustimenko, A.B., Bolegenova, S. A., Maximov, V. Yu. Gabitova, Z. Kh. Numerical simulation of pulverized coal combustion in a power boiler furnace // High temperature. – 2015. – Vol. 53, issue 3. – P. 445-452.

4. Askarova, A. S., Bolegenova, S.A., Maximov, V.Y., Bekmukhamet, A, Beketayeva, M.T. Gabitova, ZK., etc. Computational method for investigation of solid fuel combustion in combustion chambers of a heat power plant // High temperature. – 2015. – Vol. 5, issue 5. – P. 751-757.

5. Askarova, A. S., Bolegenova, S.A., Maximov, V.Y., Bekmukhamet, A, Ospanova, S.S. Numerical research of aerodynamic characteristics of combustion chamber BKZ-75 mining thermal power station // Procedia Engineering. – 2012. – Vol.42. – P. 1250-12-59.

6. Askarova A., Bekmukhamet A., Bolegenova S., Ospanova Sh., Bolegenova Symbat, Maximov V. Beketayeva M., Gabitova Z., Ergalieva A. 3D modeling of heat and mass transfer during combustion of solid fuel in BKZ-420-140-7c combustion chamber of Kazakhstan // Journal of Applied Fluid Mechanics. – 2016. – P. 699-709.

7. Askarova, A. S., Messerle V.E., Ustimenko A.B., Bolegenova, S.A., Bolegenova, S.A., Maximov, V.Y., Ergalieva A. Reduction of noxious substance emissions at the pulverized fuel combustion in the combustor of the BKZ-160 boiler of the Almaty heat electropower station using the “Overfire Air” technology // Thermophysics and aeromechanics. – 2016. – Vol 23, issue 1. – P. 125-134.

8. Askarova, A. S., Bolegenova, S.A., Maximov, V.Y., Bekmukhamet, A, Beketayeva M., Gabitova Z. Control of Harmful Emissions Concentration into the

Atmosphere of Megacities of Kazakhstan Republic // International Conference on Future Information Engineering (FIE2014), IERI Procedia. – Beijing, PEOPLES R CHINA. – 2014. –P. 252-258.

9. A. Askarova, S. Bolegenova, S. Bolegenova, V. Maximov, Manatbayev R, A. Yergaliyeva, Z. Gabitova, A. Maxutkhanova, Zh. Shortanbayeva, A. Boranbayeva, K. Berdikhan Application of 3D modelling for solving the problem of combustion coal-dust flame // Bulgarian Chemical Communications. – Special Issue E. – 2016. – P. 236-241.

10. A. Askarova, S. Bolegenova, N. Mazhrenova, Symbat Bolegenova, R. Manatbayev, I. Berezovskaya, V. Maximov, Sh. Ospanova, A. Nugymanova, Zh. Shortanbayeva 3D modelling of heat and mass transfer processes during the combustion of liquid fuel // Bulgarian Chemical Communications. – Special Issue E. – 2016. – P. 229-235.

11. A.S. Askarova, E. I. Heierle, S. A. Bolegenova, V. Ju. Maximov, S. A. Bolegenova, Manatbayev R, M. T. Beketaeva, A. B. Ergalieva CFD study of harmful substances production in coal-fired power plant of Kazakhstan // Bulgarian Chemical Communications. – Special Issue E. – 2016. – P. 260-265.

12. A.S. Askarova, S.A. Bolegenova, Symbat Bolegenova, V.Yu. Maximov, R. Manatbayev, Zh.K. Shortanbayeva, A.M. Maksutkhanova, A.N. Aldiyarova, A.E.Boranbayeva Mathematical modeling of heat and mass transfer in the presence of physical-chemical processes // Bulgarian Chemical Communications. – Special Issue E. – 2016. – P. 272-277.

13. M. Bugge, O. Skreiberg, N.E. Haugen, P. Carlsson, E. Houshfar, T. Lovas, Numerical simulations of staged biomass grate fired combustion with an emphasis on NOx emission, Energy Procedia. – Vol. 75. – 2015. – P.156–161.

14. W. Adamczyk, P. Kozolub, G. Wecel, A. Ryfa, Simulations of the PC boiler equipped with complex swirling burners, Int. J. Numer. Methods Heat Fluid Flow. – Vol. 25 (4). – 2014. – P.845–860.

15. B. Higgins, L. Yan, H. Gadalla, J. Meier, T. Fareid, G. Liu, M. Milewicz, A. Repczynski, M. Ryding, W. Blasiak, Biomass co-firing retrofit with ROFA for NOx reduction, Pol. J. Environ. Stud. – Vol. 19 (6). – 2010. – P.1185–1197.

16. F. Lockwood, S. Rizvi, N. Shah, Comparative predictive experience of coal firing, Proc. Inst. Mech. Eng. C J. Mech. Eng. Sci. – Vol. 200 (23). – 1986. – P.79–87.

17. M. Baum, P. Street, Predicting the combustion behavior of coal particles, Combust. Sci. Technol. – Vol. 3 (5). – 1971. – P.231–243.

18. L. Alvarez, M. Gharebaghi, M. Pourkashanian, A. Williams, J. Riaza, C. Pevida, J. Pis, F. Rubiera, CFD modelling of oxy-coal combustion in an entrained flow reactor, Fuel Process. Technol. – Vol. 92. – 2011. – P.1489–1497.

19. M. Cloke, E. Lester, A. Thompson, Combustion characteristics of coals using a drop-tube furnace, Fuel. – Vol. 81 (6). – 2002. – P.727–735.

20. H. Kruczek, M. Ostrycharczyk, M. Czerep, M. Baranowski, J. Zgra, Examinations of the process of hard coal and biomass blend combustion in OEA (oxygen enriched atmosphere), Energy. – Vol. 92. – 2015. – P.40–46.

21. S. Du, W. Chen, J. Lucas, Pulverized coal burnout in blast furnace simulated by a drop tube furnace, Energy. – Vol. 35. – 2015. – P.576–581.

IRSTI 44.37.29

A.M. Zhukeshov, *A.T. Gabdullina, A.U. Amrenova, M. Sagymbaeva, A. Berdalin

al-Farabi Kazakh National University, Almaty, Kazakhstan
*e-mail: gabdullyna71@gmail.com

The study of the heat power effectiveness of a parabolic solar concentrator

Abstract. In this paper, the results of research work on the development of an experimental device based on a parabolic solar concentrator. The concentrator dish was radiated by line parabolic solar imitator. The concentrator, have designed on the basic of satellite dish with different reflecting covers. Two tips of layers: aluminium plates and silver paint were used. In this work the focus of the parabolic concentrator was determined: is equal 0,56 m. The concentrator dish was radiated by line parabolic solar imitator. The temperature in the focus zone was actually obtained in full-scale tests concentrator and was 400 ^{0}C. The temperature is directly proportional to the illumination. The illumination parameter was measured by industrial luxmeter and at distance 2 m brightness of source is reduced to approximately 500 Lux. The brightness more the 500 lux concentrated on the focus area with square about 9 cm^2. The distribution of brightness on cross section area was determined.

Key words: parabolic solar concentrator, heat power effectiveness, aluminium plate, silver paint, full-scale tests, distribution of brightness.

Introduction

The acute environmental problems in the world and depletion of fossil resources set the task of developing reliable and efficient solar energy converters. In this regard, in the world there is a certain demand for power plants with a concentration of solar energy. Using a solar concentrator to focusing of the sun's rays is an effective method for obtaining an alternative energy source. Thermal radioactive transport continues to emerge as an important energy transfermechanism in a wide variety of practical systems such as high-temperature heatexchangers, boiler, rocket propulsion system and material sciences.

Many researches related to parabolic concentrators are found. J. Kleih [1] has been setting up a test facility for parabolic dish systems with power conversion unit in their focus. R.Y. Nuwayhid*et al.* [2] was realized a simple solar tracking concentrator for university research applications. C.A. Pérez-Rabago*et al.* [3] treated heat transfer in a conical cavity calorimeter formeasuring thermal power of a point focus concentrator. In work [4] A.R. El Ouederni1 *et al.*designed and experimentally studied of parabolic solar concentrator.

In general solar concentrating systems comprise a reflective surface in the shape ofparaboloid of revolution intended to concentrate solar energy on an absorbing surface,which makes it possible to reach a high temperature.This process gives the possibility to use solar energy in many high temperatureapplications. But the manufacture of the most of these systems is very expensive due tomaterials quality, dimensions and precision. So that, many authors worked to reduce thecost of this kind of systems [5, 6]. For more information, we refer to [8, 9, 10]

For Kazakhstan, which has significant resources of solar energy, the development of solar concentrator is justified. However, for the development of solar concentration power plants, it is necessary to study of their work and engineering features.In this work the task was set to develop a technique for determining the energy parameters of a laboratory installation based on a solar concentrator. It was also necessary to make an experimental station for approbation of the lighting and positioning system.

 Printed in Kazakhstan

Experimental devices

The reflector of our experimental device consists of a parabolic concentrator of 0.6 m opening diameter. Its interior surface is covered with a reflecting layer. We used two tips of layers: aluminum plates and silver paint. The reflection coefficients of this material used in the creation of the concentrators 0.78 and 0.25 respectively.

Which reflect solar rays on the face of a receiver placed at the focal position of the concentrator. The geometric parameters of the concentrator and the copper receiving disk is:

Diameter of the parabolic concentrator is equal $D = 0.6$ m.

Area of the parabolic concentrator was calculated is equal S= 0.28 m^2.

Depth of the parabolic concentrator $h = 0{,}04$m.

The focus of the parabolic concentrator determined by:

$$f = \frac{d^2}{16 \times h}$$

is equal 0,56 m. Diameter of the receiving disk: d = 5cm, thickness of the receiving disk: H = 0.08 cm and mass of the receiving disk: m = 14g. Gain factor: $k = 2{,}33$.

The concentrator dish was radiated by line parabolic solar imitator. The light source made with halogen lamp at 1500 W AT power. In this device we used nickel hard cover reflector. The light source was positioned on the centum of dish and at several distances from focus point of concentrator.

The concentrator, have designed on the basic of satellite dish with different reflecting covers, the light source and the receiving disk showed on the picture 1. The tracer system for this device was described on work [7].

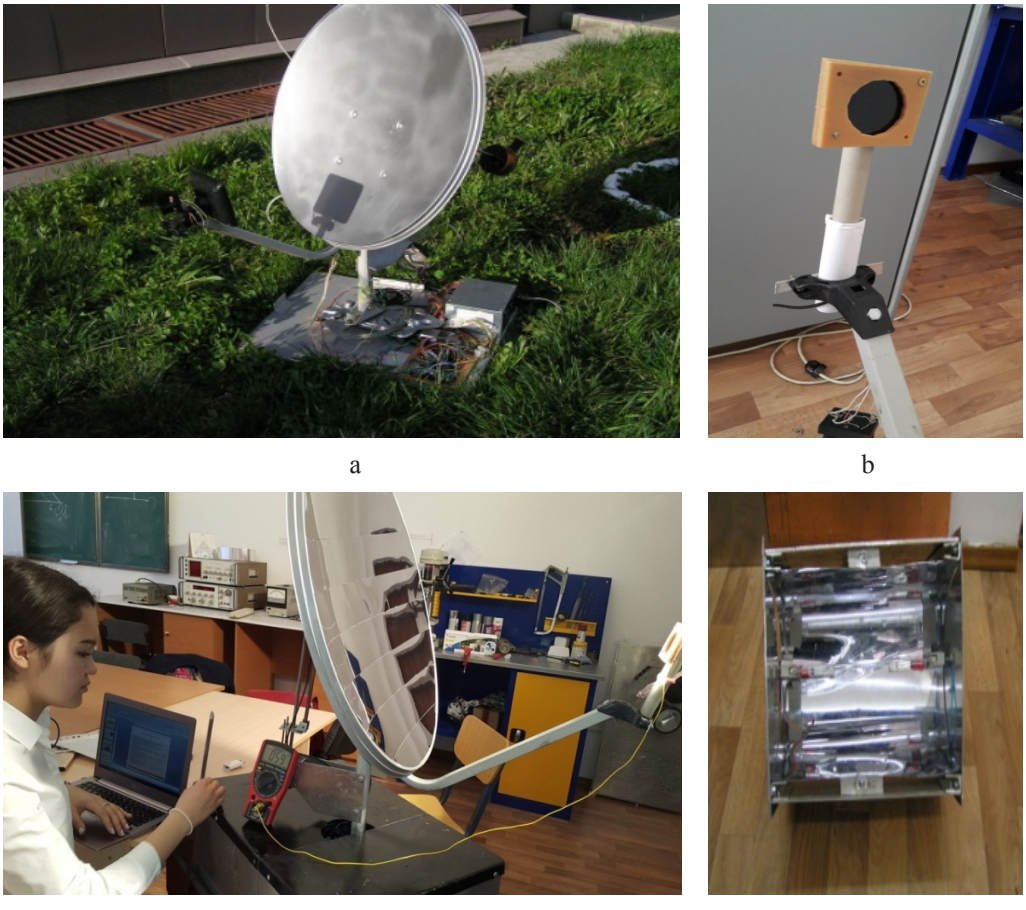

a b c d

a, c – the satellite dish with different reflecting covers; b, d – the light source and the receiving disk

Figure 1 – The experimental devices

Results

At first we determined the light source parameters. The illumination parameter was measured by industrial luxmeter. The illumination dependence from distance of light face is shown on the Figure 2. So, at distance 2 m brightness of source is reduced to approximately 500 Lux. The distribution of brightness on cross section area with square 10x10 dm^2 on this distance shown on the table 1.

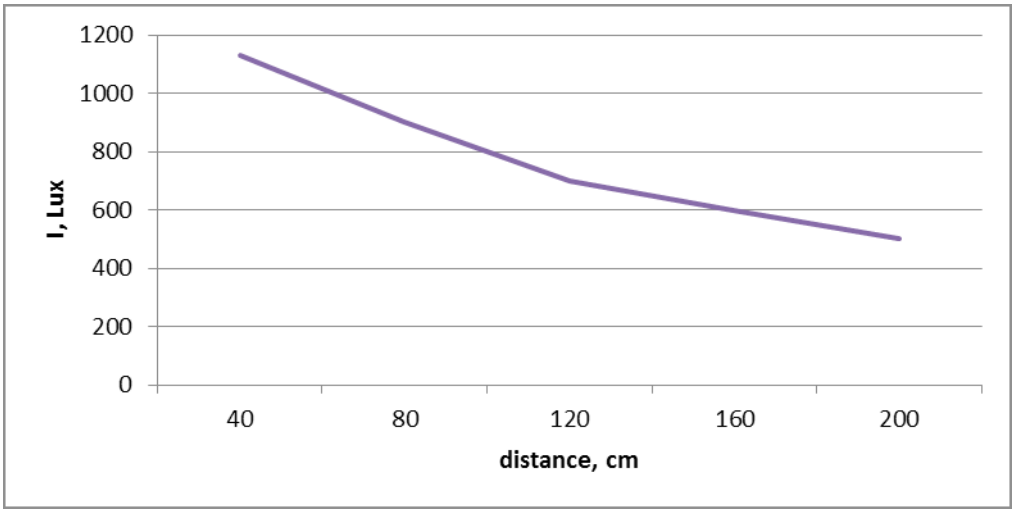

Figure 2 – The Illuminance from distance of source

Table 1 – The brightness on the wall on 2 m distance from light source

2	3	3	5	6	7	8	9	10
366	373	378	384	382	375	369	365	355
387	397	405	415	413	402	395	386	373
420	430	445	453	448	441	434	426	410
430	441	448	453	455	448	442	436	420
445	454	461	468	463	455	448	440	430
442	452	457	465	462	454	447	439	432
422	432	440	449	446	442	433	424	417
418	425	433	440	438	433	425	412	399
384	395	404	413	415	407	400	393	380
361	366	373	386	378	371	366	362	354

Then we stand light source at 2 m distance and illuminate the concentrator dish and measured the radiation parameters on their focus area. The results of experiments shown on the figure 3.

On this experiment, we determined the exact location of the focus where the receiving disk was placed, to further study the effectiveness of the focusing properties of the solar concentrator. The Illumination at the concentrator focus in lux shown on the table 2.

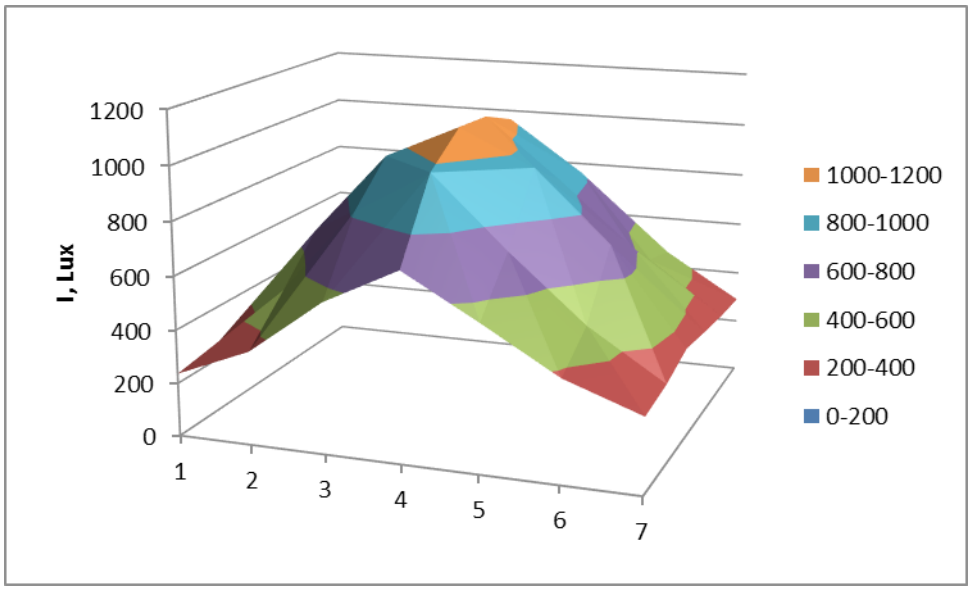

Figure 3 –The Illuminance of focus area

Table 2 – The brightness on the focus area with square 7x6 cm^2

см	1	2	3	4	5	6	7
1	236	350	560	700	543	380	280
2	257	500	820	980	720	480	300
3	260	660	964	1090	960	700	342
4	243	565	946	1080	860	623	320
5	220	470	720	1020	830	500	301
6	210	309	604	740	656	460	290

Thus, the brightness more the 500 lux concentrated on the focus area with square about 9 cm^2.

Temperature measurements. Power density

The energy of light on the focus area can determined by equation

$$Q = cm\,(T_2 - T_1)$$

where c is heat capacity of receiver material, m- mass of receiver and T2 is finish temperature.

In the steady state, the energy flux density transmitted by thermal conductivity is proportional to the temperature gradient:

$$\vec{q} = -\varkappa\,\mathrm{grad}(T),$$

where q is the heat flux density vector is the amount of energy passing per unit time per unit area perpendicular to each axis, κ is the coefficient of thermal conductivity (specific heat conductivity), and T is the temperature. The minus sign on the right shows that the heat flux is directed opposite to the grad T vector (i.e., in the direction of the soonest temperature decrease). This expression is known as the Fourier thermal conductivity law.In integral form, the same expression will be written this way (if it is a stationary flow of heat from one face of the parallelepiped to another):

$$P = -\varkappa\frac{S\Delta T}{l},$$

where P is the total heat loss power, S is the sectional area of the parallelepiped, ΔT is the temperature difference of the faces, l is the length of the parallelepiped, that is, the distance between the faces.

At first we used cylindrical copper receiver for determination of heat energy,realized on focus area, measured by calorimetrical method. On the figure 4 showed the temperature dependence on receiving disk from radiating time in the focus of concentrator by light source positioned at 2 m from dish.

The dependence of the heating temperature of the receiving disk on time in the focus of the concentrator with aluminum plates is shown in Figure 5.

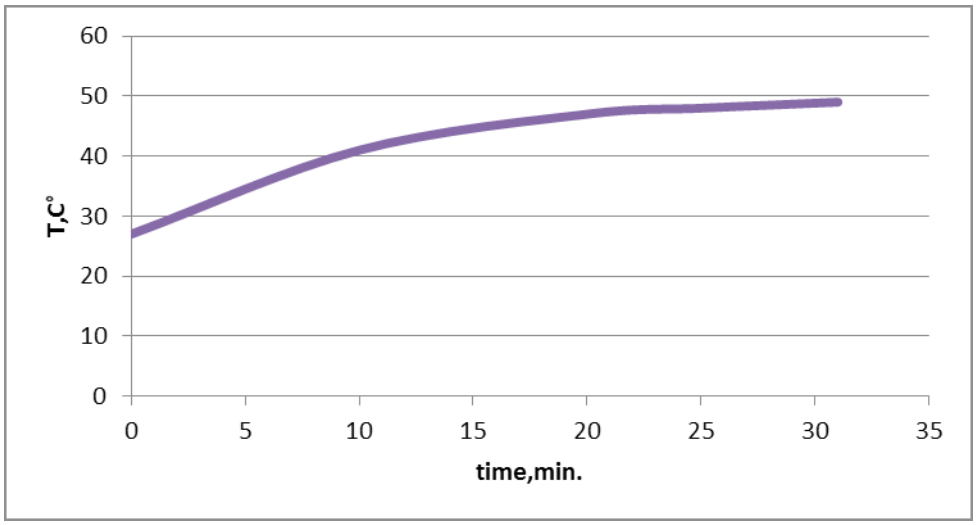

Figure 4 – Dependence of the heating temperature of the receiving disk on time with the paint coating

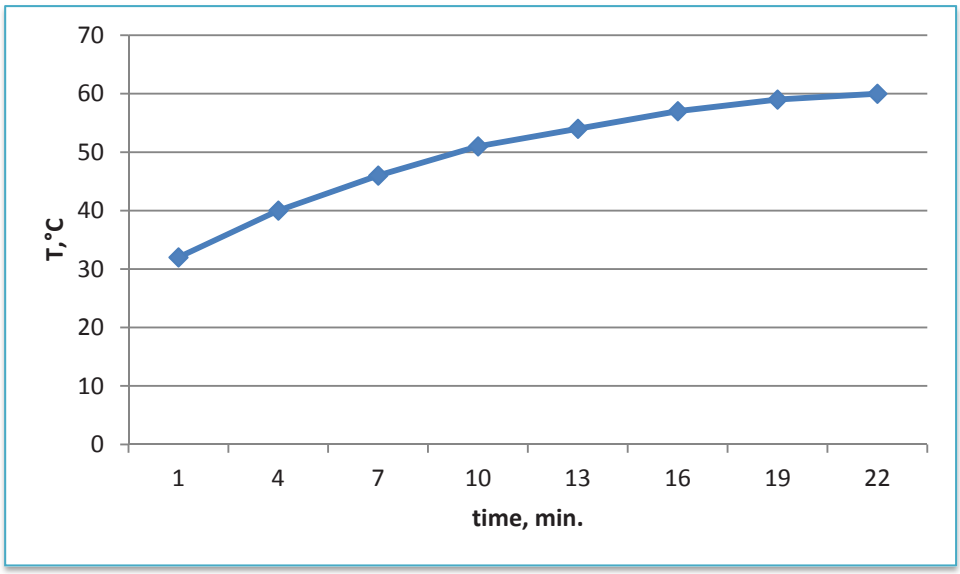

Figure 5 – Dependence of the heating temperature of the receiving disk on time with aluminum plates

Calculation of energy by this method was given 128 and 156 J for dish with paint cover and aluminum plate, respectively. As shown, with aluminum cover the maximal temperature reached fast, but this method is not enough exactly. Calculation of power density. This parameter calculated by using of Fourier method, described over. As receiver we used aluminum disks with thickness 1,1 cm.

$$P = \frac{\lambda S(T1 - T2)}{h}$$

$$P = \frac{203{,}5 \times 15{,}09 \times 1{,}8 \times 10^{-4}}{1{,}1 \times 10^{-2}} = 50{,}25W$$

$$\rho = \frac{50{,}25Bm}{15{,}09 \times 10^{-4}\,м^2} = 33{,}3\frac{\kappa W}{м^2} = 3{,}3\frac{W}{cm^2}$$

Conclusion

A parabolic concentrator with different types of coatings, as well as devices for lighting and measuring energy parameters have been developed. With an average illumination, the 500 lux light source in the focus zone received a temperature of 50 ^{0}C. If it is assumed that the temperature is directly proportional to the illumination, then in direct sunlight with a brightness of 5000 lux, the temperature in the focus zone should be 500 ^{0}C. This temperature was actually obtained in full-scale tests concentrator and was 400 ^{0}C. Two well-known methods for determining the energy and power parameters were used in the work. The obtained experience allows using these methods for calculating parameters and creating other, more powerful concentrators.

References

1. J. Kleih, 'Dish-Stifling Test Facility', Solar Energy Materials. – 1991. – Vol. 24. – P. 231-237.

2. R.Y. Nuwayhid, F. Mrad and R. Abu-Said, 'The Realization of a Simple Solar Tracking Concentrator for University Research Applications', Renewable Energy. – 2001. – Vol. 24, No. 2. – P. 207-222.

3. C.A. Perez-Rabago, M.J. Marcos, M. Romero and C.A. Estrada, 'Heat Transfer in a Conical Cavity Calorimeter for Measuring Thermal Power of a Point Focus Concentrator', Solar Energy. –2006. – Vol. 80, No. 11, – P. 1434-1442.

4. A.R. El Ouederni, A.W. Dahmani, F. Askri, M. Ben Salah and S. Ben Nasrallah. Experimental study of a parabolic solar concentrator. Revue des Energies Renouvelables CICME'08 Sousse (2008). –Vol. 193 – P. 199-193

5. S.Kalogirou, P. Eleflheriou, S. Lloyd and J. Ward, 'Low Cost High Accuracy Parabolic Troughs Construction and Evaluation', Renewable Energy. – 1994. – Vol. 5, No. 1-4. – P. 384-386.

6. I. Palavras and G.C. Bakos, 'Development of a Low-Cost Dish Solar Concentrator and its Application in Zeolite Desorption', Renewable Energ., – 2006. – Vol. 31, No. 15, – P. 2422-2431.

7. Zhukeshov A.M., Sundetov T. Calculation of the wind load of a solar concentrator with a two-axis tracker. KazNU bulletin, Physics series. – 2015. – No. 4. – P. 23-29.

8. Harmim, A., Merzouk, M., Boukar, M., Amar, M.: Design and experimental testing of an innovative building-integrated box type solar cooker. Solar Energy. – 2013. – Vol. 98. – P.422-433.

9. Hafez, A. Z., Soliman, Ahmed, El-Metwally, K. A., Ismail, I. M.: Solar parabolic dish Stirling engine system design, simulation, and thermal analysis. Energy conversion and management. – 2016. – Vol. 126. – P.60-75.

10. Tan, Woei-Chong, Chong, Kok-Keong, Tan, Ming-Hui: Performance study of water-cooled multiple-channel heat sinks in the application of ultra-high concentrator photovoltaic system. Solar Energy. – 2017. – Vol. 147. – P.314-327.

CONTENTS

Sh.R. Myrzakul, E. Gudekli, A.M. Syzdyk, K.R. Yesmakhanova
The nonlocal nonlinear Schrödinger and Maxwell – Bloch equation....4

G.T. Balakayeva, D.K. Darkenbayev, Chris Phillips
Investigation of technologies of processing of big data....13

Z.M. Abdiakhmetova, B.K. Alimbayeva, P.T. Omarova
Use of machine learning for early pre-clinical diagnostics of heart diseases....19

F.F. Komarov, A.I. Kupchishin, A.A. Kuatbayeva, T.A. Shmygaleva, D.A. Katabas, A.Yu. Ryabinin
Mathematical modelling of radiation defect formation processes in the materials irradiated with protons and alpha particles....23

A. Altybay, M. Ruzhansky, N. Tokmagambetov
On numerical simulations of the 1d wave equation with a distributional coefficient and source term....28

F.F. Komarov, A.I. Kupchishin, A.A. Kuatbayeva, T.A. Shmygaleva, K.A. Kabi, D.A. Katabas
Computer modelling of distributions processes on vacancy nanoclusters depth in the heavy targets irradiated with ions....33

G.B. Kussainova, Ye.S. Mukhametkarimov, N.R. Guseinov, O.Yu. Prikhodko
Optical properties of a-As2Se3 thin films....38

A. Issakhov, A. Abylkassymova, M. Sakypbekova
Applications of parallel computing technologies for modeling the mixed convection in backward-facing step flows with the vertical buoyancy forces....43

A.S. Askarova, S.A. Bolegenova, S.A. Bolegenova, V.U. Maximov, A.O. Nugymanova, P. Safarik
Combustion processes in furnace chambers of Kazakhstan TPPs using high-ash coal....51

A.M. Zhukeshov, A.T. Gabdullina, A.U. Amrenova, M. Sagymbaeva, A. Berdalin
The study of the heat power effectiveness of a parabolic solar concentrator....61